Università Politecnica delle Marche
Department of Life and Environmental Science
Curriculum in Ecology and Marine Biology

Cyanobacteria Sulfur Metabolism under Precambrian environmental Conditions

Tutor:
Professor Mario Giordano
Università Politecnica delle Marche – Ancona

Ph.D. candidate:
Lucia Gastoldi

Ph.D Course Coordinator:
Professor Oliana Carnevali
Università Politecnica delle Marche – Ancona

XXXII cycle
(2016-2019)

Università Politecnica delle Marche
Department of Life and Environmental Sciences - DiSVA
Via Brecce Bianche — 60131 – Ancona, Italy

Alla mia famiglia,
vicina sempre e dovunque,
con chiamate, messaggi
e pacchi per la sopravvivenza.
Grazie per la pazienza
e il supporto infiniti.

“Avanti, avanti, Cavalieri di Théodedn!
Gesta crudeli vi attendono: fuoco e stragi!
Saran scosse le lance, frantumati gli scudi,
e rosso il giorno prima dell’alba!
Cavalcate! Cavalcate! Cavalcate verso Gondor!”
Il ritorno del Re – Il Signore degli Anelli

“Arise, arise, Riders of Thjoden!
Fell deeds awake: fire and slaughter!
spear shall be shaken, shield be splintered,
a sword-day, a red day, ere the sun rises!
Ride now, ride now! Ride to Gondor!!”
The return of the king – The Lord of the Rings

ABSTRACT

One of the most important concepts in physiology highlights how the chemical characteristics of a specific environment can influence the basal metabolism of those organisms living in it. Therefore, the variations in the elements' concentration must have influenced the evolution of the metabolic pathways' observable today even though no one really knows exactly how the origin of early life took place on Earth. Nevertheless, we know from geological records that the first cell originated in an environment that was mighty different from the present one, especially considering the availability of carbon, nitrogen, sulfur, phosphate, and iron, which are the most important elements from a biological point of view. Particularly, considering those elements fundamental in microalgal metabolism, the amount of inorganic sulfur available, which is normally considered as sulfate, became important since it was considerably less compared with the actual level (which is around 28mM).

Sulfate variations before the **Phanerozoic Era** were so strong that one hypothesis speculates that sulfur availability influenced the phytoplankton evolution and radiation in the prehistoric oceans (sulfur facilitation hypothesis). With these concepts in mind, I investigated how the regulation in sulfate assimilative metabolism in picocyanobacteria may have changed through the history of Earth focusing on the first step of the assimilation pathway, which is controlled by the ATP sulfurylase (ATPS) protein.

Three events were used as milestones for the current project: (1) the origin of Cyanobacteria organisms, during the end of **Archean Eon**, (2) the evolution of oxygenic photosynthesis and (3) the consequent Great Oxygenation Event (GOE) in the **Proterozoic Eon**. These major changes in global conditions caused profound variation in the ocean chemistry, leading (a) an increase of sulfate availability, (b) a dramatic decrease of dissolved iron and other cations, and, as a final consequence, (c) an increase in sinks for reducing equivalents in the cell metabolism. Since all these environmental factors could have influenced the usage of reducing equivalents in primitive unicellular organisms, conspicuous repercussions on their metabolism regulation and resource/energy allocation and distribution are ensuing.

Despite the relevance of these matters, very little is known about these repercussions on the primary producers' metabolism, in particular, about marine picocyanobacteria. Since the early primary production mostly depended on photo-oxygenic cyanobacteria and, since, even now, cyanobacteria retain differences in the use of sulfate, we focused on this group

of organisms studying their physiological performance, their chemical composition, their mode of resource and energy partitioning in reconstructed Proterozoic chemistry and in modern ocean conditions. In order to understand the impact that environmental changes may have had on ocean ecology, we also studied their influence on cyanobacterial biomass quality, in the attempt to comprehend the consequences on the trophic webs.

The results from this work allowed to point out some information:

→ Oxygen availability variations influence growth rate in cyanobacteria,
→ Nutrient limitation combined with redox power variation has an effect on the ATPS activity, but the nutrient concentration seems to be the strongest one,
→ Nutrient limitation influences elements assimilation and macromolecular pool in cyanobacteria.

Then, it is possible to conclude that the oxygenation of the planet may not have been the only evolutive constraint for redox regulation in ATPS enzymes. Moreover, these biochemical results support the theory which states cyanobacteria evolved in the freshwater environment and only secondly conquered the seawater environment.

TABLE OF CONTENT

"Nel mezzo del cammin di nostra vita
mi ritrovai in una selva oscura,
ché la dritta via era smarrita.

Ahi quanto a dir qual era è cosa dura
esta selva selvaggia e aspra e forte
che nel pensier rinova la paura!"
La Divina Commedia
Inferno
Canto Primo – 1,6

"When half way through the journey of our life
I found that I was in a gloomy wood,
because the path which led aright was lost.

And ah, how hard it is to say just what
this wild and rough and stubborn woodland was,
the very thought of which renews my fear!"
La Divina Commedia
Hell
Chapter First – 1,6

INTRODUCTION

During the history of Earth, the chemistry of the aquatic environment changed drastically in combination with the oxygenation of the atmosphere, phenomenon that followed the evolution of oxygenic photosynthesis in Cyanobacteria during the Precambrian period (Anbar, 2008; Anbar and Knoll, 2002; Anbar et al., 2007; Farquhar et al., 2010a; Lyons et al., 2014; Saito et al., 2003; Ward et al., 2016). The most important and main consequences derived from the oxygenic photosynthesis pathway were 1) the obvious presence of O_2; 2) an increase in sulfate availability in water column (Fike et al., 2015); 3) an important decrease in dissolved iron (Johnson, 2019), which became a limiting nutrient in modern ocean (Behrenfeld et al., 1996; Greene et al., 1991; Kolber et al., 1994; Moore et al., 2001); 4) a switch from ammonium to nitrate as nitrogen source (Stüeken et al., 2016, 2016); and, finally, 5) an increase in sinks for reducing power (Falkowski and Godfrey, 2008). Indeed, molecular oxygen is the ultimate sink for reductants nowadays, meanwhile previously, under anoxic condition, which can resembles the present anoxic one, microorganisms used nitrogen (Falkowski and Godfrey, 2008), sulfate (SO_4^{2-}) (Boyle et al., 2013), elemental sulfur (S^0) (Flynn et al., 2014), iron (Fe^{3+}) or CO_2 (Cord-Ruwisch et al., 1988) as a respiratory electron sink (Boyle et al., 2013; Falkowski and Godfrey, 2008). The resulting changes in redox environmental conditions due to Earth's oxygenation could have implied a tighter control on photosynthetic cell metabolism since molecular oxygen acquires electrons with higher affinity than the oxidants present on the planet before (Chen et al., 2017) and this can have a huge effect on metabolisms. For example even today, some organisms, such as purple photosynthetic bacteria, can vary their principal metabolism depending on environmental redox conditions: they are indeed photoautotrophs under reducing conditions, while under oxidizing conditions they lose their photosynthetic capability, becoming facultative heterotrophs (Falkowski and Godfrey, 2008).

The variations in sulfur concentration influenced the evolution and the spread of photosynthetic phytoplankton since not all the cells have the same tolerance to elemental concentration. Considering that sulfur is one of the most important macronutrients in photosynthetic cells (it is thought to drive their evolution – sulfur facilitation hypothesis, Prioretti and Giordano, 2016) and since its assimilation consumed a large amount of reducing power and energy, sulfur metabolism and its variations were analyzed in this thesis to point out if oxygenation of the planet influenced somehow the first step of sulfur metabolism in cyanobacteria.

1.1 THE CYANOBACTERIA TAXON

Cyanobacteria are Gram-negative photosynthetic prokaryotic organisms (**Figure 1**) with global biomass estimated around $3 \cdot 10^{14}$ g (Cohen and Gurevitz, 2006; Whitton and Potts, 2012) and, they represent the major part of phytoplankton present today in the ocean (Falkowski, 2004). This group can be found in several environments, including the deep sea (Lindh et al., 2017) and the high temperature (Castenholz, 1969; Meeks and Castenholz, 1978; Miller and Castenholz, 2000) ones thanks to the plasticity of their metabolism. This aspect is known to influence the distribution of species in the water column allowing the coexistence of similar species in the same environment (Scanlan et al., 2009). Furthermore, cyanobacteria phytoplankton appreciably contribute (1) to global primary production (indeed, around 40-45% of the marine carbon fixation is attributable to them; Falkowski, 2004; Scott et al., 2007), and (2) to N_2 fixation (Bothe et al., 2010; Tamagnini et al., 2002).

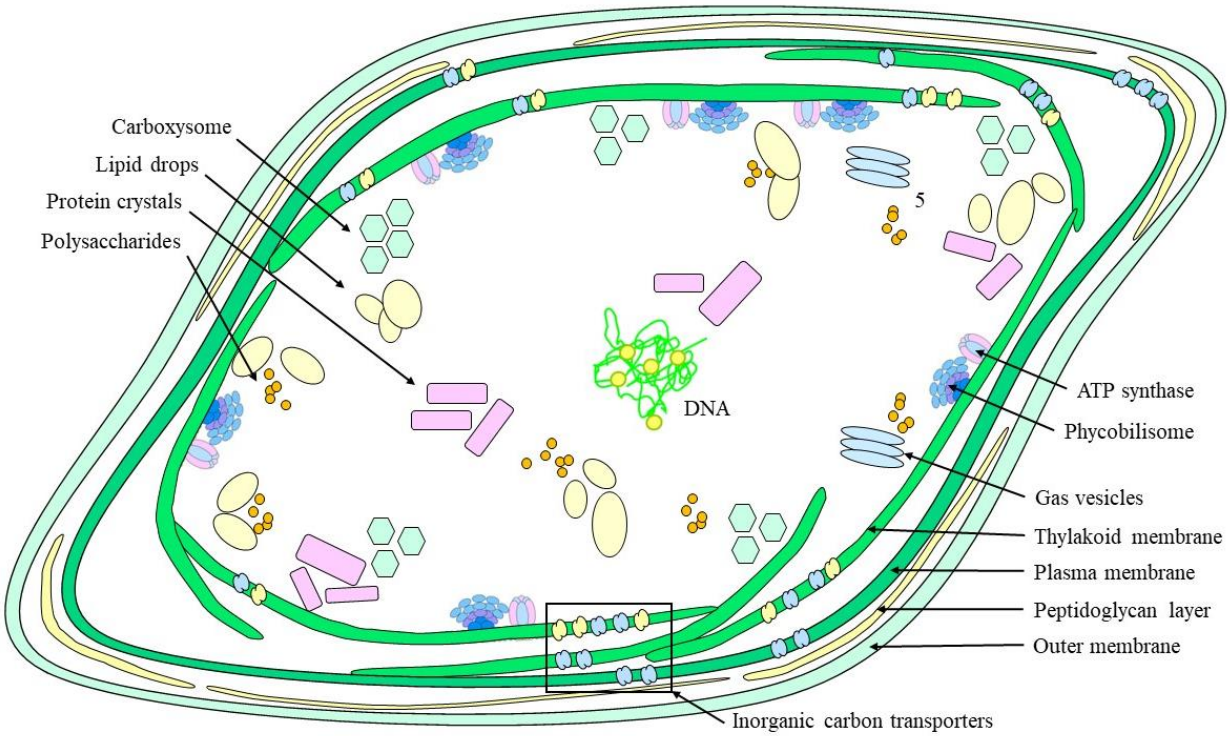

Figure 1 *Cyanobacteria cell (Bryant, 2006; Liu, 2016).*

Indeed, for example, the *Trichodesmium* genus role in oceanic nitrogen fixation is estimated at around 60 – 80 Tg N annually on the total estimated value of 100 – 200 Tg N annually (Bergman et al., 2013). Fixing N_2, they have a great role also (a) in the pelagic

food-web (Bergman et al., 2013; Karlson et al., 2015), and (b) in the oceanic microbial loop (Karlson et al., 2015) releasing bioavailable nitrogen in the water column. To our present knowledge, they are the only organisms where the **oxygenic photosynthesis** evolved and not acquired through an endosymbiotic event (McFadden, 2001). Besides it, however, cyanobacteria can perform also anoxygenic photosynthesis, based on sulfide as the electron donor and independent from photosystem II (Hamilton et al., 2016; Klatt et al., 2015; Ozaki et al., 2019). Moreover, dark respiration and fermentation are available options to survive in dark anaerobic conditions, such as mat formations or oceanic blooms (Cohen and Gurevitz, 2006). Since they are prokaryotes, the organization of the photosynthetic system is a bit different from the algal/plant one. Nevertheless, as usual as in other photosynthetic organisms, in cyanobacteria, it is possible to recognize the **thylakoid membrane** which, however, is not organized as grana (as shown in **Figure 2**, which represents a magnification of membrane organization shown in **Figure 1**).

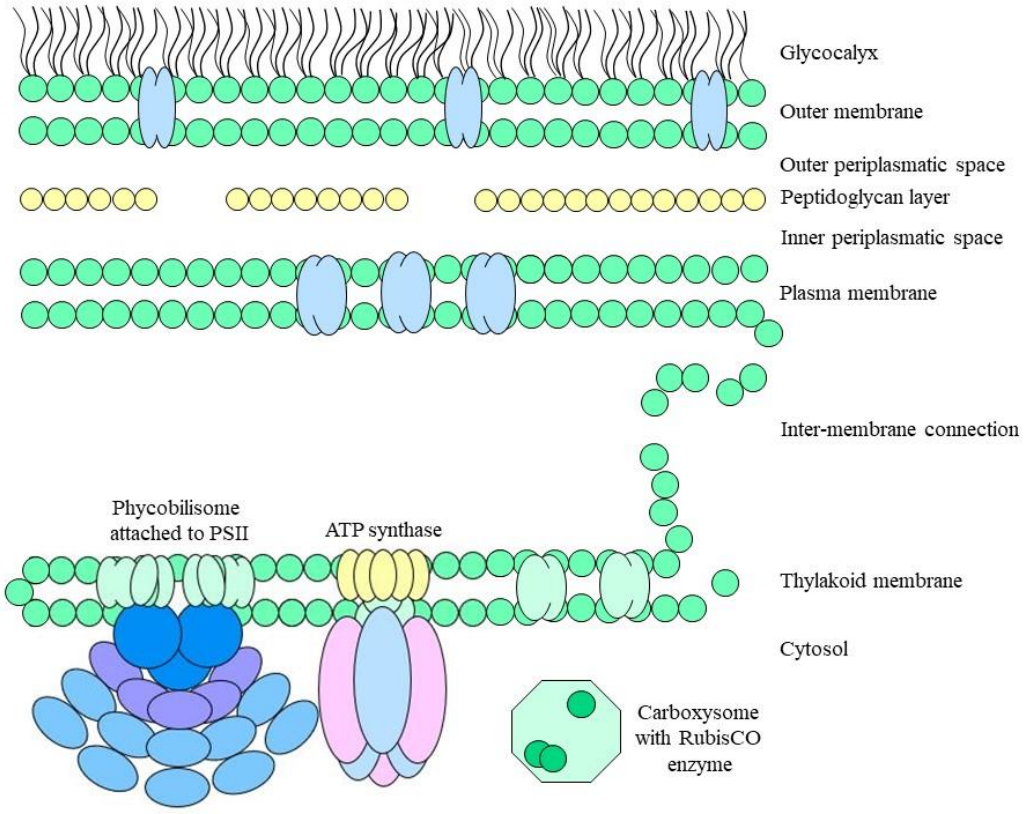

Figure 2 *Cyanobacteria membrane organization (Bryant, 2006).*

On this membrane, the **photosynthetic apparatus** is organized (**Figure 3**), constituted by the **reaction centers** (photosystem II and I), the **plastoquinone** (PQ/PQH), the **cytochrome *b_6f* complex** and the **ATP synthase** (Bryant, 2006; Liu, 2016). Moreover, some proteins involved in the respiratory electron transport chain are also present: the **NAD(P)H dehydrogenase** (NDH-1), the **succinate dehydrogenase** (SDH) and **cytochrome oxidase** (Cyt ox; indicated in **Figure 3**). Some components on the other hand, such as the cytochrome b_6/f (cyt b_6/f), the plastoquinone (PQ/PQH_2) and the **plastocyanin** (PQ) are shared by both electron transport pathways (**Figure 3** - Bryant, 2006; Liu, 2016).

During photosynthesis, the light is collected through specific pigment, both **chlorophylls** (normally chlorophyll a, with some species containing chlorophyll d - Miyashita et al., 1996) and **phycobilins** organized in the light-harvesting antenna, the **phycobilisome complex** (Bryant, 2006; Falkowski and Raven, 2013; Scanlan et al., 2009; Watanabe and Ikeuchi, 2013). The phycobilisome (PBS - **Figure 3**) is a mobile antenna connected with the PSII, formed by 3 different kinds of proteins organized as spokes of a wheel to collect the light (Scanlan, 2003; Scanlan et al., 2009). The center of the wheel is made of allophycocyanin (APC) and is the section used to connect the PBS with the PS, the spokes are instead constituted by phycocyanin (PC) or phycoerythrin (PE) in different proportion depending on the wavelength of the light that the cells used to grow (Scanlan et al., 2009; Six et al., 2007).

The PSII oxidizes water to O_2 as usual in other photosynthetic organisms. From PSII, the electrons move to cytochrome b_6/f complex and then to the PSI. Downstream PSI, reductants, as NADPH is generated. (Bryant, 2006 - **Figure 3**). In addition, the resulting proton gradient is used to synthesize ATP through the ATP synthase enzyme (Falkowski and Raven, 2013). The generated redox potential, coupled with the ATP molecules, is used to reduce the CO_2 through the fixation pathway, which is activated by the RubisCO enzyme (Falkowski and Raven, 2013). Furthermore, the ATP and NAD(P)H molecules produced through photosynthesis light reaction will be used also for the sulfur and nitrogen metabolism.

In modern cyanobacteria, RubisCO is stored in **carboxysomes** (**Figure 3**), protein shells that limit the competition between O_2 and CO_2 for the active site of the enzyme (Badger and Price, 2003; Burnap et al., 2015; Fukuzawa et al., 2012; Giordano et al., 2005; Price et al., 2008; Rae et al., 2013, 2013). The carboxysomes are part of a more complex system, the **Carbon Concentration Mechanisms** (**CCMs - Figure 4** and **Figure 5**) which

overcome the gap between the K_m[1](CO_2) of RubisCO (around 240mol/l for *Synechococcus* for example - Falkowski and Raven, 2013) and the concentration of dissolved CO_2 in the environment (Badger and Price, 2003; Burnap et al., 2015; Fukuzawa et al., 2012; Giordano et al., 2005; Price et al., 2008; Rae et al., 2013, 2013).

The ancestral form of the RubisCO enzyme evolved in an anoxic environment where the CO_2/O_2 competition didn't exist (Erb and Zarzycki, 2018) or, at least, was not an issue until the environment became completely oxygenated (Erb and Zarzycki, 2018). Once the oxygen concentration increased, competition for the active site of RubisCO became important and, due to the increase of photorespiration rate, the CO_2 reduction rate decreased. This was probably an evolutionary pressure strong enough to force the evolution of CCMs, carboxysome enclosed (Price et al., 2008; Rae et al., 2013; Six et al., 2007).

[1] K_m: Michaelis constant of the enzyme, an inverse measure of affinity between the enzyme and the substrate molecules. Practically, K_m is the concentration of substrate which allows the enzyme to reach half V_{max} (Robinson, 2015).

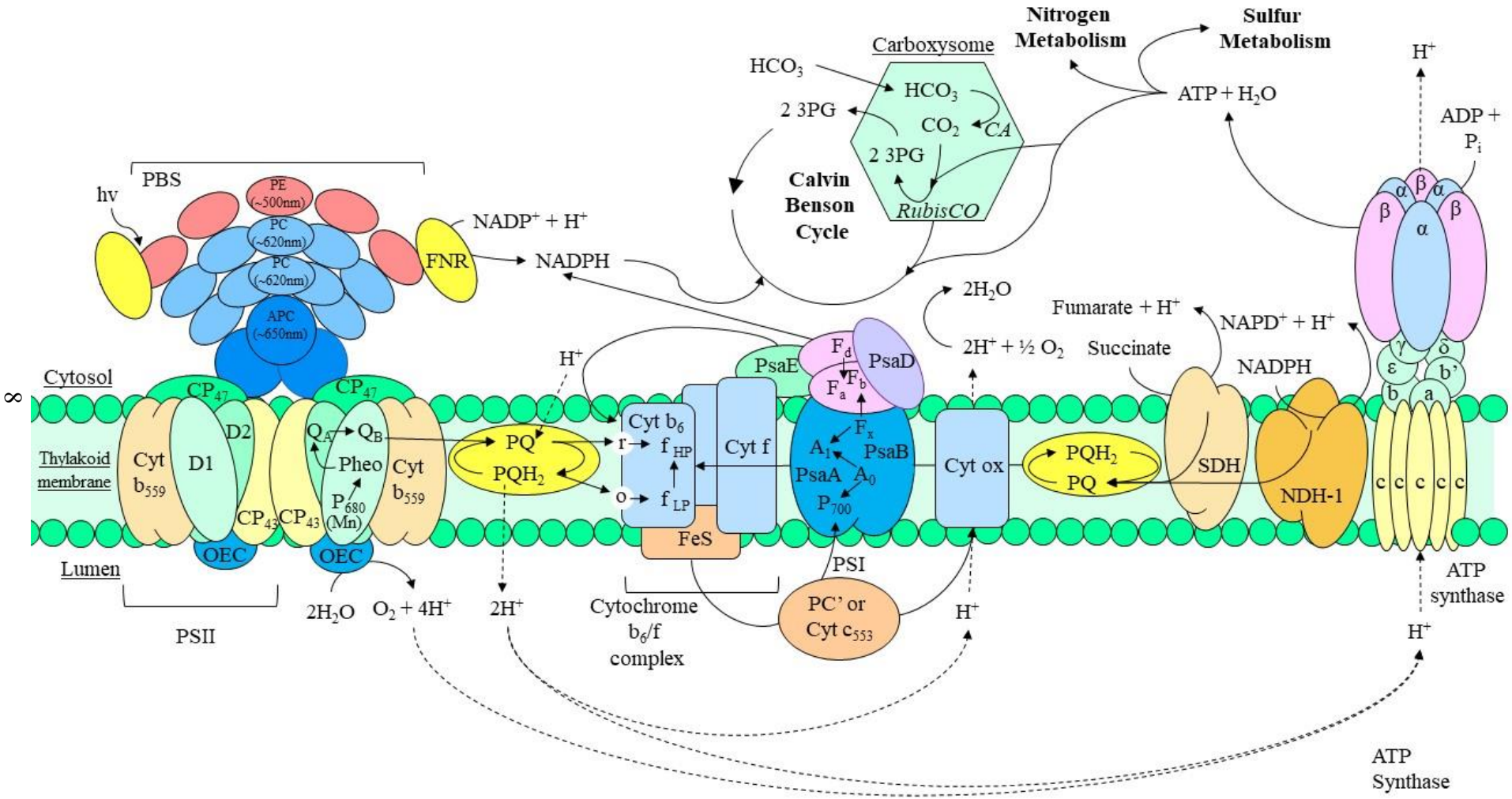
Nitrogen Metabolism
Sulfur Metabolism
Carboxysome
HCO_3^-
HCO_3^-
CO_2
CA
2 3PG
2 3PG
RubisCO
Calvin Benson Cycle
$ATP + H_2O$
H^+
ADP + P_i
PBS
hv
PE (~500nm)
PC (~620nm)
PC (~620nm)
APC (~650nm)
FNR
$NADP^+ + H^+$
NADPH
$2H_2O$
$2H^+ + ½ O_2$
Fumarate + H^+
Succinate
$NAPD^+ + H^+$
NADPH
Cytosol
Thylakoid membrane
Lumen
PSII
CP_{47}
CP_{43}
D1
D2
Cyt b_{559}
Q_A
Q_B
Pheo
P_{680} (Mn)
OEC
$2H_2O$
$O_2 + 4H^+$
PQ
PQH_2
$2H^+$
Cyt b_6
f_{HP}
f_{LP}
r
o
Cytochrome b_6/f complex
Cyt f
FeS
PsaE
F_d
PsaD
F_a
F_b
F_x
A_1
PsaA
PsaB
A_0
P_{700}
PSI
PC' or Cyt c_{553}
Cyt ox
PQH_2
PQ
SDH
NDH-1
ATP synthase
ATP Synthase
H^+

Figure 3 *Photosystem organization in cyanobacterial cells (based on bibliography, in particular, Bryant, 2006; Liu, 2016). In the picture, the reactions of photosynthesis are shown, dashed lines indicate the protons movements while the full lines underline the movements of the electrons. PBS: phycobilisome, FNR: ferredoxin, PE: phycoerythrin, PC: phycocyanin, APC: allophycocyanin, PSII: photosystem II, Cyt* b_{559}*: cytochrome* b_{559}*, D1/D2/CP47/CP43: proteins for PSII, OEC: oxygen-evolving complex, Pheo: pheophytin - intermediate electron acceptor,* $Q_{A\ or\ B}$*: non-heme iron,* PQ/PQH_2*: plastoquinone, Cyt* b_6*: cytochrome* b_6*, Cyt f: cytochrome f, PSI: photosystem I, PsaA/B/D/E: proteins in PSI, Fx: cluster 4Fe-4S, PC': plastocyanin, Cyt* c_{553} *(or* c_6*): cytochrome* c_{533}*, Cyt ox: cytochrome oxidase, SDH: succinate dehydrogenase, NDH -1: NADH dehydrogenase, CA: carbonic anhydrase, 3PG: 3 phosphoglycerate (Bryant, 2006; Liu, 2016).*

Normally, two different kinds of CCMs can be found in nature: the physical ones and the biochemical ones. Both consist of (1) the subcellular compartments (means the *carboxysome* in prokaryotes and *pyrenoid* in eukaryote), in which the RubisCO is stored, (2) the carbonic anhydrase CA, which maintain the equilibrium between HCO_3^- and CO_2 in the intracellular environment; and (3) those proteins involved in the uptake of inorganic carbon from the external environment (protein for Dissolved Inorganic Carbon, i.e. DIC, acquisition - Badger et al., 2006). In cyanobacteria the CCMs are very efficient and, thanks to their genetic regulation, they can adapt their metabolism to different CO_2 concentrations (Burnap et al., 2015).

Through several genetic and molecular studies (Badger and Price, 2003; Badger et al., 2002, 2006; Cameron et al., 2013; Price, 2011; Rae et al., 2013), it was point out that different groups of cyanobacteria (i.e. marine and freshwater groups) were characterized by different types of carboxysomes, which correspond to different forms of RubisCO. This information allowed the classification of the whole cyanobacteria taxon under a genetic point of view. These studies help also in the evolutive studies on these organisms. For example, the CCMs differences between marine and freshwater genera were underlined and, also, a close relation between picocyanobacteria RubisCO genes (i.e. *Synechococcus* and *Prochlorococcus* genera) and some of β proteobacteria genes was pointed out (Scanlan et al., 2009). Based on these studies, cyanobacteria can be classified into two main groups (Badger et al., 2006; Cameron et al., 2013; Rae et al., 2013):

1) the **α Cyanobacteria,** which identify all the open ocean species. Indeed, this group encloses all the *Prochlorococcus* genus and the major part of the *Synechococcus* one. The α cyanobacteria contain the **α carboxysomes** and the **Form1A Rubisco** (Rae et al., 2013 - **Figure 4);**

2) the **β Cyanobacteria** that enclosed all the freshwater species and those species with a peculiar environment, such as some coastal and some symbiotic species. These organisms code for the **β carboxysome** and the **Form1B Rubisco** (plant-like form - (Cameron et al., 2013; Rae et al., 2013 - **Figure 5**).

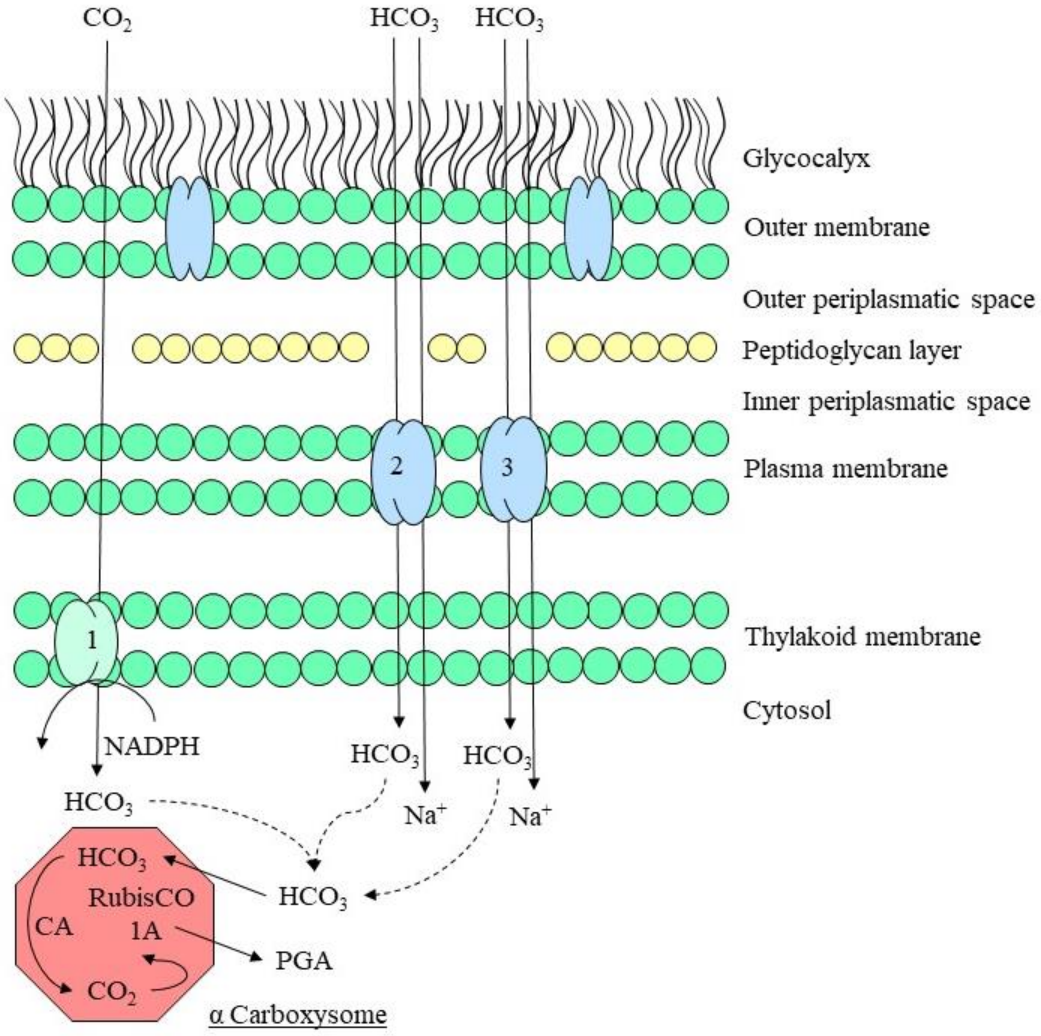

Figure 4 *α carboxysome and inorganic carbon transporters: 1) NDH -1$_4$, 2) BicA2, 3)SbtA2 (Rae et al., 2013).*

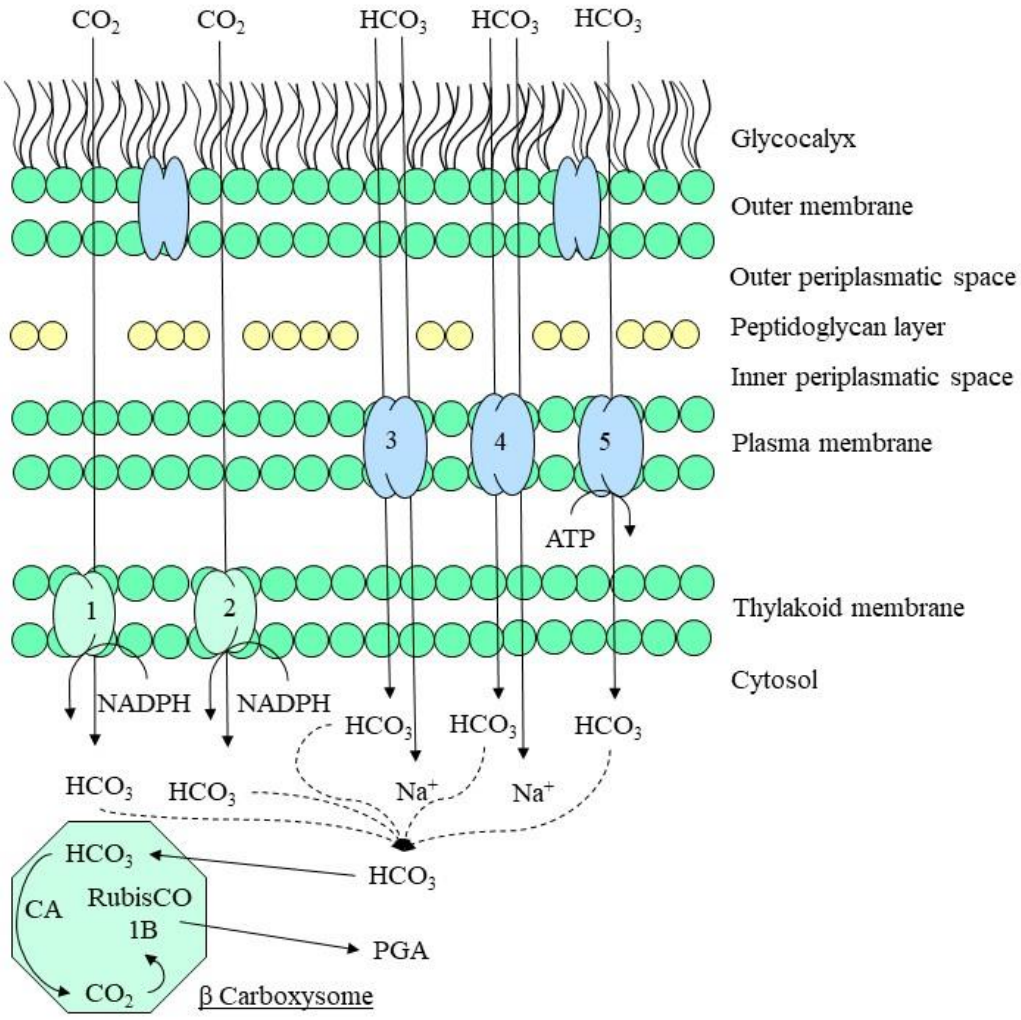

Figure 5 *β carboxysome and inorganic carbon transporters: 1)NDH -1$_4$, 2) NDH -1$_3$, 3) BicA1, 4)SbtA1, 5)BTC1 (Rae et al., 2013).*

As for carbon metabolism, which presents different proteins in different cyanobacteria subgroups related to their environment and, apparently, influenced by oxygenation on the planet, it's possible to underline the similar differences in some proteins also for sulfur metabolism. Indeed, the first step of sulfur assimilation in cyanobacteria is controlled by the ATP sulfurylase enzyme (Giordano and Prioretti, 2016), which presents two different isoforms: one in the marine and one in the freshwater subgroup. Moreover, one isoform presents a redox regulation of its activity while the second one does not (Giordano and Prioretti, 2016; Prioretti et al., 2014, 2016).

Considering this information, it can be supposed that the oxygenation of the planet, responsible for the variation of the redox power available for the cell, played a role also in the evolutionary process of ATP sulfurylase enzyme. This thesis aims to analyze this hypothesis.

1.2 CYANOBACTERIA, OCEAN EVOLUTION AND EARTH OXYGENATION

From geochemical records, 3 sequential stages are hypothesized to explain the ocean evolution during the **Precambrian** period (from 4.6Gy ago to 541My ago – **Figure 6**) as described in **Figure 7**: (1) an ***Archean ocean***, (2) a ***Proterozoic ocean*** and (3) a ***Modern ocean*** (Anbar, 2008; Anbar and Knoll, 2002; Farquhar et al., 2010b; Fischer et al., 2016a; Hamilton et al., 2016; Lyons et al., 2014; Saito et al., 2003). Despite the last stage is defined as Modern Ocean, it originated during the end of the Neoproterozoic era, after the Cryogenian period, and it lasts until the modern Anthropocene period. The chemical form and concentration of elements in the marine sedimentary rock are usually used as an index for the chemical characterization of the water column during the past eras and, therefore, of the ancient atmosphere (Anbar and Knoll, 2002; Anbar et al., 2007). Several studies have focused on the variations in the geochemical cycle during the evolution of the planet and they were used for the chemical characterization of the reconstructed proterozoic environment designed for this project.

Eon	Era	Period	Epoch	Time	
Phanerozoic	Cenozoic	Quaternary	Anthropocene	NOW	Years
			Holocene	1,950	
			Pleistocene	11,700	
		Neogene	Pliocene	2,580,000	
			Milocene	5,330,000	
		Paleogene	Oligocene	23,030,000	
			Eocene	33,900,000	
			Paleocene	56,000,000	
	Mesozoic	Cretaceous		0.066	Gyr (10^9)
		Jurassic		0.145	
		Triassic		0.201	
	Paleozoic	Permian		0.251	
		Carboniferous	Pennsylvanian	0.298	
			Mississippian	0.323	
		Devonian		0.358	
		Silurian		0.419	
		Ordovician		0.443	
		Cambrian		0.485	
Precambrian	Proterozoic	Neoproterozoic	Ediacaran	0.500	
			Cryogenian	0.635	
			Tonian	0.720	
		Mesoproterozoic	Stenian	1.00	
			Ectasian	1.20	
			Calymmian	1.40	
		Paleoproterozoic	Statherian	1.60	
			Orosirian	1.80	
			Rhyacian	2.05	
			Syderian	2.30	
	Archean	Neoarchean		2.5	
		Mesoarchean		2.8	
		Paleoarchean		3.2	
		Eoarchean		3.6	
	Hadean			4.0	
				~ 4.6	

Figure 6 *Geological Eras, the figure is based on literature used for this thesis (refer to those papers cited in the main text).*

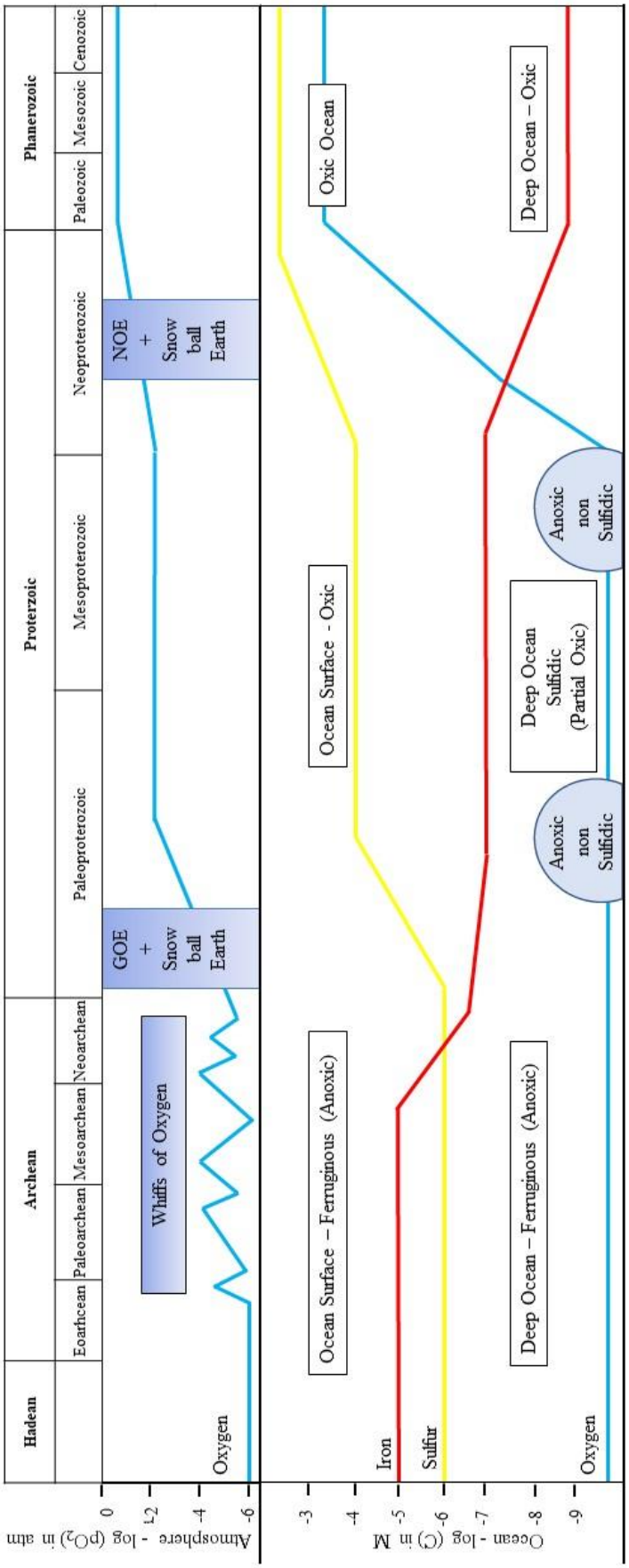

***Figure** 7 Summary of principal variation detected during Archean, Proterozoic and Phanerozoic Eons based on several papers and studies cited in the main test – In particular Anbar, 2008; Anbar et al., 2007; Farquhar et al., 2010; Fischer et al., 2016; Lyons et al., 2014; Saito et al., 2003).*

During the succession of the 3 stages of the ocean, the concentration of oxygen dissolved in the water column increased together with the dissolved sulfur, while the concentration of dissolved iron decreased and the available form of nitrogen switched from ammonium to nitrate (Anbar, 2008; Anbar and Knoll, 2002; Anbar et al., 2007; Farquhar et al., 2010b; Fischer et al., 2016a; Lyons et al., 2014; Saito et al., 2003).

In the first stage, the ***Archean ocean*** resulted to be very poor in sulfur with a concentration at least lower than 200μM (Farquhar et al., 2010b; Giordano and Prioretti, 2016; Habicht et al., 2002). In this condition the dissolved iron was much higher than today (Saito et al., 2003): some studies suggest that iron was oxidized through anoxygenic photosynthesis on the ocean surface and then brought to the deeper ocean as siliceous-iron deposits (Fischer and Knoll, 2009). Thorough time, the accumulation of oxygen in the environment implied a reduction of ferrous ions in the water column, which led to an increase of oxygenic photosynthesis over anoxygenic photosynthetic bacteria allowing the increase of dissolved oxygen (Knoll and Nowak, 2017).

Indeed, cyanobacteria oxygenic photosynthesis evolution is linked with planetary oxygenation **Figure 8**), but there are at least three different theories about when they evolved and about how big was their contribution to this phenomenon. Especially since some isotope analyses indicate the presence of free O_2 in the atmosphere during around 3 – 3.5Gyr ago (Anbar et al., 2007; Knoll and Nowak, 2017; Kump, 2008; Kump and Barley, 2007; Lyons et al., 2014; Papineau et al., 2007a), despite it was far before the **First Great Oxygenation Event** (**GOE**, 2.4 – 2.3Gyr ago; Bekker et al., 2004; Canfield, 2014; Hoffman, 2013). Yet, cyanobacteria, and thus oxygenic photosynthesis, cannot be post-dated up to that period with high precision. Indeed, although the existence of some ambiguous microfossils dated around 2 billion years ago (Butterfield, 2015; Javaux and Lepot, 2018; Schirrmeister et al., 2015), the presence of cyanobacteria on the planet remains difficult to confirm before 2.7Gyr (Shih et al., 2017; Ward et al., 2016).

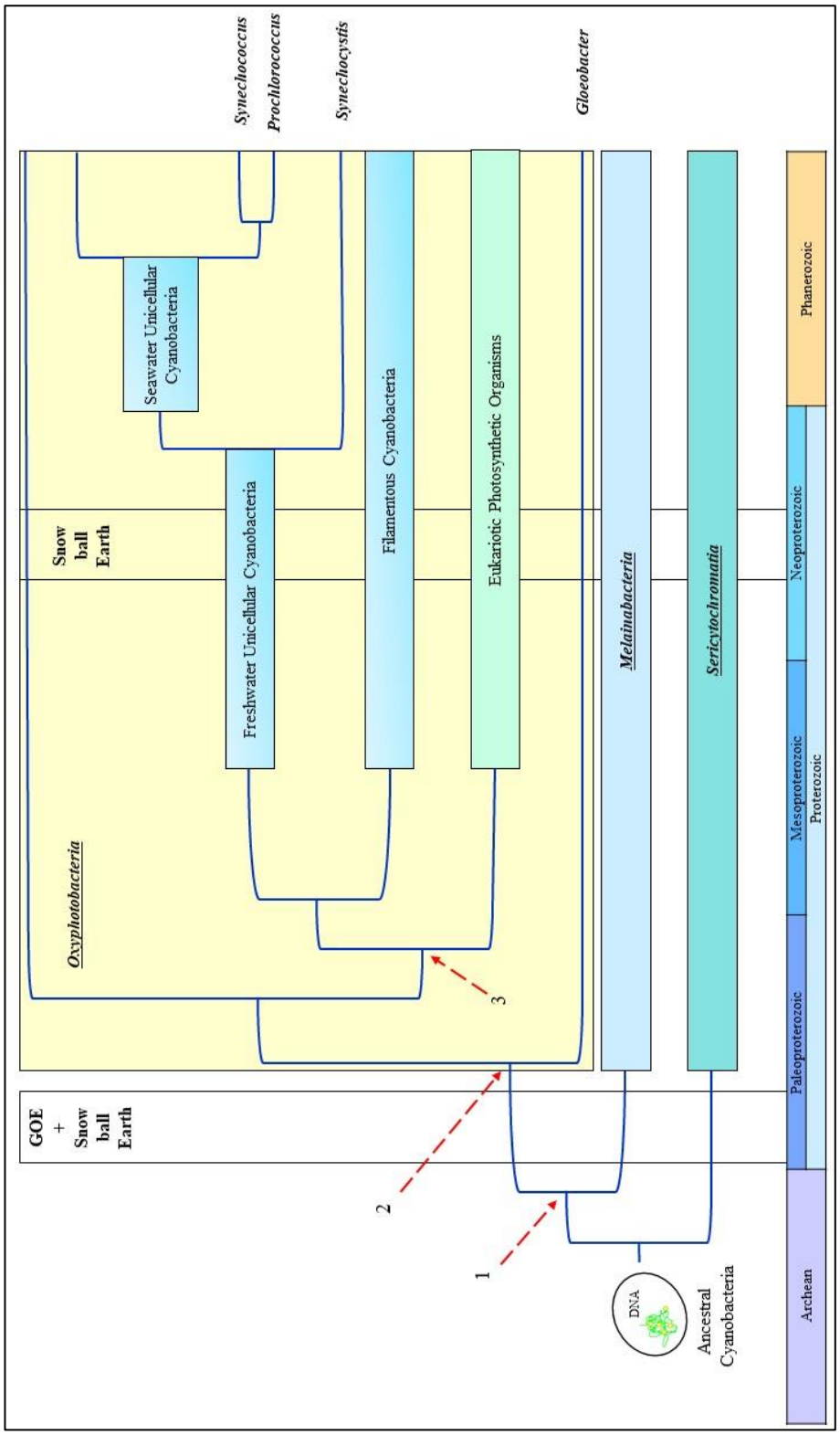

Figure 8 *Cyanobacteria principal taxon and evolution. For a proper explanation, refer to the main text and to the references in it. Legend: 1) divergence between Oxyphotobacteria and Melainabacteria; 2) origin of Crow Oxyphotobacteria; 3) plastid endosymbiosis (Shih et al., 2017).*

Thus, it can be that either oxygenic photosynthesis evolved around 2.4Gyr ago and oxygenated the atmosphere and then the oceans; or that oxygen consumption corresponded to its photosynthetic production for the first millions of years of cyanobacterial history. In the second case, the GOE would be the result of several biological and geochemical phenomena, enclosed, but not only, the increase of oxygenic photosynthesis rate (Knoll and Nowak, 2017). Based on the geological records of molybdenum (as molybdate) and sulfur isotopes, Anbar and collaborators proposed that the oxygenation of the atmosphere started during the Archean Eon as small and temporary fluctuations of gaseous oxygen (whiff of oxygen - Anbar et al., 2007; Crowe et al., 2013; Scott et al., 2008). However, it is generally accepted that before 2.5Gyr ago, the atmosphere was poor of free oxygen (at least less than 10^{-5} PAL, i.e. *Present Atmospheric Level*; Pavlov and Kasting, 2002) and overall much less oxidizing than the actual one (Papineau et al., 2007). The oxygenation of the atmosphere has continued for the most part of the **Proterozoic Eon**, during which there was the alternation of huge oxidation events (at least two) and several ice periods (Hoffman, 2016; Hoffman et al., 2017). Finally, at the beginning of **Phanerozoic eon**, the level of atmospheric oxygen arrived at the present atmospheric level, after at least 2.0Gyr from the GOE (Canfield, 2005; Hamilton et al., 2016).

Nowadays, there are several and contrasting ideas on cyanobacteria development thought eons and on their role in the oxygenation of the Earth. The main hypotheses on their origins are based on different interpretation of some geological sets of data collected (a) from chemical evidence (as, for example, specific hydrocarbon biomarkers - Brocks et al., 1999, 2003; Summons et al., 1999); (b) from isotopes analyses (Altermann and Kazmierczak, 2003; House et al., 2000; Williford et al., 2013); (c) from microfossil records and phylogenomic studies (House et al., 2000; Knoll et al., 2016; Williford et al., 2013); and, lastly, (d) from sedimentary structures, as stromatolites (Knoll et al., 2016).

Several studies, based on the above – mentioned techniques, prove the presence of bacterial life during the **Archean Eon** (lasted from 4.0Gyr to 2.5Gyr - Knoll and Nowak, 2017), but it's still hard to indicate them as cyanobacteria. Still, Brocks and collaborators (Brocks et al., 1999, 2003) suggested that the first photosynthetic cyanobacteria appeared during the Archean Eon and based their hypothesis on specific biomarkers present in the Pilbara Craton set, in particular, the 2α-methylopanes molecules (Brocks et al., 1999, 2003). Despite the reliability of these biomarkers has been seriously questioned (Rasmussen et al., 2008; Fischer, 2008), Brocks' interpretation implies that the oxygenic photosynthesis

evolved more than 2.7Gyr ago (Planavsky et al., 2014; Schirrmeister et al., 2016). This idea is enclosed in one of the 2 more important theories about cyanobacteria evolution.

The first one is based on the timing of oxygenic photosynthesis evolution and on the gain and loss of multicellularity (Schirrmeister et al., 2011, 2013, 2015, 2016) before the Proterozoic Eon, persisted from 2.5Gyr to 0.6/0.5Gyr ago (Fischer, 2008; Knoll and Nowak, 2017; Rasmussen et al., 2008). Schirrmeister and collaborators hypothesized, based on molecular clock analyses, that some ancient cyanobacteria lineages originated during the Archean Eons and evolved, as well as the oxygenic photosynthesis, the multicellularity condition before the GOE (Schirrmeister et al., 2015). According to this idea, the multicellularity would imply a change in the microbial metabolisms; including in the new evolved oxygenic photosynthesis, with a possible increase in its rate. This metabolic increase could have helped in the speed of free oxygen produced. Multicellularity and oxygenic photosynthesis could have introduced a new evolutionary pressure that broke out the differentiation and evolution of the present cyanobacteria species (Schirrmeister et al., 2015).

A second hypothesis doesn't consider the multicellularity phenomenon. Instead, it suggests that the origin of ancient oxygenic cyanobacteria occurred much closer to the GOE and not during the Archean Eon (Shih et al., 2017; Soo et al., 2017; Ward et al., 2016). According to this idea, oxygenic photosynthesis appeared about 2.6-2.5Gyr ago (Knoll and Nowak, 2017) or even later around 2.0Gyr ago with the appearance of the *Oxyphotobacteria* group (Shih et al., 2017; Soo et al., 2017). According to Shih and Soo's works indeed, after the evolution of the early cyanobacteria lineage during the Archean, three different crown groups[2] evolved from an a–phototrophic ancestral organism (**Figure 8**): (1) the *Oxyphotobacteria*, (2) the *Melainabacteri*a and (3) the *Sericytochromatia* (Shih et al., 2017; Soo et al., 2017). Then, the Oxyphotobacteria evolved the genes to perform oxygenic photosynthesis soon after the divergence from Melainabacteria (not photosynthetic cyanobacteria - Shih et al., 2017), which occurred around 2.5-2.6Gyr ago (arrows 2 and 3 in **Figure 8**).

One last hypothesis proposed a completely opposite view of the Earth's oxygenation which not enclose a big role played by cyanobacteria taxon (Kump, 2008; Kump and Barley, 2007). According to this theory, the GOE evolution should be linked with the increase in

[2] **Crown Group**: contains all extant members of a clade, their most recent common ancestor, and all extant and extinct descendants of that ancestor (Ho and Phillips, 2009).

the Paleoproterozoic subaerial volcanism that was, in turn, a direct consequence of the numerous tectonic episodes during the Proterozoic (Kump, 2008; Kump and Barley, 2007). Following this idea, it was also speculated that Cyanobacteria evolved the oxygenic photosynthesis during the Proterozoic period as a response to the environmental new conditions (Kump, 2008). It remains unclear whether the rise of oxygen was directly related to the evolution of oxygenic photosynthesis (Kopp et al., 2005; Ward, Kirschvink, & Fischer, 2015), or alternatively driven by a change in Earth's geophysical processes (Holland, 2009; Kump & Barley, 2007).

In any case, the first stable presence of oxygen in the atmosphere seems to happen between 2.4 and 2.1Gyr ago (Lyons et al., 2014). Most of the data supporting the GOE development during the Paleoproterozoic period are based on sedimentary records, in particular on the presence/absence of (1) the iron deposits and (2) of the sulfur deposits. The presence of *Banded Iron Formations* (BIFs) and pyrite in oceanic sediments (Farquhar et al., 2010b; Fischer and Knoll, 2009; Hamilton et al., 2016) along with the lack of red beds in continental sediments confirmed the lower level of oxygen in the Archean atmosphere (Canfield, 2014; Fischer et al., 2016a; Pavlov and Kasting, 2002). The presence of BIFs on the bottom of the oceans comes along with the idea that the deep ocean where anoxic, condition that could have allowed the iron deposition coupled with silica deposits (Fischer and Knoll, 2009).

More consistent data about the oxygenation event come from the isotope analyses. The general idea proposed from Farquhar (Farquhar and Wing, 2003; Farquhar et al., 2000, 2010b) and Pavlov (Pavlov and Kasting, 2002) links the presence of sulfur *mass-independent fractionation* [3](MIF – explained in the Sulfur isotope Fractionation section) in oceanic sedimentary rocks older than 2.3Gyr (i.e. pyrite) with a general value of atmospheric O_2 lower than 10^{-5} PAL (Farquhar and Wing, 2003; Farquhar et al., 2000, 2010; Pavlov and Kasting, 2002). Indeed, MIF formation can occur only when the atmosphere, and thus the aquatic environment, is reducing and sulfur can be removed from the water column under different oxidation states (Farquhar and Wing, 2003; Pavlov and Kasting, 2002). The MIF formation is substituted by the *mass-dependent fractionation* [4](MDF –

[3] **mass – independent fractionation (MIF)**, which implies that the fractionation value is not proportional to the mass differences between the considered isotopes (Smith and Morowitz, 2016);

[4] **mass – dependent fractionation (MDF)**, in which the isotopes mass influences the bonds between atoms of the molecules (Smith and Morowitz, 2016)

explained in the Sulfur isotope Fractionation section) between the last pyrites and the first red beds in the Huronian Supergroup (Canfield, 2014) which implies a huge change in the oxidant conditions of the environment. The MDF formations are linked with the microbial reduction of sulfate and provide a link between the sulfur fractionation and the evolution of the modern biogeochemical cycles (Papineau et al., 2007a).

After the GOE, the second stage of the Precambrian ocean took place and is identified as the ***Proterozoic ocean***, which is interpreted as a transitional stage. Indeed, despite the younger *Banded Iron Formations* (BIFs) deposits are dated around 1.8Gyr ago (which was interpreted as the end of the anoxic ocean), some more recent hypotheses underline the idea that the surface of the ocean was oxygenic while the deep water was still anoxic and sulfidic until the **Neoproterozoic** period in association with the **second great oxygenation event** or **NOE** (Neoproterozoic Oxygenation event - Anbar and Knoll, 2002; Canfield, 1998; Saito et al., 2003).

Dissolved sulfate increased until 1 – 5mM during the Proterozoic reaching 15mM during the **Ediacaran** (the last period of Neoproterozoic Era, between 0.65 and 0.54Gyr ago - Giordano and Prioretti, 2016). Lastly, during the **Palaeozoic** and **Mesozoic** Era seems to be sulfate has reached the present ocean level around 27mM: today the greater detected level is 28mM and represents the historical maximum (Giordano and Prioretti, 2016). As far as we know today, the Proterozoic ocean should be partially oxygenated at the surface with some deep areas still anoxic and still sulfidic (Anbar and Knoll, 2002). These conditions implied a low availability of trace metal elements which could influence somehow the biological cycle: it was speculated that this particular environment has influenced the bio-evolution of Proterozoic eukaryotes (Anbar and Knoll, 2002).

Oxygen is a strong oxidizing agent (Chen et al., 2017), because of its positive **reduction potential (E0')** that configures it as a sink for electrons. In an anoxic environment, as it could be the Archean environment before the first GOE, the anoxic bacteria used other types of oxidizing reactants rather than oxygen to perform the redox reactions, such as iron, sulfur or nitrogen (Griffin et al., 2007). Recent studies proposed an important role of anoxygenic photoautotrophs in the establishment of the intermediate redox state of the planet (Johnston et al., 2009). anoxygenic metabolism used sulfide instead of water as an electron donor, and it is observed also in some versatile cyanobacteria species (Johnston et al., 2009). In an anoxic environment, sulfide is more available for photoautotrophs than oxygen.

Once the molecular oxygen started to spread in the atmosphere and oceans, biochemical reactions could have been faster and more efficient, but at some point, oxygen was so abundant that it started to compete with other electrons acceptors acting as reactive specie and oxidizing the biological structure (Fischer et al., 2016b). Cyanobacteria and other microorganisms that survived the oxygenation of the Earth were able to evolve different mechanisms to fight the formation of Reacting Oxygen Species (ROS) which were promoted by the increase of available oxygen molecules (Fischer et al., 2016b).

1.3 THE SULFUR ELEMENT

1.3.1 Sulfur in the ocean

Sulfur is one of the fundamental elements for life together with carbon, nitrogen, and phosphate. S-containing compounds are involved in several biological pathways (Giordano and Prioretti, 2016; Prioretti et al., 2014; Ratti et al., 2011).

Sulfur concentration as sulfate can be set around 28mM in the ocean today (Giordano and Prioretti, 2016), which identifies it as the fourth most abundant solute in the water column (Fike et al., 2015) and the most important water-soluble electron acceptor for respiration (Hayes and Waldbauer, 2006; Sim et al., 2019). Normally, in aerobic aquatic environments, sulfur is acquired as sulfate, SO_4^{2-} with an oxidation number of +6 (Giordano and Prioretti, 2016; Sim et al., 2019), then it can be reduced to H_2S in a respiratory process (Drake and Akagi, 1978; Liu and Peck, 1981; Pfennig et al., 1982; Sim et al., 2019; Thauer et al., 1977) or assimilated in the biological molecules as cysteine (Giordano and Prioretti, 2016). In both options, the activation of SO_4^{2-} with ATP consumption is needed to start the process (Giordano and Prioretti, 2016; Sim et al., 2019). But, while SO_4^{2-} respiration produces energy, sulfur assimilation as cysteine does not. Instead, SO_4^{2-} reduction to cysteine molecules requires a high amount of it (Giordano and Prioretti, 2016). Sulfur metabolisms influenced greatly other element cycles (Canfield, 2004; Fike et al., 2015; Habicht et al., 1998; Sim et al., 2019). For example, respiratory microbial metabolism through sulfate reduction contributes to more than 50% of the carbon mineralization in the coastal environments (Habicht et al., 1998). Furthermore, the dissolved sulfide HS^-, produced by the microbial sulfate reduction (MSR) can react with the iron present in the water column forming pyrite Fe_2S which represents a huge redox sink for both sulfur and

iron (Sim et al., 2019). Moreover, H_2S can be oxidized to $S_2O_3^{2-}$, S^0 and SO_4^{2-} (Habicht et al., 1998) influencing greatly the oxygen balance with the atmosphere (Canfield, 2004; Fike et al., 2015; Habicht et al., 1998; Sim et al., 2019). These metabolisms were probably linked also in the proterozoic eon (**Figure 9**) and influenced the biogeochemical cycle of carbon, oxygen, nitrogen and phosphorous (Johnston et al., 2009; Knoll et al., 2016).

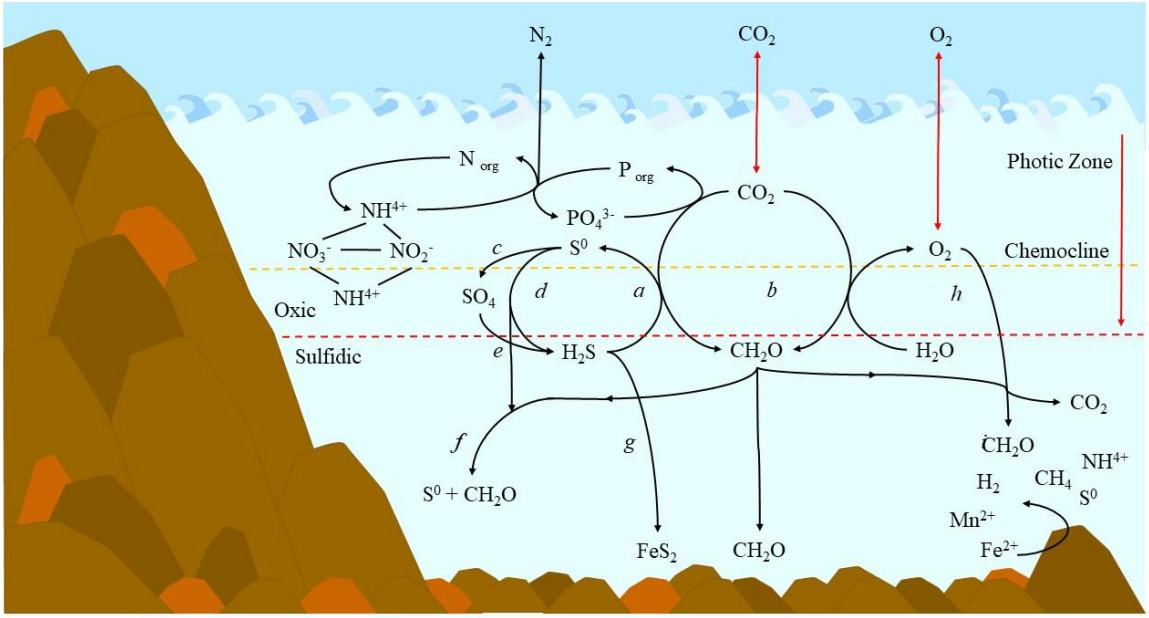

Figure 9 *Sulfur cycle in proterozoic ocean: a)anoxygenic photosynthesis, b)oxygenic photosynthesis, c)sulfur oxidation disproportion, d)S^0 respiration, e) sulfate reduction, f) S^0 export, g)pyrite formation, h)aerobic respiration (Johnston et al., 2009; Knoll et al., 2016).*

Under the present oxidizing atmosphere, the sulfate concentration is roughly stable in the ocean, with some variation related only to evaporation and freshwater supply from continental waters (Fike et al., 2015). Indeed, considering the actual fluxes, the oceanic sulfate has one of the highest response time, sets around 1.3Myr (Fike et al., 2015). Considering the biogeochemical cycle of sulfur through geological eras, it's possible to analyse the variation in the **stable isotope composition (δ)** of the sulfur species, in particular the $\delta^{34}S$ of sulfate (for a complete explanation of the geological techniques and theory which support these data, refer to the Sulfur Isotopic Fractionation section). This kind of analyses focus on different sedimentary species which represent 3 different proxies: the evaporites rocks, the barite rocks, and the carbonate deposits (CAS), that includes also the biological compound in the analyses (Canfield, 2004; Canfield et al., 2000; Farquhar et al., 2010b; Fike et al., 2015). The oceanic reservoir of sulfate has a stable isotope content (δ) for ^{34}S

around +21‰ (Fike et al., 2015). Considering the total flux of the inorganic input of sulfate (i.e. the estuarine inputs, the hydrothermal and volcanic sources, and the dust, to mention the most important), there are two different sinks for the inorganic sulfate: (1) the evaporites ($\delta^{34}S_{evaporites} \approx +21‰$) and the carbonate ($\delta^{34}S_{CAS} \approx +21‰$) burial, and (2) the pyrites produced after the microbial sulfate reduction ($\delta^{34}S_{pyrites} \approx \delta^{34}S_{SO4} + \varepsilon‰ \approx -21‰$ - Fike et al., 2015).

Back in the eons, however, the fluxes provide the sulfate supply in the ocean were not stable and, then, concentrations have varied greatly. The best way of trying to understand the evolution of the sulfate reservoir consists of the chemical analyses of fluid inclusions during the evaporation phenomenon (Fike et al., 2015). From this dataset, it can be obtained that the $\delta^{34}S_{SO4}$ of the archean ocean was almost 0‰ based on the relatively low variability of $\delta^{34}S_{pyrite}$ which it should be the most important sink for sulfate in the past. The increase in the variation of $\delta^{34}S_{pyrite}$ during eons suggests the increase in the correspondent $\delta^{34}S_{SO4}$ that reach ~20‰ during the Mesoproterozoic and then ~40‰ at the beginning of the Phanerozoic until stabilize around ~21‰ as in the present era (Fike et al., 2015). From this data, it can be speculated that during the Archean period the isotopic fractionation between sulfate and sulfite should be minimal (although there are only a few samples containing the pair sulfate – sulfide necessary to constrain fractionation). The low-level $\delta^{34}S$ fractionation is interpreted as the presence of a very low concentration of dissolved sulfate in the water column (less than 200μM) to inhibit the fractionation during the microbial sulfate reduction (Habicht et al., 2002). The increase in the fractionation between sulfate and pyrite started during the Neoproterozoic period, probably thanks to an increase in the oxidative sulfur cycle (Fike et al., 2015). The increase in sulfur availability during geological time, allowed the evolution of those microalgae containing *a* and *c* chlorophyll (Haptophytes and Diatoms) since they have a higher sulfur cell quotas (Ratti et al., 2011). The sulfur facilitation hypothesis (Giordano and Prioretti, 2016; Prioretti and Giordano, 2016; Ratti et al., 2011) proposes an interpretation of this specific evolution (**Figure 10**). This theory underlines the importance of sulfur metabolic pathway in cyanobacteria and unicellular algae, especially considering the redox power high cost of sulfate assimilation pathway (Giordano and Prioretti, 2016). This hypothesis also links sulfur metabolism with the oxidizing level of the environment as redox power available depending on how much electrons are sequestered by oxygen.

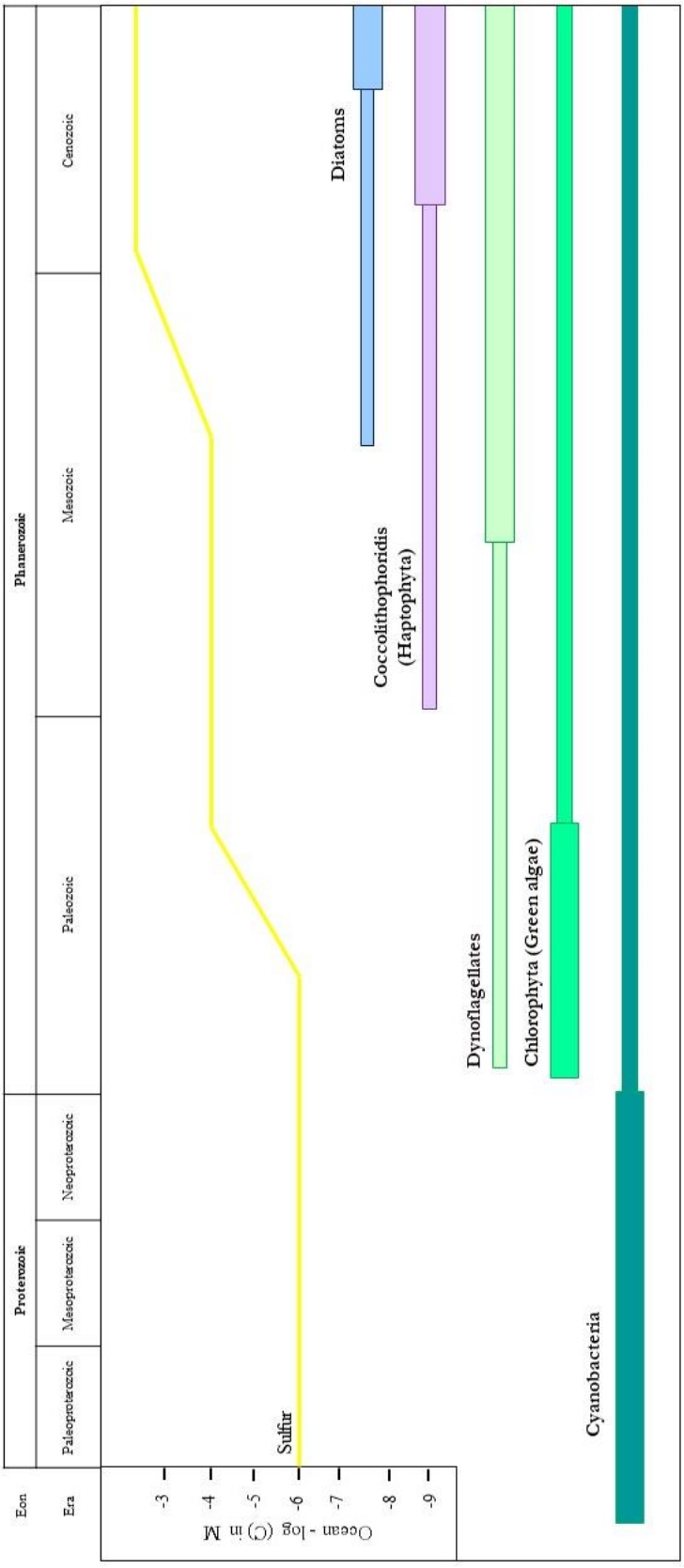

Figure 10 *Phytoplankton evolution and distribution with sulfur concentration during eons, the figure explain properly the logic behind the Sulfur facilitation hypothesis (Giordano and Prioretti, 2016; Ratti et al., 2011).*

1.3.2 Sulfur Isotope Fractionation

In natural environments, sulfur can be found as four different isotopes: ^{32}S, ^{33}S, ^{34}S, and ^{36}S. Of these, ^{32}S is the most abundant (95%; Smith and Morowitz, 2016; Thode et al., 1953). As a general rule, sulfate (SO_4^{2-}) contains heavier S isotopes than sulfides (H_2S), while organic sulfur tends to have very low levels of heavy sulfur isotopes (Thode et al., 1953) since the lighter isotopes react faster than the heavier once in any biochemical reaction. (Kendall and Caldwell, 1998).

The stable isotopes analysis of sedimentary sulfur compounds is an important part in the paleoenvironmental reconstruction of the ancient marine environment since the isotopes of sedimentary sulfides can help to understand the metabolisms and the chemical environment presented on Earth in the Precambrian period (Gill et al., 2008; Robbins et al., 2016).

Isotope fractionation (**ε_{net} ‰**) is read as the difference in **stable isotope content** (**$\delta^{34}S$** – based on the ration of ^{34}S and ^{32}S - Fike et al., 2015) between the reacts and the products of any chemical reaction relatively to one specific element and it can be measured for any kind of biochemical process (Fike et al., 2015; Kendall and Caldwell, 1998; Leavitt et al., 2015). This value can be also used to evaluate both the complete set of enzymes involved in a specific pathway and the geological cycles of a specific element (Fike et al., 2015; Habicht et al., 1998). For example, the increasing or decreasing of a minor isotope (which is one of the less abundant in nature) relative to a major one (which is the most abundant one) in a sulfur phase, is defined as **stable isotope content δ** and it is calculated as shown in the following equation (Rees, 1973):

$$\delta^{34}S_{‰} = \left(\frac{R_{sample}}{R_{standard}} - 1\right) \times 1000$$

Where R is the isotope ratio ($^{34}S/^{32}S$) of the sample and the standard materials. In this study, the international standards calibrated in a Vienna Canyon Diablo Troilite (VCDT) scaling. The relative difference between two sulfur compounds (i.e. substrate A and product B) is represented as **isotope fractionation factor α** (Leavitt et al., 2015):

$$Isotope\ fractionation\ factor\ (\alpha_{B-A}) = \frac{R_B}{R_A}$$

However, the most common and useful formula used in sulfur analyses (especially when a logarithmic scale definition is used) is:

$$\delta^{34}S_{‰} = ln\left(\frac{^{34}R_{\ sample}}{^{34}R_{\ standard}}\right) \times 1000$$

The enrichment factor is defined as:

$$^{34}\varepsilon‰ = (\alpha_{B-A} - 1) \times 1000$$

There are two principal type of isotopic fractionation: the (1) **mass – independent fractionation (MIF)**, which implies that the fractionation value is not proportional to the mass differences between the considered isotopes (Smith and Morowitz, 2016); and the (2) **mass – dependent fractionation (MDF)**, in which the isotopes mass influences the bonds between atoms of the molecules (Smith and Morowitz, 2016). The second one is the fractionation typical of both biotic and abiotic processes.

Moreover, isotope fractionation can be defined considering the chemical composition of the reacts and reagents. The **equilibrium isotope fractionation (ε_{eq} ‰)** described a chemical equilibrium in which the isotope compositions of reacts and reagent is not identical despite the isotopic rate between them is constant (Kendall and Caldwell, 1998). The **kinetic isotope fractionation (ε_{kin} ‰)** defines instead a condition during which the stable isotopes are divided depending on their mass during the unidirectional process (Kendall and Caldwell, 1998).

The **equilibrium isotope fractionation (ε_{eq} ‰)** can be useful to analyze the geological data (Kendall and Caldwell, 1998), while the **kinetic isotope fractionation (ε_{kin} ‰)** is the one suitable for the biological reactions: indeed, normally the biological pathways can be considered unidirectional (Kendall and Caldwell, 1998), as described in the *Rees' Model* (Rees, 1973).

This isotopic fractionation model was developed in order to describe the reduction process in reducing sulfate bacteria *Desulfovibrio desulfuricans*, able to convert inorganic sulfate in hydrogen sulfite (Rees, 1973). From this basal model, built simplifying as much as possible the biological reaction inside the cell, several other models have been developed to consider a more realistic view. Focusing on the sulfur element and metabolism, the whole set of biochemical sulfur reactions inside any microorganism organism should be considered linking (1) the fractionation, (2) the reverse flux of reactions from sulfide to sulfite, which seems to be influenced from the sulfide concentration in the cell (Brunner and Bernasconi, 2005; Wing and Halevy, 2014), (3) the disproportionation of thiosulfate and sulfide (Habicht et al., 1998) and (4) the metabolite concentrations (Wing and Halevy, 2014). Moreover, it should be considered the influence of other elements isotope fractionation in bacterial sulfate reduction, such as the oxygen fractionation, on the composition of the residual sulfate considering during the sulfate isotopic fractionation (Brunner et al., 2005).

As described in the followed paragraph, the sulfur acquisition performed by aquatic photosynthetic microorganisms consists of sulfate (SO_4^{2-}) acquisition from the environment, its conversion into adenosine-5'-phosphate (APS), then in sulfite (SO_3^{2-}) and finally assimilated as sulfide (S^{2-}) in the cysteine.

Simplifying as much as possible, we can consider that the reactions could be:

$$^{32}SO_4^{2-} \rightarrow APS \rightarrow {}^{32}SO_3^{2-} \rightarrow {}^{32}S^{2-}$$

or

$$^{34}SO_4^{2-} \rightarrow APS \rightarrow {}^{34}SO_3^{2-} \rightarrow {}^{32}S^{2-}$$

Applying to these reactions the *Rees' model* of sulfur isotopic fractionation and knowing that $^{32}SO_4^{2-}$ reacts faster than $^{34}SO_4^{2-}$, it can be concluded that the S^{2-} produced every instant is enriched in ^{32}S, or depleted in ^{34}S (Thode et al., 1953) means that remained sulfate will be rich in ^{34}S (Habicht et al., 1998; Thode et al., 1953).

It is possible to quantify the isotopic fractionation to a single enzyme (Sim et al., 2017, 2019)

1.3.3 Sulfur Metabolism in Photosynthetic Cyanobacteria

In the water environment, sulfur is acquired by the photosynthetic organisms as SO_4^{2-} and is then assimilates as S^{2-} in cysteine: since the first compound has the most elevated oxidation number possible (+6) and the final one has the most lower (+2), a great reducing power, -454mV, is required inside the cell to allow this process (Giordano and Prioretti, 2016; Prioretti et al., 2014; Takahashi et al., 2011).

Sulfur uptake from the environment is performed by specific transporters which differ among different photosynthetic microorganisms group (Takahashi et al., 2011). In eukaryotic algae, three kinds of transporters have been identified so far: (1) the **H^+/SO_4^{2-} transporters**, which are coded by the SULTR gene superfamily; (2) the transporters enclosed in the **SLT family**; and, (3) the **ABC transporters**.

The **H^+/SO_4^{2-} transporters** seem to be present in all algae and plants analysed so far, their high affinity for sulfate is triggered by sulfur limiting conditions (Giordano and Prioretti, 2016) and their encoding genes were found also in the *Synechocystis* sp. PCC6803 genome (Melis and Chen, 2005). Their location in the cell is on the plasmalemma membrane (Giordano and Prioretti, 2016). The transporters enclosed in the **SLT family**, once again in algae and plants, catalyse a Na^+/SO_4^{2-} antiport which is similar to those transporters found in animals (Giordano and Prioretti, 2016). These kinds of transporters are located on the

plasmalemma membrane (Giordano and Prioretti, 2016). Lastly, the **ABC transporters** are enclosed in the ATP binding cassette transporters family. They are located on the external membrane of cyanobacteria or on the chloroplast inner membrane in algae and plants (Giordano and Prioretti, 2016). They consist of a heterodimeric and transmembrane portion in which the transmembrane channel is constituted by the proteins SULP and SULP2 (Giordano and Prioretti, 2016; Melis and Chen, 2005): both of these proteins bind a sulfate-binding protein on the external site and one ATP-binding protein on the cytosolic side (Giordano and Prioretti, 2016; Takahashi et al., 2012).

Once the sulfate enters in the cell, several reactions are performed to obtain the incorporation of sulfur in biological compound as cysteine (**Figure 11**, based on Giordano and Prioretti, 2016 and references in it) which can also be further used as a substrate to produce other S-containing molecules, as glutathione or methionine (Giordano and Prioretti, 2016; Takahashi et al., 2012).

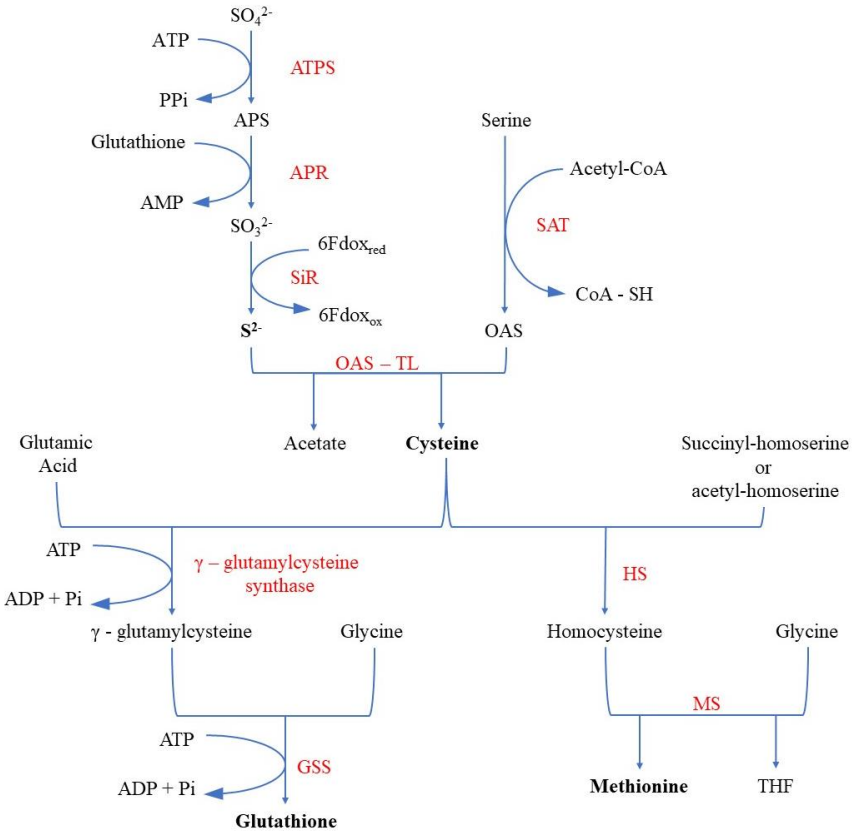

Figure 11 *Sulfur metabolism in cyanobacteria: ATPS = ATP sulfurylase: APS = Adenosine 5'-phosphosulfate; APR = APS reductase; Sir = Sulfite reductase; 6Fdox = Ferredoxin; SAT = Serine acetyl transferase; OAS = O-acetylserine; OAS -TL = OAS(thiol) lyase; HS = homocysteine synthase; MS = methionine synthase; GSS = Glutathione synthase and THR = tetrahydrofolate.*

The first reaction (**Equation a**) inside the cell consists of the activation of sulfate. The reaction is catalysed by the **ATP sulfurylase** (ATPS - EC 2.7.7.4.; Giordano and Prioretti, 2016). **Table 1** clarifies the energy level of each reaction helping to clarify why the activation of sulfate through ATP sulfurylase enzyme is so important.

$$(a)\ SO_4^{2-} + ATP \rightarrow APS + PP_i$$

Oxidant	Reductant	ΔE_0'
Sulfate SO_4^{2-}	Sulfite SO_3^{2-}	-454mV
Sulfate SO_4^{2-}	Adenosin 5-phosphosulfate	+47.4mV
Adenosin 5-phosphosulfate	Sulfite SO_3^{2-}	-0.060mV
Sulfite SO_3^{2-}	Sulfide S^{2-}	-114mV
Sulfate SO_4^{2-}	Sulfide S^{2-}	-220mV

Table 1 *Standard reduction potential E_0' (25°C, pH7, 1atm), values are expressed in mV and based on Giordano and collaborators review (Giordano and Prioretti, 2016) and http://equilibrator.weizmann.ac.il/.*

The **ATPS** enzyme is enclosed in the superfamily of α/β phosphodiesterase (Prioretti et al., 2014). This enzyme functions as sulfate activator reducing the redox potential (-454mV) of the sulfate and converting it in adenosine- 5'-phosphosulphate (APS - Giordano and Prioretti, 2016). The catalyzes by ATP has been studied in *Penicillium chrysogenum* (Farley et al., 1976), showing the ATPS requires Mg ions for its activity (Farley et al., 1976): sulfate molecule can bind the ATPS active site only after the Mg – ATP binds the protein itself (Giordano and Prioretti, 2016). Sequences similarity searches among cyanobacteria and eukaryotic algae genomes and transcriptomes available emphasize specific features of

ATPs enzyme in different groups of photosynthetic organisms (Giordano and Prioretti, 2016; Prioretti et al., 2014, 2016):

- ✓ **ATPS – A**;

  this isoform is typical of freshwater cyanobacteria, as *Synechocystis*, and of those marine cyanobacteria which are not enclosed in the *Synechococcus* or *Prochlorococcus* genera (Giordano and Prioretti, 2016; Prioretti et al., 2014, 2016). Thus, according to its distribution among species, the ATPS – A is typical of the **β – cyanobacteria** (Prioretti et al., 2016). Some studies point out that this enzyme normally contains, at least, 4 conserved cysteine residues (Prioretti et al., 2014, 2016). The quaternary structure of the protein doesn't allow the presence of disulfide bridges between the cysteine residues. For this reason, this ATPS is an enzyme not-redox regulated enzyme (Prioretti et al., 2016).

- ✓ **ATPS – B**;

  this isoform is instead the cytosolic ATPS of marine *Synechococcus* and *Prochlorococcus* genera, being thus typical of **α – cyanobacteria** (Giordano and Prioretti, 2016; Prioretti et al., 2016). It is also common in the plastids of Chlorophyta, Cryptophyta, Haptophyta, and Heterokontophyta. (Giordano and Prioretti, 2016; Prioretti et al., 2016). ATPS – B is characterized by 7 to 10 cysteine residues, 5 of which being conserved among the species holding these isoforms (Giordano and Prioretti, 2016). The model of the 3D structure of the enzyme showed that pairs of such cysteines are in enough proximity one to each other to constitute the disulphate bridges that allow the redox control of the enzyme (Prioretti et al., 2016).

- ✓ **ATPS – C;**

  this isoform is characteristic of the red algae and contains only 2 cysteine residues, of which only one is conserved (Prioretti et al., 2014).

- ✓ **ATPS – D;**

  this group of enzymes is found in those algae acquired a secondary plastid from the red lineage (Prioretti et al., 2014): in this case, the ATPSs have a kinase function beyond that synthase one (Giordano and Prioretti, 2016). In these isoforms, 8 to 10 cysteine residues are present (2 are conserved) but their positions are different compared to other groups (Giordano and Prioretti, 2016).

- ✓ **ATPS – E;**

  the last group of ATPSs is the one presents in the Dinoflagellate taxon, but the information on them regard only 2 species (Giordano and Prioretti, 2016; Prioretti et al., 2014).

Thus, the marine and freshwater cyanobacteria are also characterized by different ATPS isoforms, ATPS – A and ATPS – B, respectively. They differ for their sensitivity to redox regulation, a feature typical only of ATPS – B isoform, suggesting that the ecology of cyanobacteria may be related to differences in ATPS activity and S metabolism (Giordano and Prioretti, 2016).

It was also speculated that the evolution of ATPS isoforms could be influenced by the environmental pressures in cyanobacteria taxon (Prioretti et al., 2016), especially since the ATPS isoforms distribution follows the carboxysomes one in cyanobacteria, which has been stimulated by the variation in the CO_2/O_2 rate. Furthermore considering elements concentrations rather than gases rate, it must be pointed out that ATPS genes and enzyme activity can be down or up-regulated as an answer to the sulfur availability (Prioretti et al., 2014): for example in *Synechococcus* sp. WH7803 it was observed that the ATPS activity increased when sulfur was limiting (Prioretti et al., 2014). Finally, its activity can change also answering the variations in other elements concentration, to the elements' stoichiometry or to the temperature variations (Prioretti et al., 2014). All this information justifies this project set up and allow speculation about the evolutive creation of ATPS redox control itself.

After the ATPS catalyses the adenosin-5'-phosphosulfate (APS) formation, this compound is reduced to sulfite through the action of an APS reductase (APR) which uses glutathione as electron donor realising AMP (**Equation b**).

$$(b)\ APS + glutathione \rightarrow SO_3^{2-} + AMP$$

Afterwards, the ferredoxin-dependent sulfite reductase (SiR) reduces the sulfite to sulfide (**Equation c**) which reacts with the O-acetylserine (OAS) through the action of the OAS (thiol) lyase realising acetate and cysteine (**Equation d -** Giordano and Prioretti, 2016; Takahashi et al., 2011, 2012).

$$(c)\ SO_3^{2-} + Fdx_{red} \rightarrow S^{2-} + Fdx_{ox}$$

$$(d)\ S^{2-} + \text{O} - \text{acetylserine} \rightarrow \text{Acetate} + \text{Cysteine}$$

In addition, to enter the above described reductive pathway, APS and cysteine are substrates to produce several other S-containing molecules.

(1) An alternative step in this pathway can be performed after the APS formation and consists of the sulfation (**Equation e**) which is a non – reductive step that adds SO_4^{2-} to proteins. The APS kinase (APK) used the APS to produce the 3-phosphoadenosin5-phosphosulfate (PAPS) which is the first step for the sulfolipids formation (Giordano and Prioretti, 2016).

$$(e)\ APS + ATP \rightarrow PAPS$$

In cyanobacteria, the sulfolipids, particularly the **sulfoquinovosyldiacylglycerol (SQDG)**, can constitute 10-20% of the total lipids of the membrane. In *Synechococcus* and *Prochlorococcus* genera, it can reach up at 66%. Its synthesis in these species is stimulated by nitrogen and phosphate starvation, a condition that planktonic species might experience in their natural environment, thus explaining the high level in those oceanic genera (Mooy et al., 2006).

(2) Once the cysteine is produced, it can react with the glutamic acid by the action of γ-glutamylcysteine synthase enzyme starting the metabolic pathway leading to glutathione production (**Equation f_1** and **f_2**; **Figure 11**, based on Giordano and Prioretti, 2016) which represents the other major non-protein thiol group in the photosynthetic cells. It also plays a key role in Reactive Oxygen Species (ROS) detoxification.

$$(f_1)\ Cysteine + Glutammic\ Acid + ATP \rightarrow \gamma Glutamincysteine + ADP + P_i$$

$$(f_2)\ \gamma Glutamincysteine + Glycine + ATP \rightarrow Gluthatione + ADP + P_i$$

Glutathione is also used from the cell itself as an indicator of the sulfur concentration in it (Giordano and Prioretti, 2016; Takahashi et al., 2012). Finally, in the eukaryotic algal cell, it is also used to produce the phytochelatin. Such molecules contribute to heavy metal

scavenging in the cell, allowing their transfer in the vacuoles (Giordano and Prioretti, 2016; Takahashi et al., 2011).

(3) Cysteine is also the substrate for the formation of methionine although this reaction is catalyzed by different enzymes and in different cell compartments in different photosynthetic groups. In cyanobacteria, the process for the methionine production involved the homocysteine synthase (HS) for the homocysteine formation and then the METH for the final step (**Equation g_1** and **g_2** -Giordano and Prioretti, 2016).

$$(g_1)\ Cysteine + succinyl/acetyl - homoserine \rightarrow Homocysteine$$
$$(g_2)\ Homocysteine + Glycine \rightarrow Methionine + Tetrahydrofolate$$

In general, in eukaryotic photosynthetic organisms, the pathway is divided in one reaction performed in the chloroplast (and which involved the cystathionine synthase (CGS) with the formation of the homocysteine) and in one performed in the cytosol through the methionine synthase (MS – the METE in the vascular plant and the METH in the other organism) and which results in the methionine production (Giordano and Prioretti, 2016; Takahashi et al., 2011). In many photosynthetic microorganisms, methionine is the precursor of the 3-dimethylsulfoniopropionate (DMSP) which is an osmoprotectant, an antioxidant and a cryoprotectant (Giordano and Prioretti, 2016; Ratti et al., 2011) and from which the dimethyl sulfide (DMS) derives (Giordano and Prioretti, 2016; Ratti et al., 2011).

AIM OF THE PROJECT

During the Precambrian period, the availability of redox power has been changed as a consequence of the oxygenation of atmosphere and oceans consequent to the appearance of oxygenic photosynthesis. Indeed, once the oxygen concentration rises to appreciable levels, oxygen became the most important sink for electrons and thus, it started to compete with other molecules for them. Moreover, considering the evolution of cells in an anoxic environment, it could have been also toxic.

Consequently, it is possible that tight control in the distribution of redox power among the main assimilatory pathways became increasingly important in an environment progressively more oxidizing. If so, it can be consistent to think about an effect on elemental composition and on the organic pool in the cell driven by the shift in the environmental oxidizing level.

In this work, the sulfur metabolism of cyanobacteria was analysed since sulfur is one of the essential macronutrients for photosynthetic organisms and its assimilation consumes a high amount of reducing power. I investigated how, through the history of Earth, the regulation in sulfate assimilation metabolism in cyanobacteria may have changed. Specifically, I focused on the enzyme catalyzing the first step of sulfate reduction in these microorganisms: the ATP sulfurylase (ATPS). This enzyme is not redox-regulated in coastal and freshwater cyanobacteria, supposedly, the most primitive cyanobacteria, whereas it is subjected to redox regulation in oceanic cyanobacteria, interpreted as the most recent evolution of this taxon.

The redox regulation of sulfate assimilation is relevant to the distribution of the reducing power inside the cell and is likely to be important at (a) high sulfate availability and under (b) energy/redox power limitation. Indeed, considering the high sulfate availability (at the ecosystem level) of the first case, it can deviate reducing power from nitrate and carbon reduction to sulfate reduction. In the second case instead, low energy would reduce power (in this case the reducing equivalents in the cell, i.e. electrons) limiting and thus underling the importance of its partitioning.

To address this idea, cyanobacteria with not-redox and in redox-regulated ATPS were grown under two different and diametrically opposed environmental conditions: (1) the Modern ocean and (2) simulated Proterozoic ocean conditions which differed from the former one both for the chemistry of the waters and for the gas phase in equilibrium with the liquid culture (~2500% PAL CO_2 and 10% PAL O_2). One more condition was introduced in the experimental set up to obtain a middle ground between the previous two: the Transitional Condition, characterized by the present atmospheric level of gasses and the nutrient concentration present in the Proterozoic Eon. The Proterozoic conditions were selected because the Great Oxygenation Event (GOE) occurred in that period.

Whole-cell physiology, ATPS activity, sulfur assimilation, cell stoichiometry, and carbon allocation were used to understand how the different growth conditions, i.e. the redox state and resource availability (especially S, O_2 and CO_2), affected S assimilation and redox power utilization in cyanobacteria.

“Considerate la vostra semenza:

fatti non foste a viver come bruti,

ma per seguire virtute e canoscenza.”

La Divina Commedia
Inferno
Canto Ventiseiesimo – 118,120

“Bethink you of the seed
whence ye have sprung; for ye were not created
to lead the life of stupid animals,
but manliness and knowledge to pursue.”
La Divina Commedia
Hell
Chapter Twenty-sixth – 118,120

MATERIAL AND METHODS

2.1 EXPERIMENTAL ORGANISMS

Cyanobacteria classification has undergone several reorganizations after the application of modern genomic techniques showing no one of the previous subsection was monophyletic and that were several transitions that were not considered previously (Schirrmeister et al., 2013). Starting with the idea that those Cyanobacteria enclosed in the ancestral marine phytoplankton have played a fundamental role in the oxygenation of the Earth but didn't survive to the GOE (Sánchez-Baracaldo, 2015), we focused on those unicellular species that originated in ancient period and that, on the other hand, are still common today in the marine or freshwater environment. Furthermore, species with different ATPS isoforms and regulations were considered to obtain a useful comparing between their hypothetically different reactions in our experimental environment.

2.1.1 Synechocystis sp. PCC6803

Synechocystis sp. PCC6803 (**Figure 12** – 1) was isolated in 1968 from a lake in California and is enclosed in the β cyanobacteria, it was selected because it is one of the oldest freshwater species originated during the Mesoproterozoic period (Sánchez-Baracaldo, 2015). Originating before the Neoproterozoic Eons which starts around 1 Gyr ago, it can be considered an "ancient" species and we can assume that ancestral characters are more likely to be present in this organism. As recent studies have shown (Prioretti et al., 2014, 2016), this specie possess an ATP sulfurylase enclosed in the group A, typical of freshwater cyanobacteria and seawater cyanobacteria strains not enclosed in the *Synechococcus* and *Prochlorococcus* genera. Particularly, it presents 4 cysteine residues along with its structure that is too far from each other to constitute a disulfide bridge (Prioretti et al., 2016)

2.1.2 Synechococcus sp. WH7803

Synechococcus sp. WH7803 strain (**Figure 12** – 2) was selected as a modern specie that originated less than 0.5Gy ago during the first period of the Phanerozoic Eon (Sánchez-Baracaldo, 2015). *Synechococcus* is a genus of unicellular phototrophic cyanobacteria widespread in both fresh and seawater, we focused only on the marine taxon enclosed in

this genus and recognized as α cyanobacteria with dimensions less than 3µm (Scanlan, 2003). Particularly, *Synechococcus* sp. WH7803 is a rod shape marine α cyanobacterium with dimensions around 2µm and a genome size of 2.37Mbp, isolated in the Sargasso Sea (Dufresne et al., 2008) and known to be able to colonize several coastal environments (Zwirglmaier et al., 2008). The structure of its phycobilisome is peculiar because it contains a high concentration of phycoerythrin which gives the characteristic red/pink color to the colony (Six et al., 2007).

Most important, this *Synechococcus* specie is enclosed in the modern ocean picoplankton, which consists, nowadays, of two major genera, *Synechococcus* and *Prochlorococcus*, which is its sister taxon. Both genera are able to compete with other micro oxygenic organisms both in the open ocean and in the coastline environment (Scanlan et al., 2009), indeed, they are considered the most important organism which contributed to the global primary production (64% according to Uitz et al., 2010), playing an important role also at the base of the marine food webs (Partensky and Garczarek, 2010; Zwirglmaier et al., 2008). Despite their similar role and close evolutionary relationship, their genetic differences allow them to coexist in the same areas (Moore et al., 2002; Partensky et al., 1999; Scanlan, 2003; Scanlan et al., 2009).

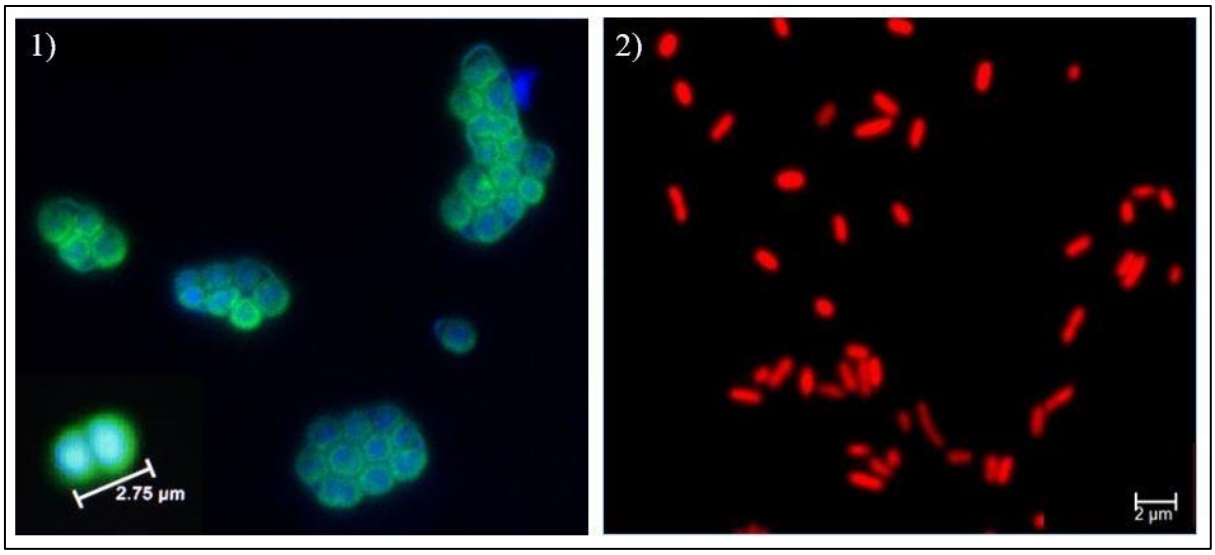

Figure 12 *1) Synechocystis sp. PCC6803 with LEICA epifluorescence microscope: the green color represents the autofluorescence of chlorophylls inside the cell (artificially recolored) while the blue fluorescence represents the nucleus marked with the DAPI color. 2) Synechococcus sp. WH7803 with LEICA epifluorescence microscope: the red color represents the autofluorescence of chlorophylls inside the cell.*

The time of evolution of these species is shown in **Table 2**, (Sánchez-Baracaldo, 2015) while **Table 3** shows the current taxonomy of the cyanobacteria used during this study.

Specie	Strain	Period
***Synechocystis* sp.**	PCC6803	Mesoproterozoic
***Synechococcus* sp.**	WH7803	Phanerozoic

Table 2 *Evolution period (Sánchez-Baracaldo, 2015).*

Specie	Family	Order	Class	Phylum	α/β
***Synechocystis* sp. PCC6803**	Merismopediaceae	Synechococcales	Cyanophyceae	Cyanobacteria	β
***Synechococcus* sp. WH7803**	Synechoccaceae	Synechococcales	Cyanophyceae	Cyanobacteria	α

Table 3 *Currently accepted taxonomy for experimental species (http://www.algaebase.org/, https://utex.org/products/utex-lb-2587, Rae et al., 2013; Shih et al., 2016).*

2.2 CULTURE SET UP

All the experiments were set up to allow a comparison between the modern environmental and the one presents in the ancient eon: indeed, thanks to several studies about Proterozoic ocean chemistry (as shown in the first chapter of this thesis), it was possible to set up an artificial environment that resembles these oceans in terms of resource availability. Moreover, we asked for the advice of professor Andrew H. Knoll, at Harvard University, that provided us information about the atmosphere and the ocean of the Precambrian Era.

At first, the selected cyanobacteria species were studied in the **Standard Condition (ST)**. The same species will also be cultured in the **Proterozoic Condition (PR)** to investigate the difference in the physiological response and ATP sulfate activity and quantification rather than cell composition in the two environments. To these two conditions, one more was added: the **Transitional Condition (TR)** characterized by the present atmospheric level of gasses and the nutrient concentration present in the Proterozoic Eon (**Table 4**).

Condition	Atmosphere	Growth Medium	Light	Temperature
Standard (ST)	Modern Atmosphere (**Table 5**)	Standard nutrient conditions (**Table 6** and **Table 7**)	50µmol photon /m^2s	20°C
Transitional (TR)	Modern Atmosphere (**Table 5**)	Proterozoic nutrient conditions (**Table 6** and **Table 7**)	50µmol photon /m^2s	20°C
Proterozoic (PR)	Proterozoic Atmosphere (**Table 5**)	Proterozoic nutrient conditions (**Table 6** and **Table 7**)	50µmol photon /m^2s	20°C

Table 4 *Summary of experimental conditions*

The incubation chamber (KCLH – 1400LEDDT – F model) has been set up to contain several semi-continuous cultures. The chamber was provided with 3 different gas sources (one tank of 20%CO_2, one tank of 100%N_2 and one air pump) to allow the set up a reconstructed Proterozoic atmosphere. Each flask had a plug that ensures the isolation from the external atmosphere. As said previously, each cyanobacteria strain involved in these experiments was tested for each experimental condition and, in all cases, three biological replicates (for each experimental replicates) were present.

Moreover, each plug will be provided with two different needles (**Figure 13**):

- **Needle n°1**, it was long enough to arrive at the liquid culture to maintain the cultures bubbled continually with the atmosphere required. Each of these needles also provided with an air filter to prevent any kind of contamination.
- **Needle n°2**, it was set up to not reach the liquid culture in the flask and provided a filter (again to prevent any contamination) to ensure the output of gasses.

Figure 13 *Set up of cultures: the blue arrow indicates the "input" of the gas and the red arrow the "output". In this picture, the pink bottles are the Synechococcus culture, while the green are the Synechocystis ones, in both cases, 3 biological replicates are present for each condition with the fourth one as a back up (in this photo you can see the Standard Conditions). Photo by Nerissa Escanlar.*

2.2.1 Atmosphere characterization

For the experiments, we need two different atmosphere conditions, organized as shown below (**Table 5**) – PAL: Present Atmospheric Level –

- **Condition A**: Modern Atmosphere – control: present atmospheric level
- **Condition B**: Proterozoic Atmosphere – proterozoic atmospheric level

Gas	%	Present atmosphere level (ppm)	Flow rate	Proterozoic atmospheric level controlled through flow rate (ppm)
CO2	20	~ 407.8ppm	20ml/min	10'000ppm (~ 2'450% PAL)
O2 (in air)	21	~ 209'460ppm	5ml/min	20'000ppm (~ 10% PAL)
N2	100	----	200ml/min	Compensation gas

Table 5 *Flow rate set up during the experiment to reflect the proterozoic environment.*

2.2.2 Light and Temperature

For our purposes, the light and the temperature in the incubation chamber were set up as follow:

- Daily cycle: 12 hours dark and 12 hours light
- Light: white LED lamps with irradiance at 50µmol photon /m^2s
- Temperature: 20°C

By mixing, the light and the nutrients become available for all the cells of the colony. Thus, the experimental design implies the mixing by bubbling gases through the colony continually. Moreover, each bottle was gently blended manually twice a day to avoid any sedimentation of the cells.

2.2.3 Growth medium

We assume that, above the atmosphere, there must be some differences also between the present and ancient ocean (as literature and previous studies confirm). Thus, the experimental plan used one saline medium for the *Synechococcus* cultures and one freshwater medium for the *Synechocystis* ones. The AMCONA medium (Artificial Multipurpose COmplement for the Nutrition of Algae, **Table 6**) is the one set up for the marine species with salinity at 30psu (Practical Salinity Unit) and pH8.1 as a standard condition. On the other hand, the BG11 medium (Stanier et al., 1971) was used for the freshwater condition with pH7.6 as condition zero (**Table 7**).

Then, several components were modified, as shown in the reference table, to reflect realistically the present seawater/freshwater condition and the Proterozoic ocean/lakes. All the solutions used during this work were made using Milli-Q water as the solvent and, before adding the vitamin stock (in AMCONA medium only), they were autoclaved to prevent any contaminations.

During the experiments, each flask was filled up with a volume of 70ml of the medium, 10ml of which were the strain inoculum and 60ml were fresh medium.

For this work, 2 different media were set up as follow:

- **Condition A**: Solution n°1, Modern Ocean – standard nutrient conditions
- **Condition B**: Solution n°2, Proterozoic Ocean – proterozoic nutrient conditions

As you can see from **Table 6** and **Table 7**, the differences are mostly about the concentration of the chemical components, one exception is the nitrogen: indeed, during the modern age, it can be found in the ocean as nitrate (NO_3) while during proterozoic it could be represented as ammonium (NH_4). This difference is probably due to the simplicity of using NH_4 in low oxygen conditions. The values expressed in the following tables are however estimated from geological datasets and want to reflect the general condition estimated in the proterozoic period. Thus, they can be debated.

AMCONA Medium Components	[C] in AMCONA Medium	[C] in Modern Ocean	[C] in Proterozoic Medium
NaCl	363 mM	363 mM	363 mM
Na_2SO_4	**25.0 mM**	**29 mM**	**3 mM** (Ratti et al., 2011)
KCl	8.04 mM	8.04 mM	8.04 mM
$NaHCO_3$	2.07 mM	2.07 mM	2. 07 mM
KBr	725 µM	725 µM	725 µM
H_3Bo_3	372 µM	372 µM	372 µM
NaF	65.7 µM	65.7 µM	65.7 µM
$MgCl_2$	41.2 mM	41.2 mM	41.2 mM
$CaCl_2$	9.14 mM	9.14 mM	9.14 mM
$SrCl_2$	82 µM	82 µM	82 µM
Nitrogen	$NaNO_3$ (549 µM)	$NaNO_3$ (13.7 µM)	**NH_4Cl_3 (100 uM)**
NaH_2PO_4	21 µM	1.5 µM	21 µM (as today)
$NaSiO_3$	105 µM	18.63 µM	105 µM (as today)
$CuSO_4$	40.0 nM	40.0 nM	40 mM
$FeCl_3$	6.56 uM	2 nM	**200 nM**
Na_2EDTA	6.56 µM		200 nM
$ZnSO_4$	254 nM	0.5 nM	**0.0 nM** (Ratti et al., 2011)
$CoCl_2$	5.69 nM	5.69 nM	5.69 nM
$MnCl_2$	2.42 µM	2.42 µM	2.42 µM
$NaMoO_4$	105 nM	105 nM	**10.5 nM** (Ratti et al., 2011)
H_2SeO_3	1.00 nM	1.00 nM	1.00 nM
$NiCl_2$	6.30 nM	6.30 nM	6.30 nM
Na_2EDTA	8.29 µM	8.29 µM	8.29 µM
Tiamine HCl	297 nM	297 nM	297 nM
Biotine	4.09 nM	4.09 nM	4.09 nM
B12	1.47 nM	1.47 nM	1.47 nM
Tris HCl	**10 mM**	**10 mM**	**40 mM**

Table 6 *Recipe for AMCONA medium (Fanesi et al., 2014) with modified concentration to mimic the Modern and Proterozoic Environments.*

BG11 Medium Components	[C] in BG11 Medium	[C] in Proterozoic Freshwater
$NaNO_3$	17.65mM	**0.0035mM (as NH_4Cl_3)**
K_2HPO_4	0.23mM	0.23mM
$MgSO_4$	0.304mM	**0.035mM**
$CaCl_2$	0.245mM	0.245mM
Citric acid	0.031mM	0.031mM
Ammonium ferric citrate green	0.6g/L stock 10ml stock/1L medium	**0.6g/L stock** **10ml stock/1L medium**
$EDTANa_2$	0.0027mM	0.0027mM
Na_2CO_3	0.0189mM	0.0189mM
Tris HCl	10mM	10mM
H_3BO_3	0.0463mM	0.0463mM
$MnCl_2$	0.0091mM	0.0091mM
$ZnSO_4$	0.00077mM	0.00077mM
Na_2MoO_4	0.0016mM	0.0016mM
$CuSO_4$	0.00032mM	0.00032mM
$CoCl_2$	0.000172mM	0.000172mM

Table 7 *Recipe for BG11 medium (Stanier et al., 1971) with modification to mimic the modern and proterozoic environments.*

2.2.3.1 Dissolved oxygen in the media

Dissolved oxygen in the medium was detected to characterize the environment in which the cyanobacteria were cultured and validate the experimental conditions.

Oxygen level was expected to be proportional to the oxygen concentration present in the gas used for the bubbling of the culture itself. The quantification was performed with Oxygen Sensor Spots (OXSP5 - https://www.pyroscience.com/) set inside a bottle reflecting the setup of each culture conditions (i.e. amount of growth medium, needles and bubbled gas): the sensor was calibrated for the minimum oxygen level (it was gassed with 100% N_2) and for the maximum level (it was gassed with an air pump) and then the detection of oxygen levels was performed for 78 minutes to be sure that the detected value was stable.

2.3 CHARACTERIZATION OF THE CELL PHYSIOLOGY

The first step of this study was based on the detection of physiological and chemical parameters corresponding to the different environmental conditions. Furthermore, several experiments about protein profiling have been added and the activation of sulfate, once it has entered in the cell, was analysed from two different points of view in selected Cyanobacteria strains: (1) with a physio-biological approach, underlining the variations in the activity, in the regulation and in the amount of the ATP sulfurylase (ATPS) under different experimental conditions, and (2) a more physic-chemistry approach, which analysed the sulfur isotope fractionation variations.

2.3.1 Determination of the growth curve and growth rate

To maintain a semi-continuous culture in its exponential phase, it's necessary to detect the **specific growth rate** (linked with the growth curve), which allows evaluating the volume of the daily dilutions performed adding a specific volume of fresh medium to replace the same volume of the old culture. The standard procedure to obtain the growth curve is to count the cell daily and from this cell quantification during the time it is possible to identify the exponential phase of the culture itself from which the specific growth rate can be obtained.

To set up the growth curve, we decided to link the values of the optical density (OD) of each culture with the corresponding cell counting under the microscope. In this way, it was possible to obtain a ratio (coded by a trendline) that allows obtaining a realistic cell number simply with the detection of the OD. The optical density was read at 750nm (Schulze et al., 2011) through an EnSpire Multilabel Reader (PerkinElmer) while the microscopic cell counting was performed using Bürker Counting Chambers or, alternatively, analyzing a 0.2µm isopore filter with a LEICA fluorescence microscope taking advantage of the natural fluorescence of chlorophylls and analyzing the captured picture with the Fiji software (https://imagej.net/Fiji).

The specific growth rate (µ) was then obtained from the exponential portion of the growth curve itself, in accordance with the Yamamoto's equation (Yamamoto and Shiah, 2010):

$$\mu = \frac{\ln(N2/N1)}{t2 - t1}$$

where N is the number of cells counted at time 1, which is the day in which the exponential growth phase started; and at time 2, which represents the end of the exponential growth phase. Assuming that, X_n doubles with respect to X_0, then the **doubling time (T)**, defined as the mass doubling time of the culture, can be calculated as (Painter and Marr, 1967):

$$T = \frac{ln(2)}{\mu}$$

which consents to calculate the volume required for the daily dilution.

2.3.2 Quantification of oxygen production during photosynthesis

Evolved oxygen quantification during photosynthesis was detected with a Respiration Vials with Integrated Optical Oxygen Sensors (OXVIAL4 - https://www.pyroscience.com/) on 4ml of concentrated culture after 30 min of dark. To be sure that the inorganic carbon couldn't be a limiting factor in this experiment, the cells were resuspended in 4ml of the inorganic carbon enriched medium before the beginning of the experiment.

Light from a white led lamp was orientated to the front of the electrode within the vial and the light intensity (quantified with a light sensor) was adjusted to increase it according to the experimental design described below:

- 30 min of dark at 20°C
- 3 min at 10/25/60/80/100/200/300/400/500/700 µE/m^2s.

Chlorophyll a content was quantified through the pigment extraction with 90% acetone and the extinction coefficient from Porra's work (referred to section 2.4.1 for the full method explanation - (Porra et al., 1989). Important parameters were obtained as shown in **Figure 14**.

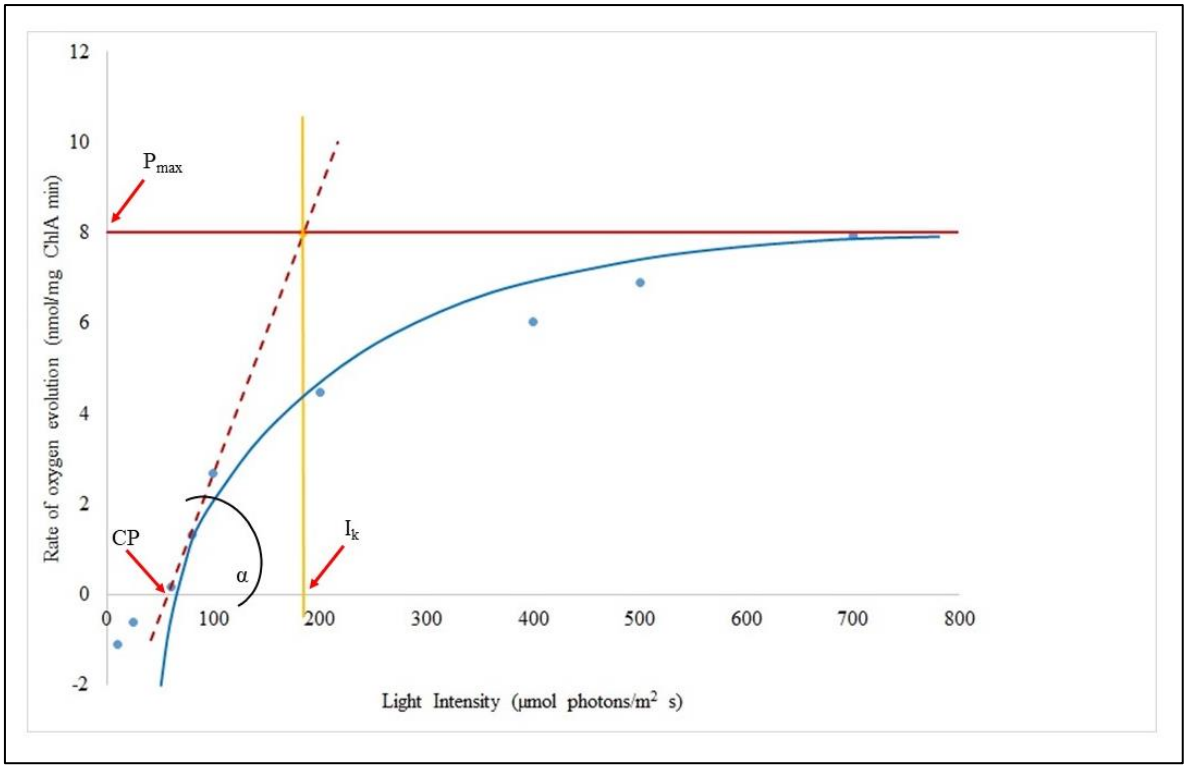

Figure 14 *Mathematical model for the oxygen evolution rate saturation light intensities (Pmax), theoretical saturation light irradiance (Ik), the apparent photosynthetic light use efficiency (α) and the amount of light irradiation when oxygen evolution should compensate the respiration (CP).*

2.3.3 Quantification of ATPS activity

2.3.3.1 Sample preparation for protein extraction and activity evaluation

At first, cells from each culture were collected by centrifugation (6'000 x 5min) and washed with a solution of ammonium formate which was iso-molar to the growth medium in which the tested cells were grown. To start the extraction procedure, 800µl of Extraction Buffer (containing 50mM of TRIS-HCl pH8.1, 10mM of MgCl2 and 1mM of EDTA; (Burnell, 1984; Giordano et al., 2000; Prioretti et al., 2016) were added to the pellet. Then, mortar and pestle in ice were used to ensure a complete enzyme extraction without its degradation. Subsequently, a solution of TritonX100 (0.1% v/v) and glycerol (10% v/v) was added to each sample to reach a total volume of 1ml *per sample*. After 30 minutes of incubation in ice to allow Triton to completely solubilize the proteins, the sample was sped down at 4°C (12'000g x 15min) and the supernatant was collected and transfer in a new tube. 50µl from each tube was transferred at -30°C overnight to allow the quantification of the total amount of protein extraction through the Lowry/Peterson procedure performed as

explain above (4.3.1): to reach the initial working volume of 500µl, 450µl of SDS Solution (containing 1% SDS, sodium dodecyl sulfate; m/v, and 0.1M NaOH) were added to each crude extract.

The ATP sulfurylase activity was tested spectrophotometrically at 25°C for 15 minutes and only the exponential phase of the assay (almost 10 minutes) was considered for the data analyses, as described in previous works (Burnell, 1984; Giordano et al., 2000): the reaction mixture used contains APS (1mM), PPi (as Na4P2O7, 1mM), MgCl2 (5mM, glucose (5mM), NADP (300µM), hexokinase and glucose-6-P dehydrogenase from baker's yeast (5units/ml, BIOCON (JAPAN) LTD.) and TRIS-HCl pH8.1 (50mM). To avoid any kind of problem with the solution in which the hexokinase and glucose-6-P dehydrogenase enzymes were suspended (i.e. 3.2M ammonium sulfate), the solution itself was centrifuge and the enzyme resuspended in 25%glycerol (stock at -30°C) before the analyses.

The reaction in which the ATPS is involved is very fast and is very difficult to determine in the forward direction, for this reason, the assay exploits the reverse reaction: during the procedure, this reaction is linked with the reactions allowed by the presence of ATP and glucose-6-phosphate and by the hexokinase and glucose-6-P dehydrogenase (equations below). The final product of that coupled reaction is the NADPH, which can be detected at 340nm spectrophotometrically.

$$(1) APS + PPi \rightarrow ATP + SO_4^{2-} \quad \underline{\text{catalyzed by } \mathbf{ATPS}}$$

$$(2)\ Glucose + ATP \rightarrow Glucose\ 6\ phosphate + ADP \ \underline{\text{catalysed by Hexokinase}}$$

$$(3) Glucose\ 6\ phosphate + NADP \rightarrow \boldsymbol{NADPH} + 6phosphogluconate$$

$$\underline{\text{catalyzed by G6P Dehydrogenase}}$$

The rate of NADPH production was recorded for 15 minutes at 340nm, using the EnSpire Multilabel Reader (PerkinElmer). The values of the absorbance were then converted to enzyme activity using the Lambert-Beer law:

$$Activity\ \left(\frac{\mu mol}{min \times ml}\right) = \frac{\frac{\Delta Abs_{340nm}}{\Delta T}}{\varepsilon \times d} \times \frac{V_{tot}}{V_{sample}}$$

$$\text{where: } Reaction\ rate = \frac{\Delta Abs_{340nm}}{\Delta T}$$

where ΔT are the 10 minutes during which the experiment was in exponential phase, ε is the coefficient of extinction of NADPH at 340nm (i.e. 6.22mM/cm), d is the optical path length in cm (which correspond to the height of the sample contained in the well during the

analyses for this multiplayer reader), Vtot is 0.200ml, which is the total volume of the sample, while Vsample is the volume of crude extract used for the assay. The specificity activity of the ATPS was then calculated dividing the activity in μmol/min × ml^{-1} for the concentration of the protein in mg/ml detected in the crude extract through the Lowry/Peterson technique. To ensure realistic quantification, a specific volume of the Extraction Buffer and Triton Solution were used to equilibrate the calibration line.

2.4 CHARACTERIZATION OF THE CELL COMPOSITION

2.4.1 Quantification of chlorophylls

The quantification of chlorophylls was used to normalize the results of oxygen production. For this kind of experiment, 5ml of each culture was collect and centrifugated at 6000g for 5 minutes. After the removal of the supernatant, the cells were broken soaking the eppendorf in liquid nitrogen three times. The pellet was then resuspended in 1ml of extraction buffer and vortexed for 5 minutes. The extraction buffer used for cyanobacteria strains was a solution of 90% Acetone. After this passage, the samples were incubated overnight at 4°C in the dark. Once the incubation was completed, the samples were energetically vortexed and centrifuged once again.

Chlorophyll concentration was measured analyzing the supernatant with the Beckman DU 640 Spectrometer (Beckman Coulter), working with Cyanobacteria, we measured only the Chlorophyll *a* (Ruan et al., 2018):

$$\boldsymbol{Chl\ a}\ (\boldsymbol{mg/ml}) = A664 \cdot 11.41$$

2.4.2 Characterization of biochemical composition

2.4.2.1 Quantification of total proteins through spectrophotometrically analyses

Protein concentration was determined spectrophotometrically using the method described by Peterson (Peterson, 1977), which is based on the Lowry's method (Lowry et al., 1951). The cells were harvested at 6000g for 5 minutes. The pellet was then resuspended in 500μl of an SDS solution containing 1% SDS (sodium dodecyl sulfate; m/v) and 0.1M NaOH: the SDS allows the complete solubilization of the membrane proteolipids while the NaOH maintain the stability of the solution (Peterson, 1977). Meanwhile, the calibration

line for the quantification of the protein was set up with different concentrations of BSA (bovine serum albumin).

After a few seconds of vortexing, 500µl of Reagent A Solution (**Table 8**) were added to each sample and to each eppendorf which was used for the calibration line. This mixture contained copper and Na-K tartrate: the first compound specifically binds to proteins in an alkaline environment while the tartrate is used to stabilize Cu ions (Lowry et al., 1951). The samples were then vortex and incubated for 10 minutes at room temperature. Finally, 250µl of Reagent B Solution (**Table 8**) were added to each eppendorf. Solution B contained the Folin & Ciocalteu's phenol reagent (Sigma-Aldrich), which oxidizes the Cu-protein complexes giving a blue color to the protein solution (Lowry et al., 1951; Peterson, 1977). The samples were then incubated for about 30 minutes at room temperature to allow complete development of the reaction and, thus, of the blue color. The absorbance of the solutions was measured at 750nm in an EnSpire Multilabel Reader (PerkinElmer). Protein concentration was calculated by interpolating the absorbances of the samples into the calibration line based on the BSA.

Reagent		**Concentration**
	<u>Solution A</u>	
CTC	• $CuSO_4$ 0.1% (m/v) • NaK tartrate 0.2% (m/v) • Na_2CO_3 10% (m/v)	25%
SDS 10%		25%
NaOH 0.8M		25%
milliQ H2O		25%
	<u>Solution B</u>	
Folin & Ciocalteu's phenol reagent (Sigma-Aldrich)		16.7%
milliQ H2O		83.3%

Table 8 *Reagent Solution compositions for protein quantification.*

2.4.2.2 Determination of carbon and nitrogen composition

Carbon, nitrogen and sulfur presence in the sample was detected through the Elemental Analyser ECS 4010 (Costech International S.p.A., Pioltello, Mi, Italy) that allows analyzing the elemental composition of the sample through a gas chromatography performed after the complete burning of the sample itself.

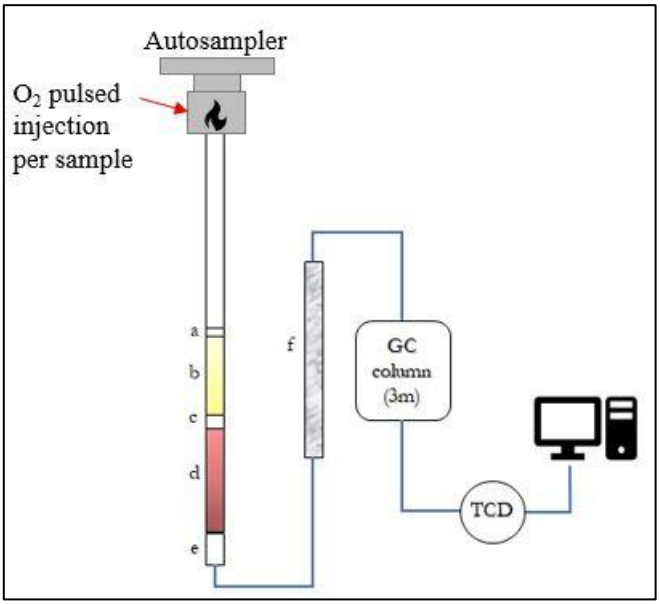

Figure 15 *Elemental analyzer setup. a) 1cm of quartz wool; b)5cm of tungstic oxide catalyst; c) 2cm of quartz wool; d) 11cm of copper wires with sulfur; e) 4cm of quartz wool; f) carbon dioxide trap and the gas chromatography (GC).*

The instrument is composed of 3 different parts (**Figure 15**): (1) the *combustion unit*, (which enclosed the *reactor*), (2) the *detector* and (3) the *handling data system*. The *combustion unit* allows the complete disruption of the sample through combustion regulated by an oxygen flux and ensured by the presence of a little amount of Vanadium (V_2O) in the tin cup used as a sample unit. Everything results from the combustion of the sample (which means gases as CO_2, H_2O, N_2, and NO_x) is driven in the *reactor*, which consists of a column fill whit quartz reduced, copper and tungsten trioxide and that reaches 980°C. The ashes from the combustion remain at the beginning of the reactor itself.

In the end, the gasses arrive in the gas chromatography (GC) column where they are separated and detected by the *thermal conductivity detector* (TCD). The detector generates a signal which is proportional to the amount of the elements in the original sample. The results from this analysis are detected in the last part of the instrument, i.e. the *handling data system*. During the analyses, the gasses which are being analyzed, are carried by an inert gas

(i.e. helium) and, furthermore, before arriving in the detector, they pass through a small column filled with magnesium perchlorate that retains water and humidity.

In order to have the best possible signal to noise ratio, the TCD set up was changed depending on the size of the analyzed samples. For those with a weight lower than 1mg, the TCD control panel was set with a high range switch (x10) and a gain control of 1, while, when the samples were more than 1mg of dry pellet, the TCD was set with a low range switch (x1) and a gain control of 3.

Another important parameter set up during the analyses was the amount of oxygen used for the combustion of the sample at the beginning of the process and define as μ, the amount of the injection of O_2 per sample.

To work, the instrument needs three different gasses: helium, which is the gas carrier for the transportation of all the gasses derived from the sample combustion, oxygen to allow the combustion of the samples at the beginning, and, lastly, air to make the autosampler working properly. The setup of the flow of those gasses was performed as follow:

- Helium: 100ml/min
- Oxygen: 30ml/min
- Air: 80ml/min

The following time cycle parameters were adopted:

- Autosampler is activated and the sample dropped into the combustion reactor;
- 12s of sample delay which is the time that each sample needs to reach the combustion reactor. The samples should arrive at least 2 seconds before the oxygen flow;
- 20s of sample stop = it determines the time of sample combustions;
- 40s of Oxy stop = time waiting for electro valves from activating of autosampler before starting
- to refill the instrument of oxygen volume needed for the next samples;
- 70s of run time = it is the time from the beginning of a cycle to the end of it.

2.4.2.2.1 Sample preparation for CNS analyses

The cells were collected from the culture and centrifuged at 6000g for 5 minutes. The pellet was then washed with a solution of ammonium formate (isotonic to the growth

medium, which means 0.5M for seawater and 0.03M for freshwater) to eliminate all the residual salts of the growth medium. The final pellet was resuspended in 50µl of 0.5mol/L of ammonium formate and dried at 80 °C for, at least, 24 hours. Ones the weight of the sample was stable, it was considered completely dry and the analyses with the CNS analyzer were performed with a range of 1-3mg. As said above, a little amount of vanadium (~0.500mg) was always added to the sample to ensure the complete combustion and a known amount of sulphanilamide (from ~0.030mg to ~0.800mg to cover the whole range of samples) was used as a standard during the construction of the calibration line. Data acquisition and data analyses were performed with the EAS software package (Costech Instruments).

2.4.2.3 Determination of trace element

Each time a molecule is hit by a beam of short-wavelength X-rays (~ 0.01-10nm), the elements that constitute it undergo ionization (**Figure 16**). This means that the atom may pass to an excited state by transferring one (or more) electron from the inner shell to the higher orbital.

In this condition, the atom becomes unstable, an electron from the higher energetic level is then forced to fall down to replace the gap left by the excited electron: during this passage, the electron releases a specific amount of energy equal to the energetic difference between the two orbitals involved. This released energy is in the form of a photon (Compton, 1923).

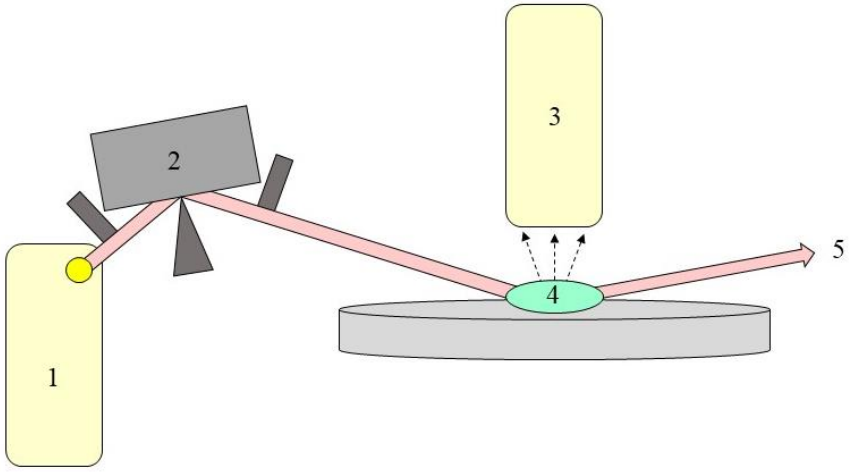

Figure 16 *TXRF – S2 PICOFOX: 1) X-ray tube, 2) reflector, 3) detector, 4) sample, 5) totally reflected beam. The red arrows represent the fluorescence radiation.*

The wavelength of the emitted radiation is characteristic for each atom and its intensity is proportional to the element concentration in the sample. This technique allows detecting the elemental composition of a complex system like a cell with a high level of accuracy.

The peculiarity of the total X-ray reflection technique is that it takes advantage of the feature of the X-ray radiation to be totally reflected in the vacuum that, in combination with the fluorescence of the elements, allows to measure the latter. In fact, under the presence of X-ray radiation, every material has a lower optical density, then a lower refractive index, with respect to the vacuum whose refractive index is 1. This means that when X-ray radiation hits a solid, it will be totally reflected in the vacuum. In this regard, one of the most important components of the instrument is the monochromator: this is directly connected with the X-ray radiation source and has the function of defining the spectral distribution and geometric quality of the excitation beam towards the sample (von Bohlen, 2009).

2.4.2.3.1 Sample preparation for S2 PICOFOX analyses

The number of cells required for the experiment was collected from the culture and centrifuged at 6000g for 5 minutes. The pellet was then washed with a solution of ammonium formate (isotonic to the growth medium, which means 0.5M or 0.03M depending on the growth medium) in order to eliminate all the residual salts of the growth medium and organic molecules that may have been released during growth.

The final pellet was resuspended in 1ml of ammonium formate with 5µl of a solution containing Gallium (Ga, 1g/L) in HNO_3 (v/v 5%). Gallium was chosen as an internal standard since is an unusual element for cyanobacteria cells. The concentration of each element in the samples was then calculated with respect to the signal obtained from Gallium. For the analyses, an aliquot of 10µl was placed on the quartz sample holder and dried at 60°C until completely evaporated. The measurements were recorded for 1000 seconds, the X-ray spectra obtained for each sample were analyzed using the software SPECTRA 6.1 (Bruker AXS Microanalysis GmbH).

2.4.2.4 Quantification of organic pools

The variations of the organic pools (i.e. proteins, carbohydrates, and lipids) inside the cells were analyzed for each species applying the Fourier Transform to Infrared Spectroscopy. The analyses were performed using an FT – IR TENSOR 27 Spectrometer

(Bruker Optik GmbH) and the resulting data were investigated through the software OPUS 6.0 (Bruker Optik GmbH).

The FT – IR (i.e. Fourie Transform Infrared Spectrometry) is a kind of Infrared Spectrometry that is based on the Fourier Transform[5]. In general, analyses with the infrared spectrometry can detect the molecules present in a sample and quantify the concentration in which they are present (Smith, 2011). The analysis is centered on the identification of specific chemical groups based on the different ways in which the incident infrared light (which has a wavelength between 700nm and 1mm) is absorbed in the presence of different chemical bonds, which identify the functional groups (Smith, 2011).

All the processes are based on the theory according to which, when a molecule absorbs an infrared beam, its chemical bonds vibrate according to its three-dimensional organization. Indeed, postulating that each atom enclosed in the molecule has 3 degrees of freedom (indicating the 3 directions in which it can move on three Cartesian axes) there are two different equations that allow obtaining the specific vibration modes of the molecule:

$$Vibration\ modes = (3 \cdot N) - 5$$
$$Vibration\ modes = (3 \cdot N) - 6$$

where N is the number of atoms in the molecule. 5 and 6 are constants that were chosen to indicate a linear and a non-linear molecule respectively (Settle, 1997).

Therefore, different functional groups are subjected to a specific kind of vibrational motion adsorbing a determined quantity of energy. This energy can be detected by a spectrometer and displayed in the form of an IR absorption spectrum (**Figure 17** - Settle, 1997).

[5] **Fourier transform**: is a mathematical transformation which facilitates signal analysis: it allows to write a function which depends on time as a frequency dependent function.

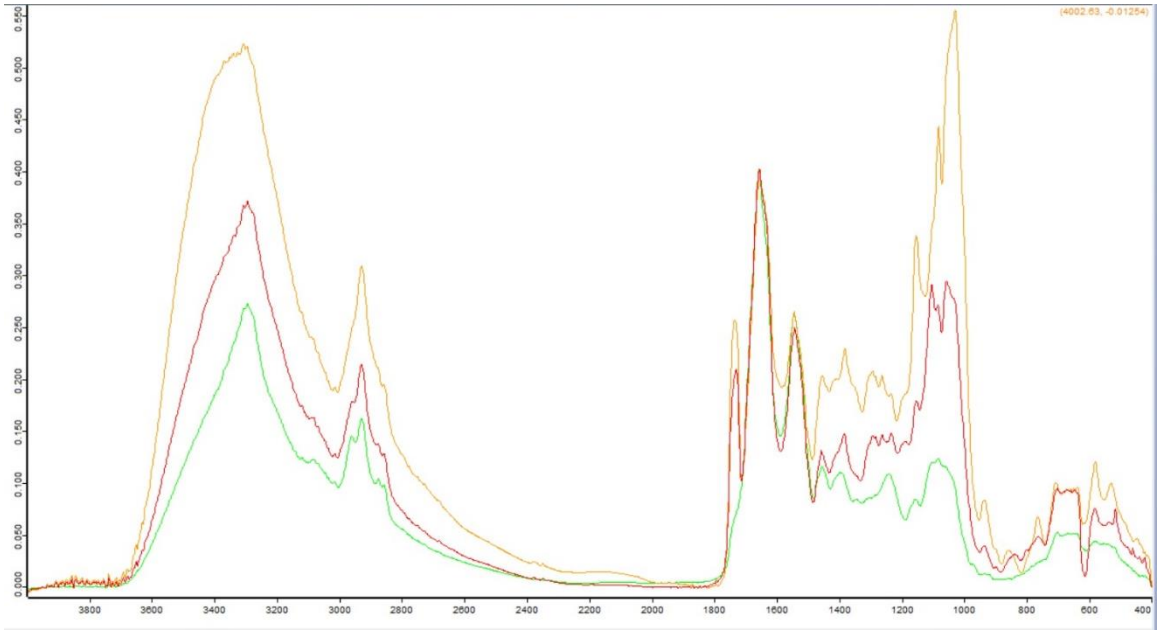

Figure 17 *Example of IR absorption spectrum. In this particular case, each line represents a different growing condition for Synechocystis sp. PCC6803: the 3 spectra were normalized on the protein peak at 1650nm.*

At the end of the analyses, the resulting Infrared Spectrum presents several peaks that are proportional to the concentration of the functional group in the sample. For spectra being used in analyses like ours, the absorbance must be considered in the final spectra. Indeed, according to Lambert-Beer law (3):

$$A = \varepsilon \cdot b \cdot \mathrm{C}$$

From which it can be obtained:

$$A = log\left(\frac{incident\ light}{trasmitted\ light}\right)$$

where ε is the molar extinction coefficient, b is the optical distance and C is the concentration of the sample in the liquid volume analyzed (mol/L).

The central part of an FT – IR spectrometer is Michelson's interferometer (**Figure 18**) which is constituted by four arms that hold three mirrors: the collimator mirror which makes the light rays parallel once they left the light source, the fixed mirror, and the moving mirror. The fourth arms hold the detector and the samples. In the middle of this structure, there is a *beam-splitter* that reflects part of the light to the moving mirror and transmits the second part of the light bean to the fixed mirror. After the moving and fixed mirrors have reflected the light beans back to the beam-splitter, it recombines them in one new light bean that will pass through the sample (Smith, 2011). Plotting the intensity of light spotted by the detector with the optical distance which travels the two reflected light beams, the instrument

can obtain an *interferogram*. The interferogram is then transformed, thanks to the Fourier Transform, in an absorption spectrum that can be analyzed. The practical problem, easily skipped, is that the Lambert-Beer Law assumes a homogeneous sample. It becomes necessary then, to assume the hypothetical homogenization of the sample (reached following a strict protocol) and compare the absorbances with real values obtained through alternative experiments, as explained in the next section.

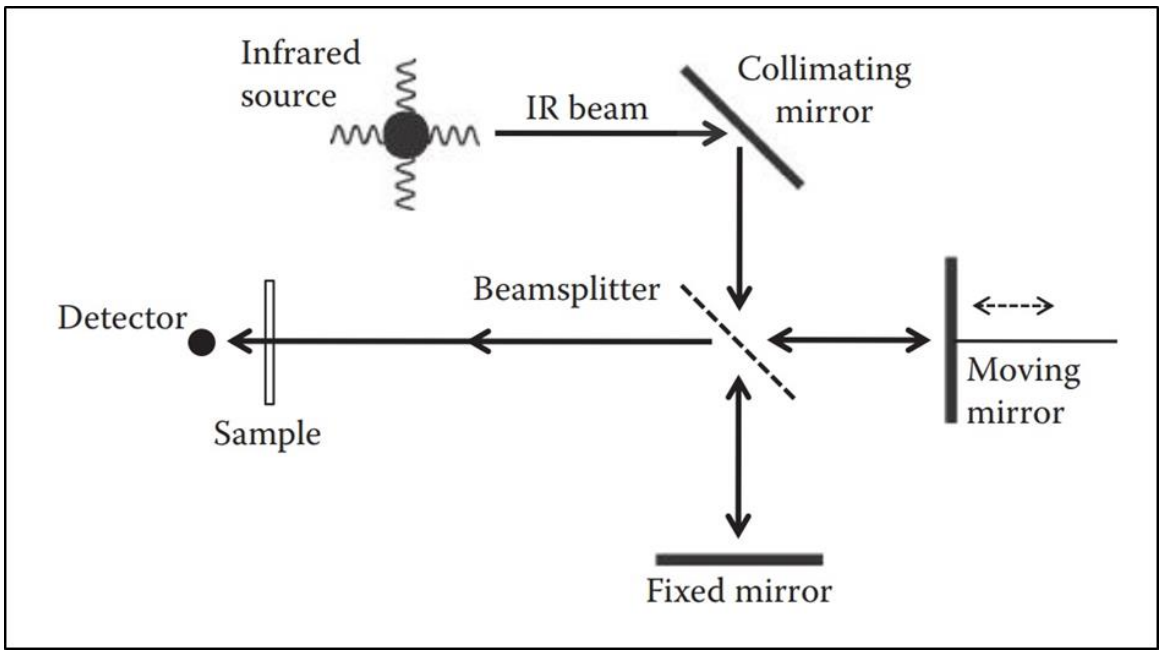

Figure 18 *Michelson's interferometer (Smith, 2011).*

2.4.2.4.1 *Sample preparation for FT-IR analyses*

As described in section 4.3.3.1, the cells were collected from the culture and washed. The final pellet was resuspended in 50µl of 0.5mol/L of ammonium formate, transferred on the FT-IR samples support and dried at 80 °C for 24 hours. To perform the analyses, 50µl of ammonium formate was used as a blank. Spectra acquisition was then performed: three instrumental and three or two biological replicate spectra were acquired for each species and culture condition to obtain a statistically significant analysis.

Each peak of the FT-IR spectrum was interpreted as a specific macromolecular pool in accordance with Giordano and collaborators' previous studies (Giordano et al., 2001; Palmucci et al., 2011). The pools analyzed during this work are described in **Table 9** and, more specifically in **Table 18** in the results section.

Wave Number (cm^{-1})	Assignment	Comments
3025-3006	=CH	C=C bonds
~ 2953	$-CH_3$	C-C bonds
~ 2924	$-CH_2$	C-C bonds
~ 1740	Stretching of C=O of ester functional groups	Primarily from lipids and fatty acids
~ 1650	Stretching of C=O of amides associated with proteins	Usually called the amide I band
~ 1200-900 (focus on 1024, 1050 and 1150 peaks)	Stretching of C-O-C of polysaccharides	Primarily due to carbohydrates, might be obscured by silicate when present
~ 1075	Stretching of Si-O of the silicate	Considered for diatom analyses

Table 9 *Band assignment for FT-IR spectroscopy used in this study(Giordano et al., 2001).*

For this work, the second derivative function for each spectrum was calculated with the software OPUS 6.0 to clarify the position, the width and the height of every single peak. This passage allows also to minimize the variation between replicate spectra. The resulting spectra were then deconvoluted (using the function CURVE FIT of the same software - **Figure 19**) and, at the end of the analysis, the integral value of each peak was obtained. Each peak was then used as a measure of the corresponding macromolecular pool.

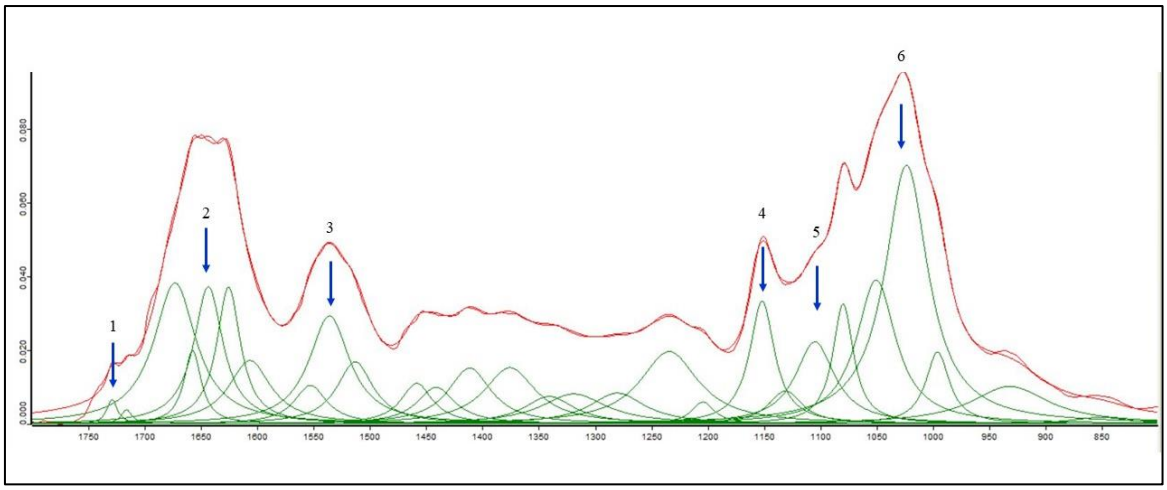

Figure 19 *Representative FT-IR spectra (1800 – 800cm^{-1}) after deconvolution, in this case, data for Synechococcus sp. WH7803 in standard conditions. 1) lipids, 2) amide I, 3) amide II, 4 – 5 – 6) carbohydrates.*

This type of analysis does not allow to obtain an absolute quantification of the macromolecular pools; it was possible, however, to estimate the size of the pool using a semiquantitative computational procedure (Palmucci et al., 2011). To do that, the protein content was determined through a quantitative method (measured as described in section 4.3.1) and the resulting value was used to determinate the carbohydrates and lipids content made using the following equations:

$$C(carb) = \frac{Abs(carb)}{Abs(prot)} \cdot C(prot) \cdot \frac{\varepsilon(prot)}{\varepsilon(carb)}$$

$$C(lip) = \frac{Abs(lip)}{Abs(prot)} \cdot C(prot) \cdot \frac{\varepsilon(prot)}{\varepsilon(lip)}$$

where *C(carb)* corresponds to carbohydrates pool size and *C(lip)* to the lipids pool size in the sample, *C(prot)* is the quantification of protein pool determined spectrophotometrically; *Abs(carb)*, *Abs(lip,)* and *Abs(prot)* are the FT-IR absorbances value; *ε(carb)*, *ε(lip),* and *ε(prot)* are their extinction coefficients. We assume the extinction coefficient values more than 0, while their ratio in the formulas is assumed to be constant for all the species, thus omitted from all the calculations (Palmucci et al., 2011). Moreover, it is possible to estimate the level of reduction of organic compounds through the formula below:

$$Reduction\ index = \frac{Abs(CH_2) + Abs(CH_3)}{Abs(CH)}$$

Again, these numbers are not a realistic quantification of the molecules inside the samples, they represent the relative proportion of the CH_n groups inside the samples themselves.

2.5 STATISTICAL ANALYSES

All measurements were done in triplicates: each number enclosed three biological replicates, and, where necessary and physically possible, three instrumental replicates for each biological one as well. Results are shown as mean with standard deviation in brackets.

The software RStudio (https://www.rstudio.com/products/rstudio/download/) was used for the statistical calculations: the BARTLETT test was used to verify the homogeneity of the variances while the SHAPIRO one was used to test the normality of the data. During the whole work, the data were assumed, independent.

One-way ANOVA tests were performed as a parametric test for the analyses of the variance, while the KRUSKAL – WALLIS tests were performed for the analyses of variance of non – parametric values. The results were considered for p-value < 0.05 and the TUKEY test (for the parametric analyses) and PAIRWISE – T-Test (for the non-parametric analyses) were used as post hoc test to determinate the statistical significance between the different sets of data.

In the case of *Synechococcus* specie, since the comparison was possible only between two conditions, the t-Test was used for the statistical analyses performed with the GraphPad software (https://www.graphpad.com/scientific-software/prism/).

All the graphics were made with RStudio and the *ggplot2* package.

“E caddi come corpo morto cade.”

La Divina Commedia
Inferno
Canto Quinto – 142

“And I fell as falls a body that is dead.”

La Divina Commedia
Hell
Chapter Fifth – 142

RESULTS

3.1 Dissolved gas in the growth media

3.1.1 Dissolved Oxygen and Dissolved Inorganic Carbon

The amount of dissolved oxygen in the media (**Table 10**) varied significantly (one-way ANOVA, $p<0.05$) justifying the assumption that the proterozoic conditions were realistic for the entire duration of the experiment.

Conditions	Media	$[O_2]$ in µmol/l
Standard Conditions	BG11 Standard concentrations	251[a] (0.26)
	AMCONA Standard concentrations	214[b] (0.47)
Proterozoic Conditions	BG11 Proterozoic concentrations	48.9[c] (0.18)
	AMCONA Proterozoic concentrations	39.1[d] (0.47)

Table 10 *Oxygen dissolved in the media underwent continuous bubbling, different letters indicate a statistical significance.*

3.2 Characterization of the cell physiology

3.2.1 Specific Growth Rate

In the freshwater conditions, the differences in *Synechocystis* growth rate (**Figure 20** and **Figure 22**) and maximal cell density (**Figure 22**) among the standard condition, the transitional and the proterozoic ones are statistically significant. Comparing the standard

with the transitional condition and then the transitional with the Proterozoic one, it can be underlined that the effect of low nutrients concentration is higher than the effect of low oxygen available. Indeed, the difference between the standard and the transitional conditions appears to be more significant respect to the one between transitional and proterozoic ones (standard vs. transitional: *p-value* = $7.0 \cdot 10^{-6}$; transitional vs. proterozoic: *p-value* = 0.015).

Marine *Synechococcus*, on the other hand, was unable to grow under proterozoic condition, a strong effect of oxygen availability was then hypothesized (**Figure 22** and **Figure 20**). The growth rate in the transitional condition resulted higher than in the standard one while the opposite trend was shown by cell density (**Figure 22**): a lower cell density in the transitional condition can be explained by the lower Fe, N, S concentrations in the medium.

In conclusion, both dissolved oxygen concentration and nutrient concentrations in the medium have an effect on growth rates (**Figure 22**, **Table 11** and **Table 12**). In the freshwater environment, the lower the availability of dissolved oxygen and nutrients, the lower the growth rates and cell density (**Figure 22**).

Specific Growth rate (days $^{-1}$)	**Standard Condition**	**Transitional Condition**	**Proterozoic Condition**
***Synechocystis* sp. PCC6803**	0.26^{a} (0.01)	0.09^{b} (0.02)	0.05^{c} (0.01)
***Synechococcus* sp. WH7803**	0.19^{a} (0.02)	0.25^{b} (0.01)	N.A.

Table 11 *Specific growth rates of experimental organisms under different experimental conditions. Standard deviation is indicated in brackets.*

Doubling Time (hours)	**Standard Condition**	**Transitional Condition**	**Proterozoic Condition**
***Synechocystis* sp. PCC6803**	63.8^{a} (2.27)	189^{b} (40.1)	352^{c} (49.9)
***Synechococcus* sp. WH7803**	86.7^{a} (10.1)	66^{b} (2.81)	N.A.

Table 12 *Doubling time of experimental organisms under different experimental conditions. Standard deviation is indicated in brackets.*

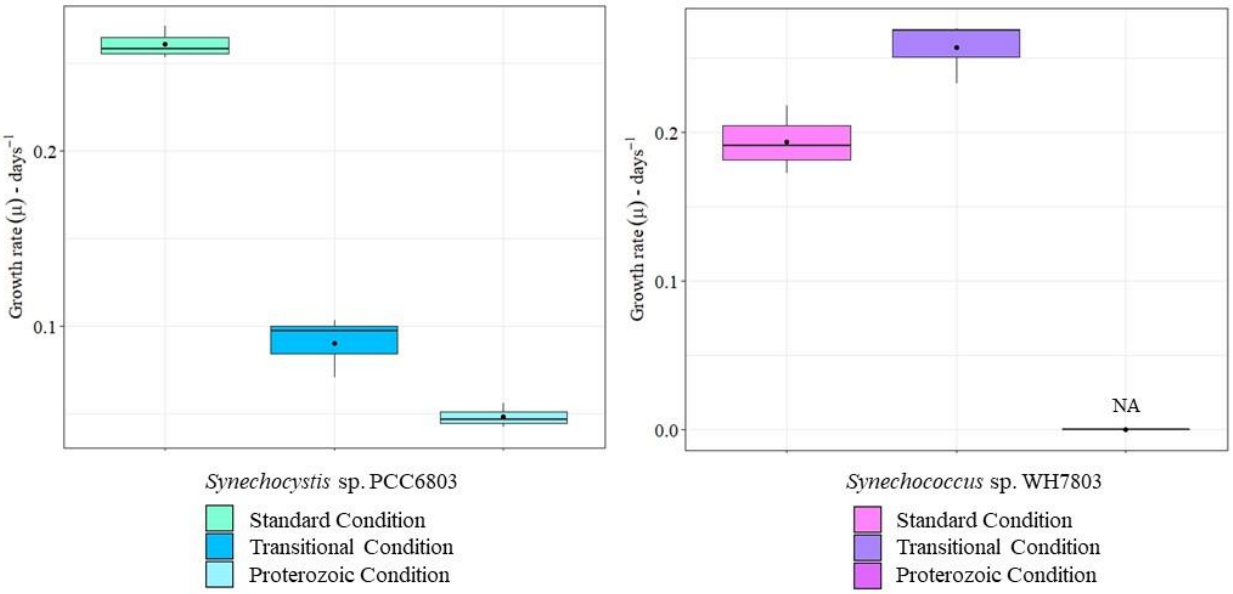

Figure 20 *Specific growth rates of experimental organisms under different experimental conditions. Each box represents the interquartile range of a specific condition: the black spot represents the mean of the sample while the black line is the median and represents the second quartile Q_2. Above the line is the upper quartile Q_3 while below the line is the lower quartile Q_1. The lines that come out from each box represent the minimum (lower) and the maximum (higher) value in the data. NA indicates the impossibility to perform the experiment.*

3.2.2 Dry weight and biomass productivity

The results concerning the dry weight (**Table 13** and **Figure 21**) underline that both for *Synechocystis* and *Synechococcus* the weight of a single cell doesn't change significantly despite the setup of different environments (**Figure 23** – 1). It's also clear from the results that the size of *Synechocystis* cells is 10 times bigger than *Synechococcus* once, as was also observed from the microscope picture. From the dry weight, it's also possible to obtain the biomass productivity (**Table 14**) normalizing data on the growth rates (**Figure 23** – 2): the results show how, despite the maintenance of the dry weight *per cell,* the production of biomass in the culture decrease significantly for *Synechocystis* from standard to transitional condition. The difference between the transitional and the proterozoic condition in a freshwater environment is not statistically significant. For *Synechococcus*, the variation in biomass productivity is not statistically significant (**Figure 22**). In both species, biomass productivity trend follows the growth rate.

Dry Weight (pg/cell)	Standard Condition	Transitional Condition	Proterozoic Condition
***Synechocystis* sp. PCC6803**	0.098[a] (0.011)	0.103[a] (0.021)	0.098[a] (0.031)
***Synechococcus* sp. WH7803**	0.014[a] (0.004)	0.014[a] (0.002)	N.A.

Table 13 *Dry weight for different species in different experimental conditions. Standard deviation is indicated in brackets. NA indicates the impossibility to perform the experiment.*

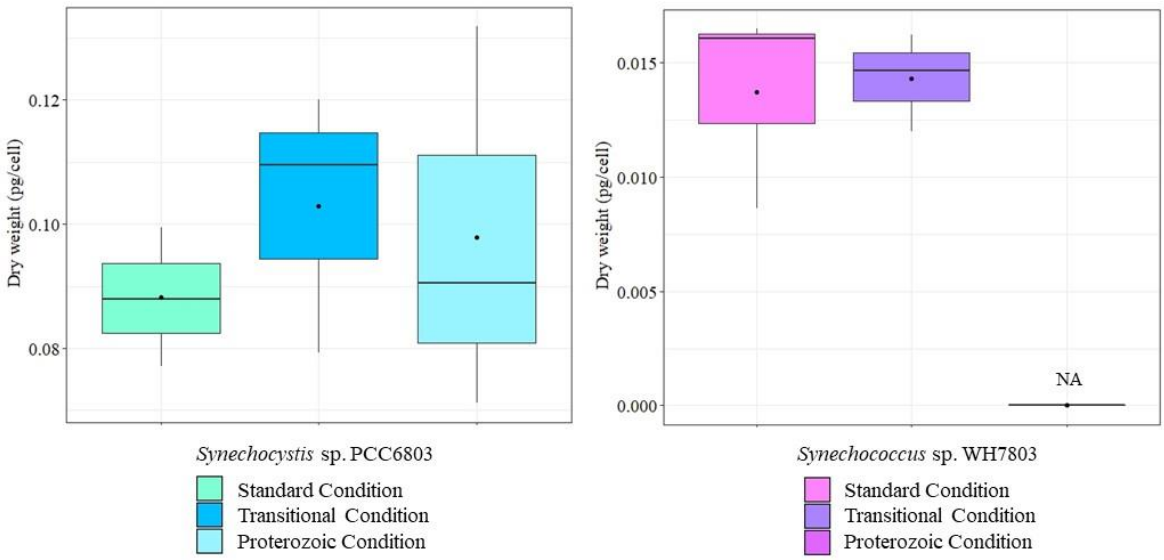

Figure 21 *Dry weight for different species in different experimental conditions. Each box represents the interquartile range of a specific condition: the black spot represents the mean of the sample while the black line is the median and represents the second quartile Q_2. Above the line is the upper quartile Q_3 while below the line is the lower quartile Q_1. The lines that come out from each box represent the minimum (lower) and the maximum (higher) value in the data. NA indicates the impossibility to perform the experiment.*

Biomass Production (pg/cell · days^{-1})	Standard Condition	Transitional Condition	Proterozoic Condition
***Synechocystis* sp. PCC6803**	0.023[a] (0.002)	0.009[b] (0.002)	0.005[b] (0.001)
***Synechococcus* sp. WH7803**	0.003[a] (0.001)	0.004[a] (0.001)	N.A.

Table 14 *Biomass production for different species in different experimental conditions. Standard deviation is indicated in brackets. NA indicates the impossibility to perform the experiment.*

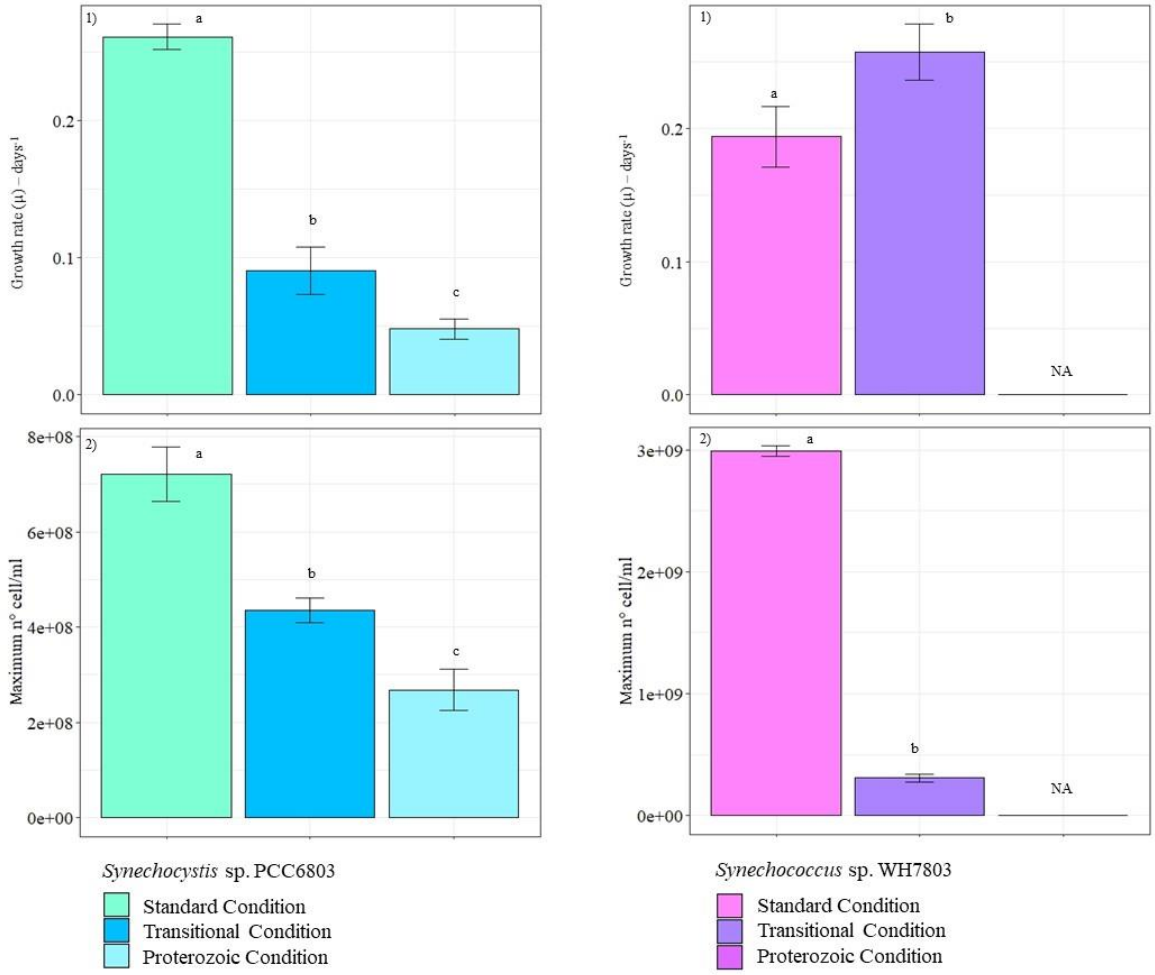

Figure 22 *<u>Synechocystis sp. PCC6803</u>: 1) growth rates, the error bars represent the standard deviations and different letters indicate statistically different values. Each column is representative of 3 biological replicates (p = 0.027; KRUSKAL – WALLIS test and PAIRWISE test as post hoc); 2) maximal cell density in different culture conditions, the error bars represent the standard deviations while different letters indicate statistically different values. Each column is representative of 3 biological replicates (p = 4.26 · 10^{-5}; One-way ANOVA test and Tukey test as post hoc).*

<u>Synechococcus sp. WH7803</u>: 1) growth rates, the error bars represent the standard deviations and different letters indicate statistically different values. Each column is representative of 3 biological replicates (p = 0.02413; KRUSKAL – WALLIS test and PAIRWISE test as post hoc). 2) maximal cell density in different culture conditions, the error bars represent the standard deviations while different letters indicate statistically different values. Each column is representative of 3 biological replicates (p = 0.02413; KRUSKAL – WALLIS test and PAIRWISE test as post hoc). NA indicated the impossibility to analyze/perform the experiment for the proterozoic condition.

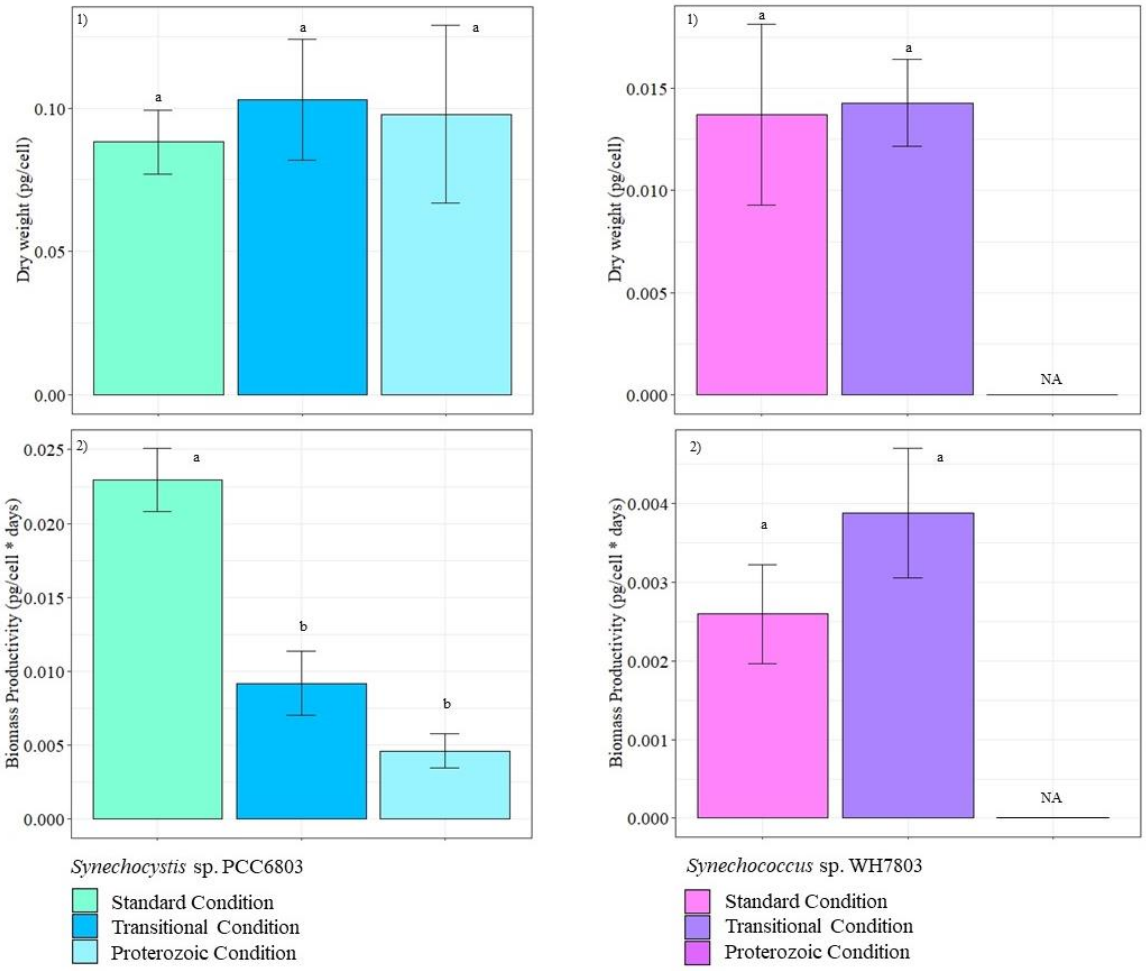

Figure 23 *Synechocystis sp. PCC6803: 1) dry weight in Standard, Transitional and Proterozoic conditions, the error bars represent the standard deviations (all of them are less than 35%), there is no statistical significance. Each column is representative of 3 biological replicates (p >0.05; KRUSKAL – WALLIS test and PAIRWISE test as post hoc); 2) biomass productivity under the 3 different experimental conditions, the error bars represent the standard deviations while different letters underline different statistical significance. Each column is representative of 3 biological replicates (p = 5.22E-5; ANOVA test and TUKEY test as post hoc).*

Synechococcus sp. WH7803: 1) dry weight in Standard, Transitional and Proterozoic conditions, the error bars represent the standard deviations (all of them are less than 35%), there is no statistical significance. Each column is representative of 3 biological replicates (p >0.05; t-Test); 2) biomass productivity under the 3 different experimental conditions, the error bars represent the standard deviations (all of them are less than 25%), there is no statistical significance. Each column is representative of 3 biological replicates (p >0.05; t-Test). NA indicated the impossibility to analyze/perform the experiment in the proterozoic condition.

3.2.3 Quantification of oxygen production during photosynthesis

Net oxygen production as a function of light intensity was also tested: the exponential phase O_2 production of each culture was compared and results were normalized

on the chlorophylls content of the cells (**Table 15**). Both *Synechocystis* and *Synechococcus* showed light intensity-dependent oxygen evolution (**Figure 24**) in both standard and proterozoic conditions (not tested for *Synechococcus*).

Chlorophyll A (pg/cell)	Standard Condition	Proterozoic Condition
***Synechocystis* sp. PCC6803**	1.286[a] (0.113)	0.092[b] (0.034)
***Synechococcus* sp. WH7803**	0.054 (0.011)	N.A.

Table 15 *Chlorophyll A content for different species in experimental conditions used to test oxygen evolution. Standard deviation is indicated in brackets. NA indicates the impossibility to perform the experiment.*

In standard condition, both species reached the Maximum Production (P_{max}) around 10µmolO_2/mg ChlA min^{-1} with a similar Compensation Point (**Table 16**). On the other hand, *Synechocystis* under the proterozoic environment reached the P_{max} at 28.2 µmolO_2/mg ChlA min^{-1} with a higher compensation point (190.86 µE/m^2s). After 600µE/m^2s the production of oxygen arrives at a plateau for *Synechocystis* in standard condition while a decrease was observed in *Synechococcus* in standard condition. Moreover, the onset of the saturation is statistically different too between both standard conditions (199.813µE/m^2s for *Synechocystis* and 159.1µE/m^2s for *Synechococcus*) and the proterozoic one (583.9µE/m^2s).

Furthermore, *Synechocystis* in the Precambrian environment seemed to be able to keep producing oxygen also with a light intensity higher than 500µE/m^2s.

Specie	Conditions	α	Maximum Photosyntetic Rate (P_{max})	Compensation Point	Onset of Saturation (Ek)
***Synechocystis* sp. PCC6803**	Standard	0.06[a] (0.03)	8.83[a] (1.61)	23.6[a] (6.92)	200[a] (73.5)
	Proterozoic	0.07[a] (0.04)	28.2[b] (10.9)	191[b] (56.2)	584[b] (39.7)
***Synechococcus* sp. WH7803**	Standard	0.12[a] (0.02)	13.6[a] (4.13)	34.2[a] (13.2)	159[a] (33.2)
	Proterozoic	NA	NA	NA	NA

Table 16 *Photosynthetic parameter for oxygen evolution during light reactions. The apexes letters indicated a different statistical significance calculate with t-Test analyses. NA indicates the impossibility to perform the experiment.*

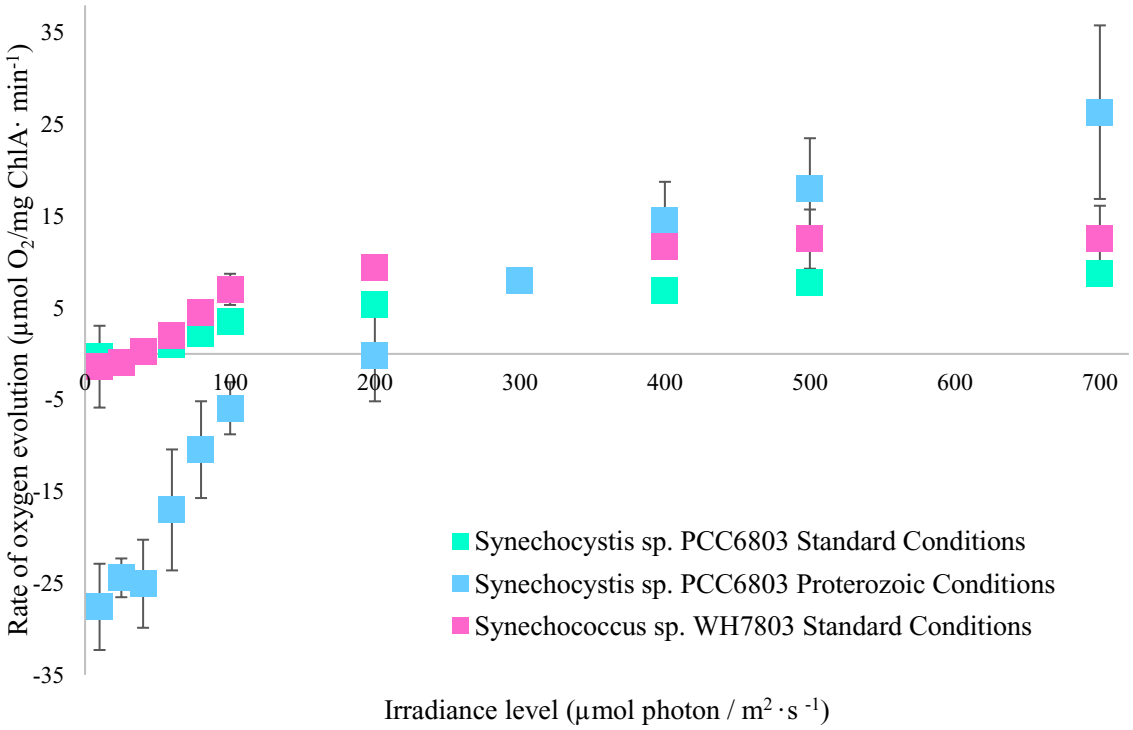

Figure 24 *Oxygen evolution during photosynthesis, each spot in the graph represents the average of 3 biological replicates while the bars represent the standard deviation. The values in the corresponding table were obtained graphically from each bio-replicate and then averaged.*

3.2.4 Quantification of ATPS activity

As results showed, the activity of the ATP sulfurylase enzyme varies greatly under different environmental conditions (**Table 17**). In *Synechocystis*, the activity decreases greatly between standard condition (1459nmol/min mg^{-1}) and transitional one (164nmol/min mg^{-1}) as shown in **Figure 25** and **Figure 26**. Moreover, there is an increase of the enzyme activity between the transitional condition and the proterozoic one where the value is 634nmol/min mg^{-1}. Despite the difference between the average, the error was huge. Regarding *Synechococcus*, there is a huge decrease in the activity from 2689nmol/min mg^{-1} in the standard condition to 32nmol/min mg^{-1} to transitional one (**Figure 25**). The

experiment was, ones again, not possible for the seawater proterozoic condition since the *Synechococcus* was not able to survive in there.

ATP Sulfurylase Activity (nmol/min · mg of protein^{-1})	Standard Condition	Transitional Condition	Proterozoic Condition
***Synechocystis* sp. PCC6803**	1459^{a} (277)	164^{b} (82.6)	635^{c} (213)
***Synechococcus* sp. WH7803**	2689^{a} (1096)	32.2^{b} (5.54)	N.A.

Table 17 *ATPS activity for different species in experimental conditions used to test oxygen evolution. Standard deviation is indicated in brackets while different letterers underline a different statistical significance. NA indicates the impossibility to perform the experiment.*

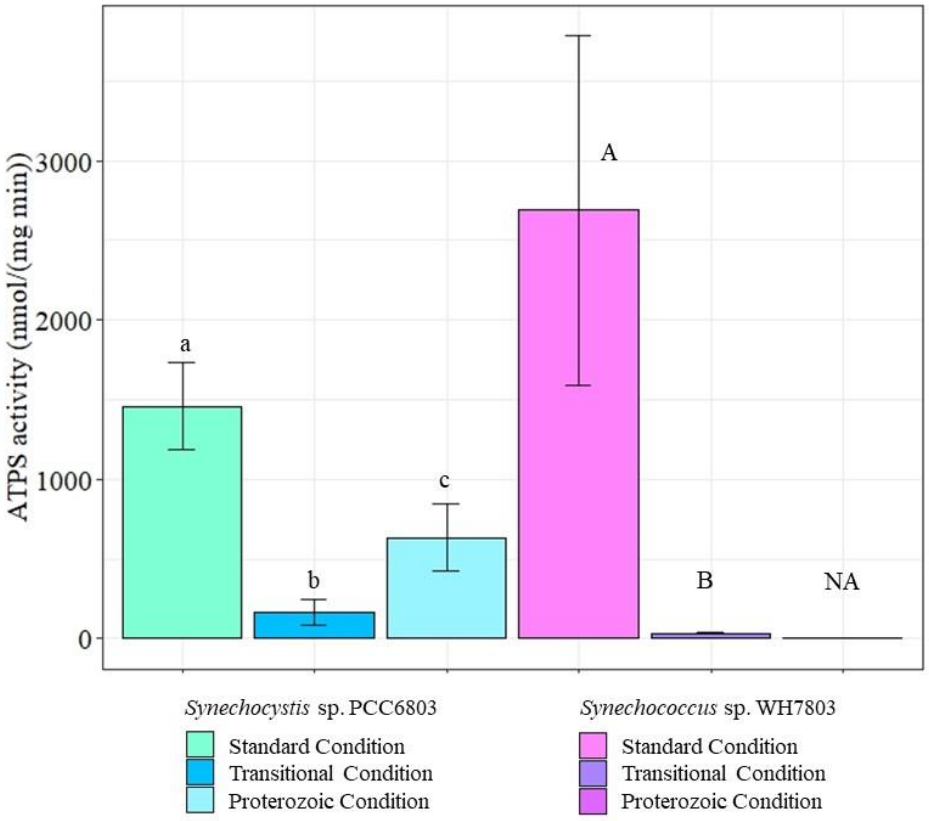

Figure 25 *ATPS activity variations. In both Synechocystis sp. PCC6803 ($p < 0.05$; sequential t-Test) and Synechococcus sp. WH7803 ($p < 0.05$; sequential t-Test) each letter represents statistically significance differences. Each bar represents the average of 3 biological replicates and the error bars represent the standard deviations. NA represents the impossibility of performing the experiment in proterozoic seawater conditions.*

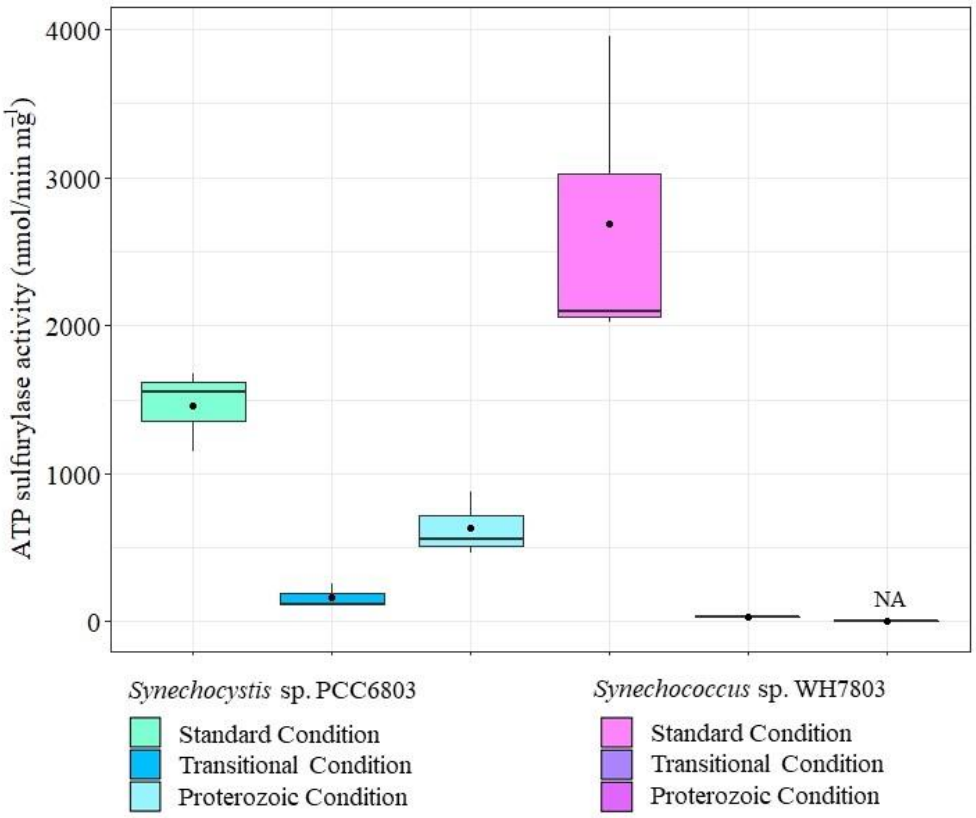

Figure 26 *ATP sulfurylase activity. Each box represents the interquartile range of a specific condition: the black spot represents the mean of the sample while the black line is the median and represents the second quartile Q_2. Above the line is the upper quartile Q_3 while below the line is the lower quartile Q_1. The lines that come out from each box represent the minimum (lower) and the maximum (higher) value in the data. NA indicates the impossibility to perform the experiment. NA indicates the impossibility to perform the experiment.*

3.3 Characterization of cell composition

3.3.1 Protein spectrometric quantification

In *Synechocystis* (**Figure 27** – 1) the picograms of proteins *per cell* decrease between standard (0.079pg/cell) and transitional (0.053pg/cell) conditions while they seem to be constant between standard and proterozoic one (0.082pg/cell). On the other hand, in *Synechococcus* (**Figure 27** – 2) the amount increases from standard (0.013pg/cell) to transitional (0.032pg/cell) condition. Furthermore, comparing the two species, it's clear how the amount of proteins present in freshwater cells is higher than the one present in seawaters, which is explained by the different cell dimensions.

The statistical analyses in *Synechocystis* return a *p value* of 0.047, underling a statistical difference that it's possible to see in **Figure 27**. Nevertheless, one of the post hoc was applied, the corresponding *p values* were >0.05. This finding justifies why there are no letters on top of *Synechocystis* bars. Despite this, a difference between the transitional condition and the other two is clearly detectable.

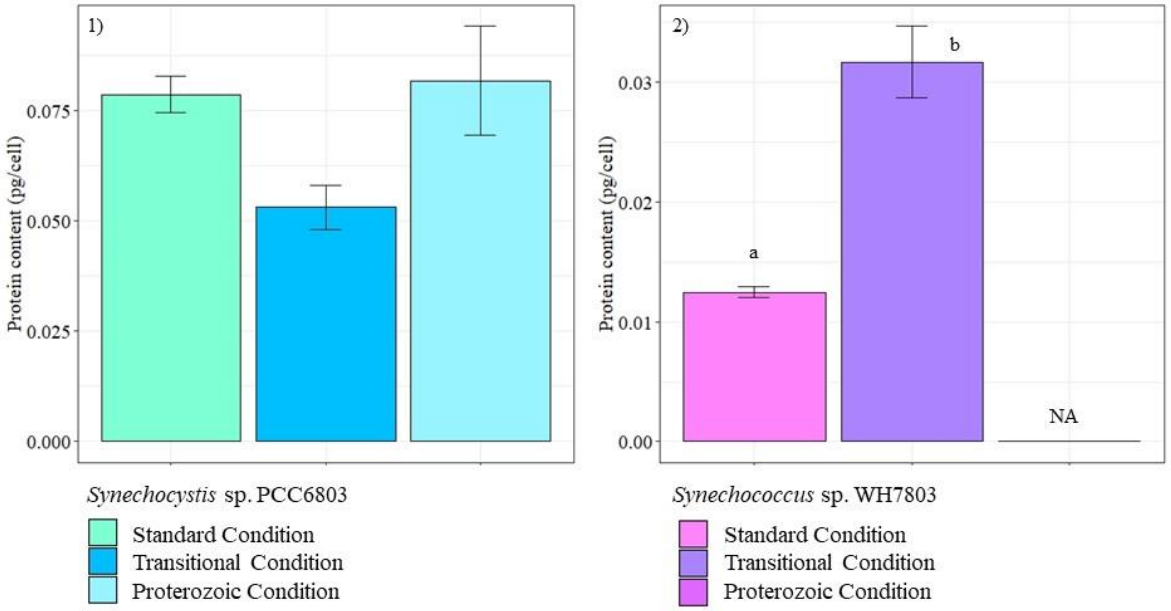

Figure 27 *Proteins content per cells grown in different environments, each bar represents the average of 3 biological replicates, the error bars represent the standard deviations and different letters indicate statistically different values. 1) p = 0.047; One-way ANOVA test and Tukey test as post hoc; 2) t-Test; p = 0.0004; NA indicates the impossibility of performing the experiment for the seawater proterozoic condition.*

3.3.2 Macromolecular composition

The macromolecular compositions of cells were analysed through infrared spectrometry. In total, 3 spectra for each biological replicate in standard conditions and 2 spectra for each biological replicate in other conditions were collected and the peaks reflecting the carbohydrate, lipid and protein pools were averaged and compared. The following two figures show the resulting spectra for *Synechocystis* (**Figure 28**) and for *Synechococcus* (**Figure 29**) underling the fundamental peaks that are described in **Table 18**. All spectra have been normalized to the amide I band (Domenighini and Giordano, 2009; Kansiz et al., 1999; Palmucci et al., 2011).

Wavenumber (cm^{-1})	Letters in the spectra	Assignment	Reference
~3015	a	-CH	(Palmucci et al., 2011)
~2950	b	$-CH_3$	(Palmucci et al., 2011)
~2920	c	$-CH_2$	(Palmucci et al., 2011)
~1740	d	ν C=O Lipids and fatty acid	(Giordano et al., 2001; Kansiz et al., 1999)
~1650	e	C=O associated with proteins (Amide I)	(Giordano et al., 2001)
~1540	f	N-H associated with proteins (Amide II)	(Giordano et al., 2001; Kansiz et al., 1999)
~1455	g	δ_{as} CH_3 and δ_{as} CH_2 of proteins	(Giordano et al., 2001; Kansiz et al., 1999)
~1230	h	ν_{as} P=O of the phosphodiester backbone	(Giordano et al., 2001; Kansiz et al., 1999)
~1150	i	ν C-O-C of polysaccharides	(Giordano et al., 2001)
~1075	j	ν Si-O of silicate compound (normally frustules)	(Giordano et al., 2001)
~1050	k	ν C-O-C of polysaccharides	(Giordano et al., 2001)
~1024	l	ν C-O-C of polysaccharides	(Giordano et al., 2001)

Table 18 *Band assignment for FT-IR graph, letters referred to both Synechocystis and Synechococcus graph in* ***Figure 28*** *and* ***Figure 29****.*

As shown in the sections II and III of **Figure 28**, important differences can be detected in the lipid and in the carbohydrate pools. In section II, an increase in the spectrum intensity is observed in both transitional and proterozoic conditions. The most important variation is observed in the range of 1200-950cm^{-1}, which corresponds to the absorption of C-O-C of polysaccharides. Moreover, with the increase of the spectrum intensity in this region, is detected also a symmetrical increase in the SiO_2 functional group at ~1075cm^{-1} and a variation in the shape of the peak at ~1230cm^{-1}(phosphodiester group PO_2). A correlation exists also between the lipid peak at ~1740cm^{-1} and the region between 3020 and 2900cm^{-1}: indeed, while the ~1740cm^{-1} correspond to the C=O bond of lipid, the ~3000cm^{-1} region corresponds to the vibration of the C-H in which are enclosed the long carbon chain of fatty acid and lipids molecules. In **Figure 28**, it is shown that the presence of a strong and higher peak at ~1740cm^{-1} in transitional and proterozoic conditions corresponds to an

increase in the peaks enclosed in the ~3000cm^{-1} region (~3015/~2950/~2920cm^{-1}). Another important difference is detected in the peak at ~1455cm^{-1} which is much stronger in the transitional condition than in the other two.

A similar comparison was made on *Synechococcus* variations showed in **Figure 29**. Yet, in this case, the variations between standard and transitional conditions show different trends considering different ranges of wavelengths. Despite the lipid peak at ~1740cm^{-1} is almost constant between standard and transitional conditions, there is an increase in the protein peaks not used to normalize the spectra. The intensity of the amide II (~1540cm^{-1}) peak and the one of the -CH_n protein bonds (~1455cm^{-1}) show an increase in the transitional condition. On the other hand, in the range of carbohydrates detection, it is observed an important decrease in the spectra intensity from standard to transitional condition.

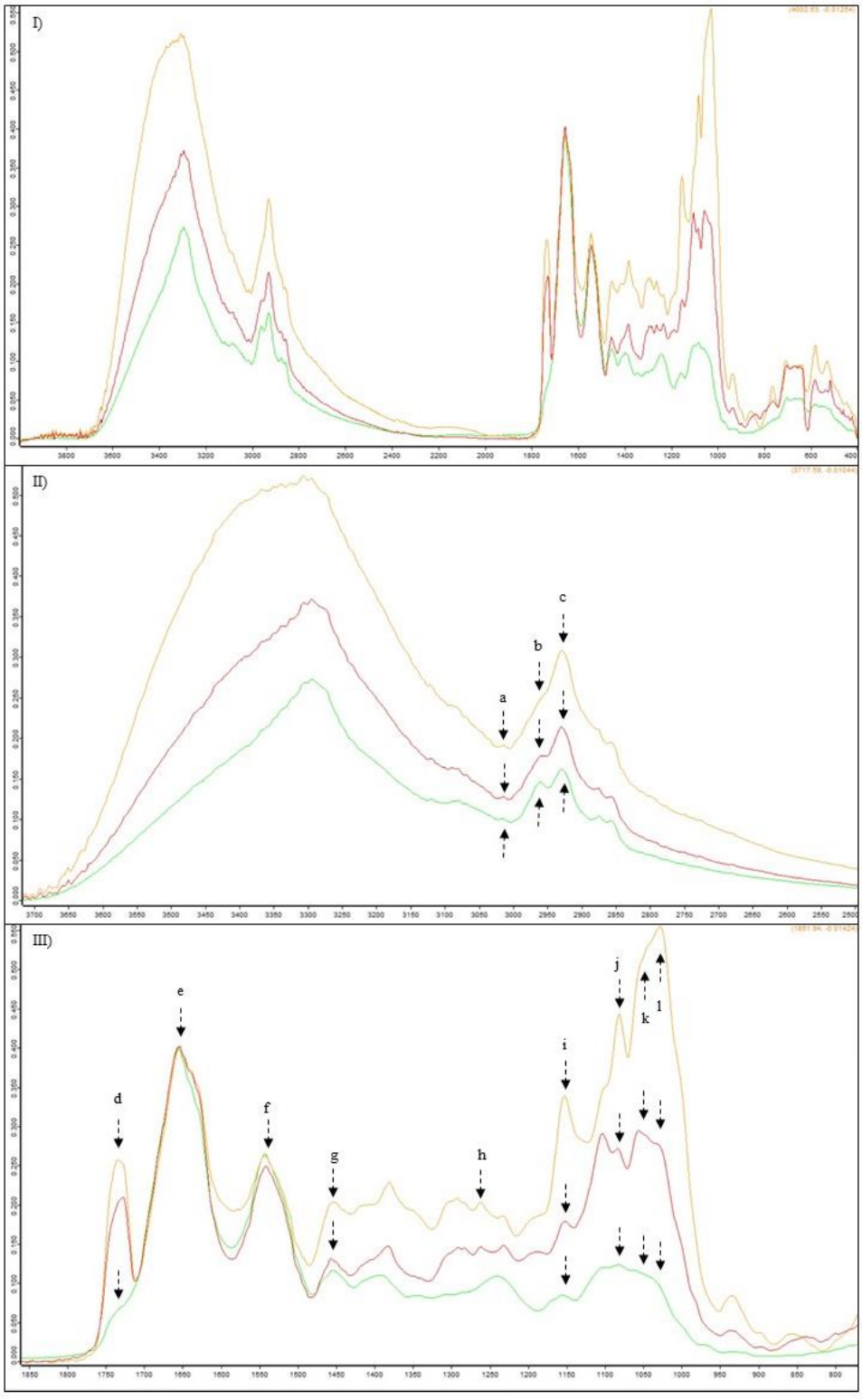

Figure 28 *FT-IR spectra of Synechocystis sp. PCC6803 in the three conditions. Transitional and proterozoic spectra were normalized to the amide I peak at ~1650cm^{-1} of standard condition spectra. Legend: green line: standard condition; red line: proterozoic condition; orange line: transitional condition. Sections II and III are the magnification of section I.*

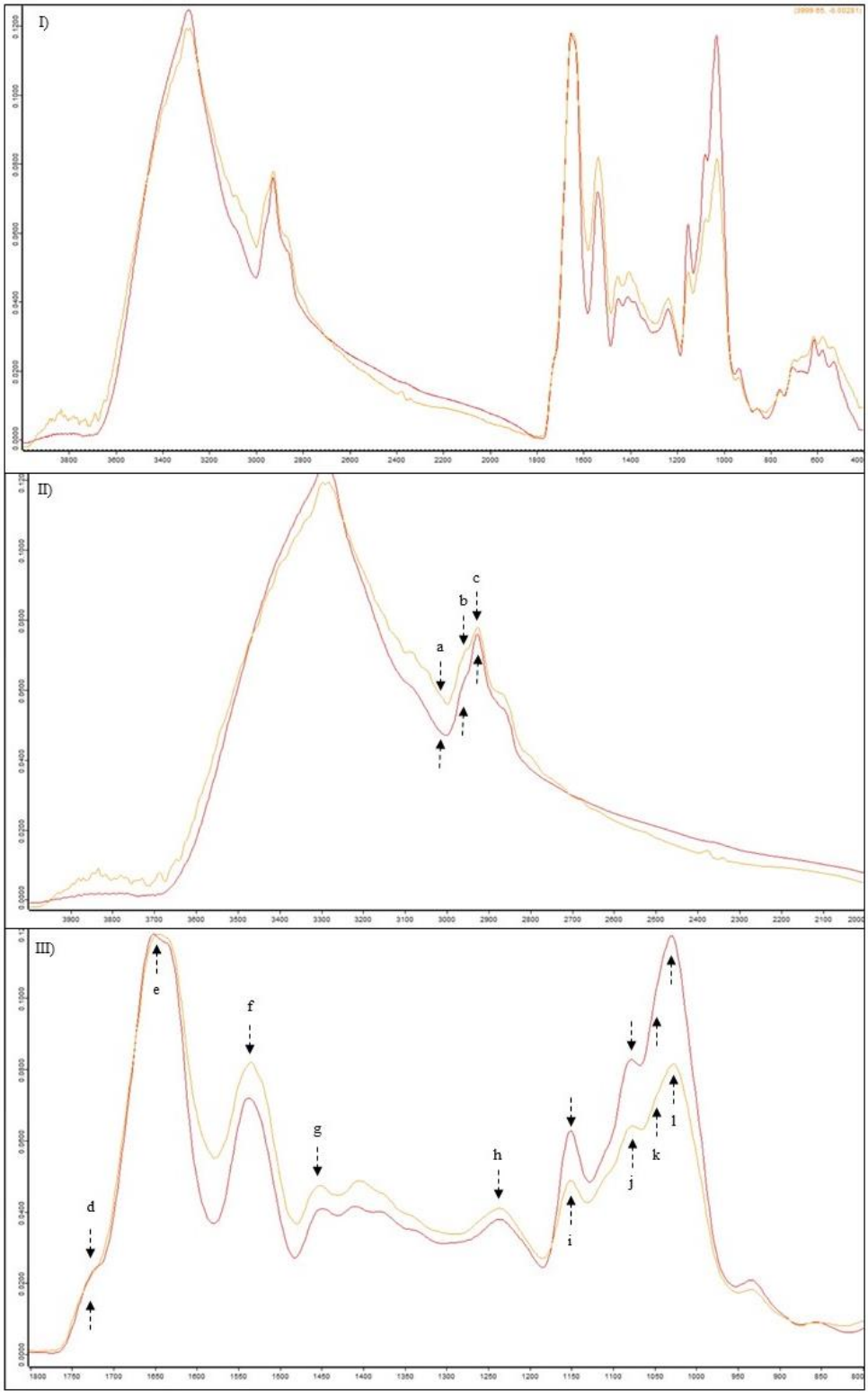

Figure 29 *FT-IR spectra of Synechococcus sp. WH7803 in the two conditions. Transitional spectrum was normalized to the amide I peak at ~1650cm^{-1} of standard condition spectra. Legend: red line: standard condition; orange line: transitional condition. Sections II and III are the magnification of section I.*

In addition to the above qualitative differences between the analyzed spectra, the reduction index (**Figure 30**) of the cells was obtained from infrared spectrometry data. In general, the variation of this index underlines a modification in the saturation of carbon bonds inside the cell: in this case, its increase indicates a decrease in the unsaturated carbon bonds.

As shown in **Figure 30**, in both *Synechocystis* and *Synechococcus* there is an increase of this index. In *Synechocystis* is possible to underline that the variation between standard and transitional condition is statistically significant while the variations between standard and proterozoic and, secondly, between transitional and proterozoic, are not. On the other hand, in *Synechococcus,* the variation between standard and transitional conditions is very high increasing by more than thirty times. One again, the comparison with the proterozoic condition in *Synechococcus* was not possible.

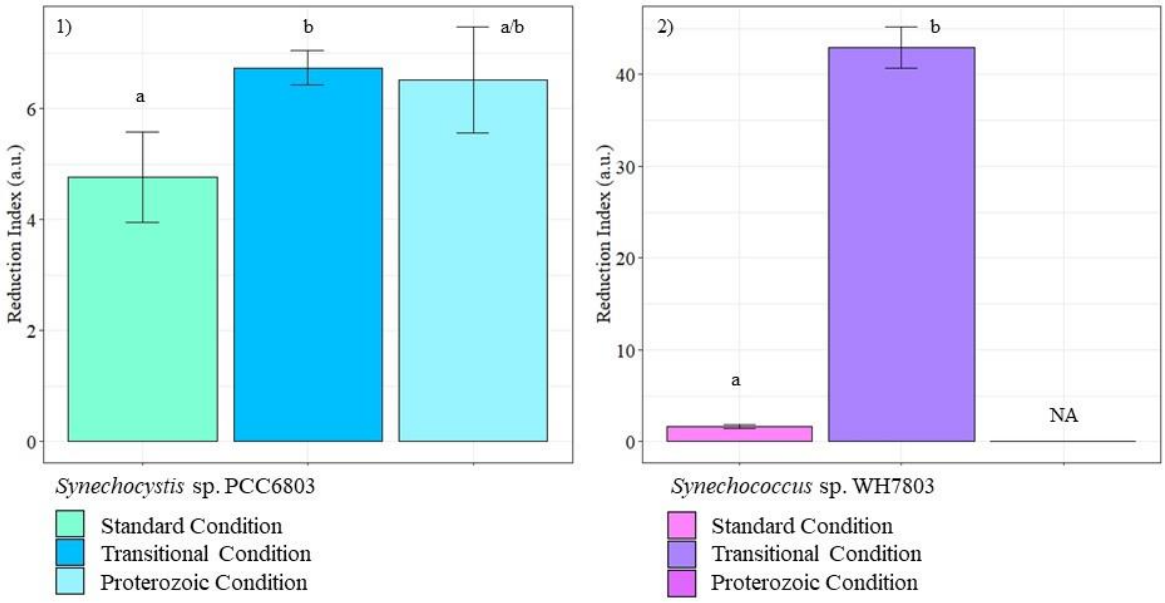

Figure 30 *Reduction index. 1) Synechocystis sp. PCC6803; the error bars represent the standard deviations and different letters indicate statistically different values. Each column is representative of 3 biological replicates (p = 0.03; ANOVA and Tukey test as post hoc). 2) Synechococcus sp. WH7803; the error bars represent the standard deviations and different letters indicate statistically different values. Each column is representative of 3 biological replicates (t-Test, p <0.0001). NA indicates the impossibility to analyze/perform the experiment for the proterozoic condition.*

Thanks to the semiquantitative evaluation of macromolecular pools (Palmucci et al., 2011), it was also possible to normalize the organic pools' values detected in the experimental conditions to those found in the standard one (**Table 20** and **Table 21**, **Figure 31** and **Figure 33**).

Specie	Macromolecular Pool	Standard Condition	Transitional Condition	Proterozoic Condition
***Synechocystis* sp. PCC6803**	Protein (pg/cell) - spectrometric quantification -	0.079^{a} (0.004)	0.053^{a} (0.005)	0.077^{a} (0.017)
	Carbohydrate (a.u)	0.049^{a} (0.015)	0.240^{b} (0.018)	$0.146^{a/b}$ (0.076)
	Lipid (a.u)	0.004^{a} (0.002)	0.057^{b} (0.005)	0.049^{b} (0.030)
***Synechococcus* sp. WH7803**	Protein (pg/cell)	0.013a (0.0004)	0.032b (0.003)	N.A.
	Carbohydrate (a.u)	0.024^{a} (0.006)	0.056^{b} (0.013)	N.A.
	Lipid (a.u)	0.0009^{a} (0.0002)	0.0026^{b} (0.0007)	N.A.

Table 19 *Molecular pools quantification, the pg/cell values are referred to as protein spectrometric quantification. The arbitrary unit (a.u) indicates those values derived from the semi quantification method (Palmucci et al., 2011). Standard deviation is indicated in brackets while different letters underline statistically significant differences.*

Specie	Macromolecular Pool	Standard Condition	Transitional Condition	Proterozoic Condition
***Synechocystis* sp. PCC6803**	Protein (a.u.)	1 (Set up)	0.68 (0.064)	0.98 (0.221)
	Carbohydrate (a.u.)	1^{a} (Set up)	4.94^{b} (0.375)	$3.00^{a/b}$ (1.56)
	Lipid (a.u)	1^{a} (Set up)	13.11^{b} (1.25)	$11.23^{a/b}$ (6.92)
***Synechococcus* sp. WH7803**	Protein (a.u.)	1^{a} (Set up)	2.54^{b} (0.24)	N.A.
	Carbohydrate (a.u.)	1^{a} (Set up)	2.31^{b} (0.52)	N.A.
	Lipid (a.u)	1^{a} (Set up)	3.29^{b} (0.85)	N.A.

Table 20 *Macromolecular quantification: the arbitrary values (a.u.) for each pool were normalized to the standard condition one. Standard deviation is indicated in brackets while different letters underline statistically significant differences.*

Ratio	Specie	Protein (a.u.)	Carbohydrate (a.u.)	Lipid (a.u.)
Standard vs Transitional	*Synechocystis* sp. PCC6803	1:0.7	1:5	1:13
	Synechococcus sp. WH7803	1:2.5	1:2	1:3
Standard vs Proterozoic	*Synechocystis* sp. PCC6803	1:1	1:3	1:11
	Synechococcus sp. WH7803	---	---	---
Transitional vs Proterozoic	*Synechocystis* sp. PCC6803	0.7:1	5:3	13:11
	Synechococcus sp. WH7803	---	---	---

Table 21 *Macromolecular pools comparison: the arbitrary values (a.u.) are based on those present in* ***Table 20***

As shown in **Figure 31**, the amount of proteins in *Synechocystis* varies slightly between standard and transitional conditions. During the statistical analyses performed for protein compound, the ANOVA test underlines a *p value* <0.05, applying the post hoc (Turkey test) the differences are not significant despite from the graph is possible to see a difference between the transitional condition and the other two. Instead, there is a significant increase in the carbohydrates and lipid amounts considering the standard and transitional conditions. Moreover, there is also a variation between the transitional and proterozoic conditions in both carbohydrates and lipids, but since the error is large there is no statistical significance of the difference in the means.

If we consider the distribution of the biological replicates within each sample (**Figure 32**) instead of the average (**Figure 31**), it's possible to observe that values in standard conditions are more constant than those in the transitional one.

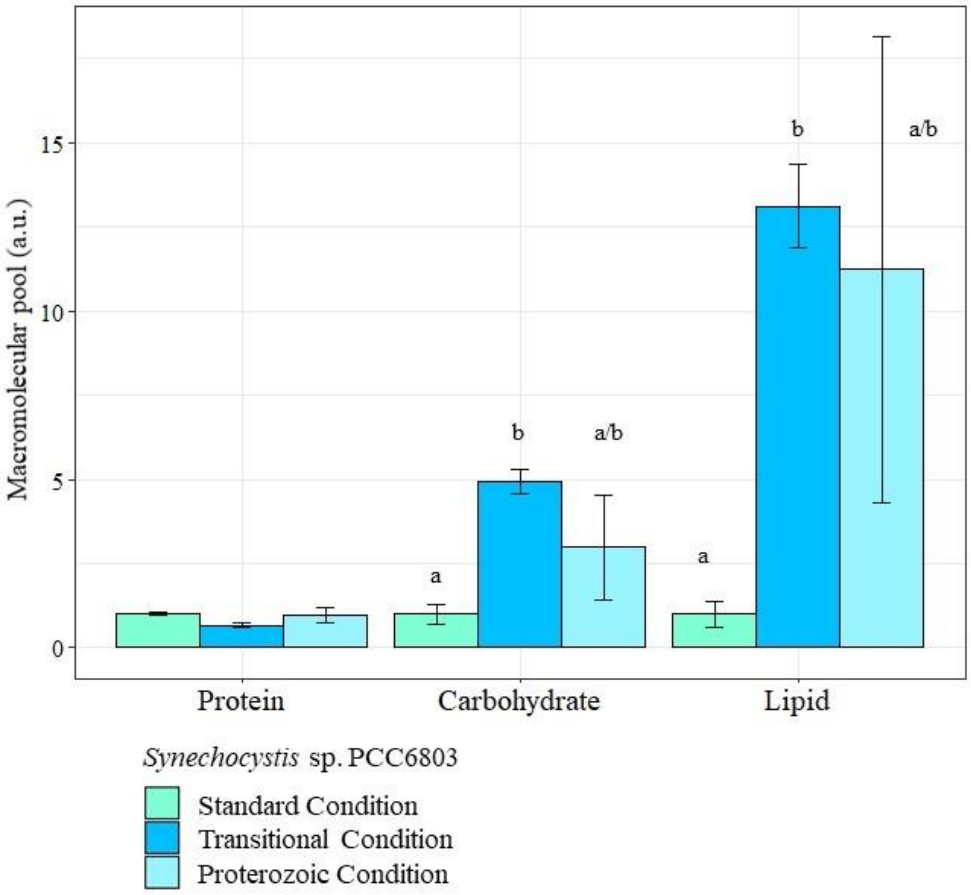

Figure 31 *Macromolecular amount comparison in arbitrary unit (a.u.) in Synechocystis sp. PCC6803. The values of macromolecular pools in transitional and proterozoic conditions were normalized to the values in the standard condition. The error bars represent the standard deviations, different letters indicate statistically different values. Each column is representative of 3 biological replicates. For each molecular pool, an ANOVA was performed. Standard values were set as 1.*

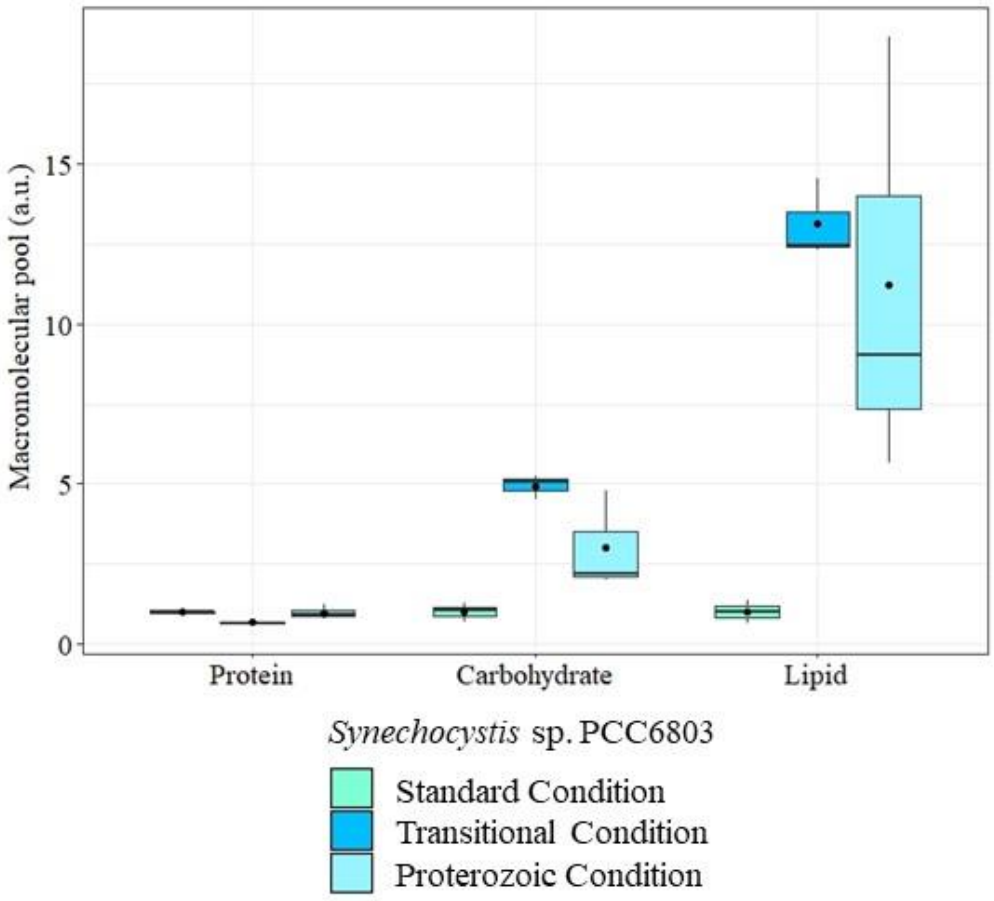

Figure 32 *Macromolecular in arbitrary unit (a.u.) in Synechocystis sp. PCC6803. The values of macromolecular pools in transitional and proterozoic conditions were normalized to the values in the standard condition. Each box (3 biological replicates) represents the interquartile range of a specific condition: the black spot represents the mean of the sample while the black line is the median and represents the second quartile Q_2. Above the line is the upper quartile Q_3 while below the line is the lower quartile Q_1. The lines that come out from each box represent the minimum (lower) and the maximum (higher) value in the data. For each molecular pool, an ANOVA was performed. Standard values were set as 1.*

In *Synechococcus* (**Figure 33**), despite the variations are spread in all the organic pool considered, the increase of carbohydrates and lipids are less important than those occurring in *Synechocystis*. Indeed, in the seawater specie, the increases are always around the triple of the standard values (**Table 21** and **Figure 33**), while in *Synechocystis* the gap is higher. For example, for lipids, the proterozoic value is more than ten times higher than the standard value (**Table 21**).

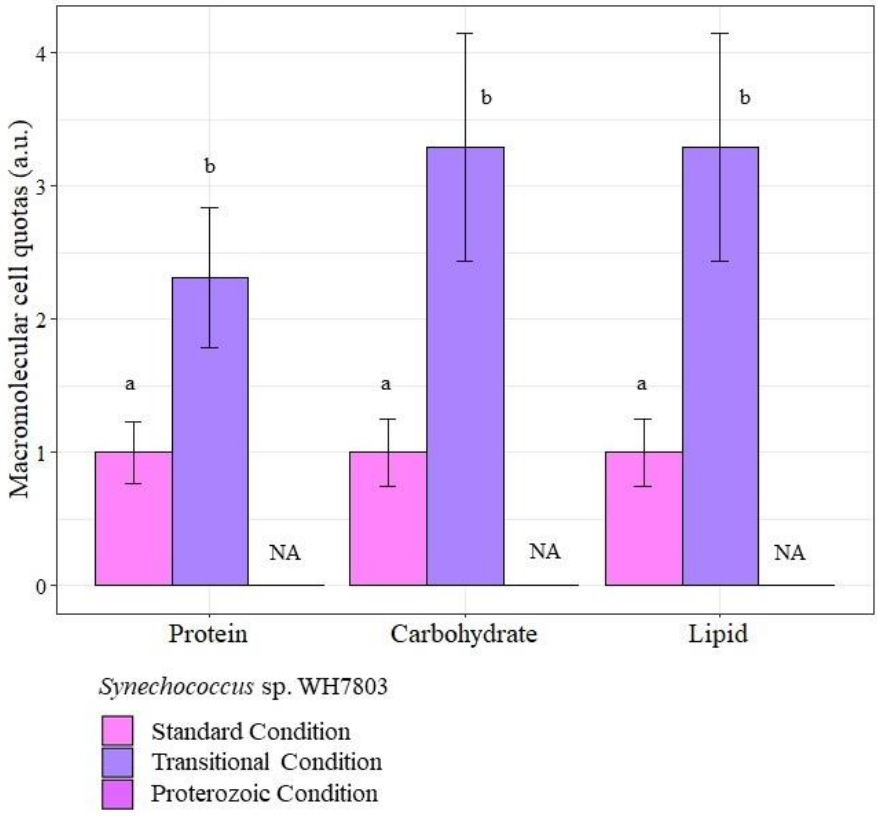

Figure 33 *Macromolecular cell quotas in arbitrary unit (a.u.) in Synechococcus sp. WH7803. The values of macromolecular pools in transitional and proterozoic conditions were normalized to the values in the standard condition. The error bars represent the standard deviations, different letters indicate statistically different values. Each column is representative of 3 biological replicates. For each molecular pool, a t-Test was performed. NA indicates the impossibility to analyze/perform the experiment for the proterozoic condition.*

Again, if we consider the biological replicates instead of the average as in **Figure 34**, it's possible to observe that values in standard conditions are more constant than those in the transitional one. In both species, it is also possible to underline how the protein value presents a lower variability (i.e. a lower error between biological replicates) probably due to the direct detection method. Indeed, carbohydrates and lipids are in any case derived from an indirect procedure and thus, they are more subject to errors.

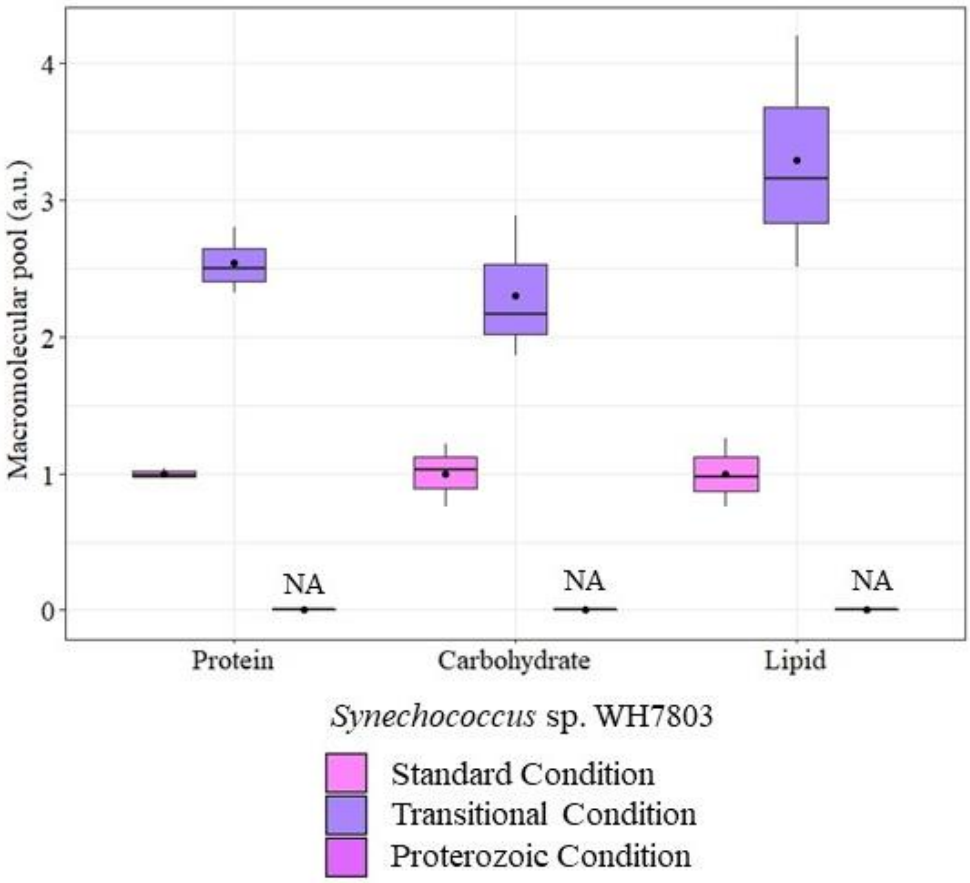

Figure 34 *Macromolecular cell quotas in arbitrary unit (a.u.) in Synechococcus sp. WH7803. The values of macromolecular pools in transitional and proterozoic conditions were normalized to the values in the standard condition. For each molecular pool, a t-Test was performed. Each box (3 biological replicates) represents the interquartile range of a specific condition: the black spot represents the mean of the sample while the black line is the median and represents the second quartile Q_2. Above the line is the upper quartile Q_3 while below the line is the lower quartile Q_1. The lines that come out from each box represent the minimum (lower) and the maximum (higher) value in the data. NA indicates the impossibility to perform the experiment.*

Furthermore, infrared spectrometry is also used to obtain arbitrary ratios between principal macromolecular pools using the absorbances obtained from the spectra (**Table 22**). Variations in these ratios underline variation in the quality of the molecular pools themselves and represent the cell response to environmental redox conditions and nutrient availability.

As shown in **Figure 35**, the ratio between carbohydrate and lipid polls decrease in both specie from standard to proterozoic condition. Considering *Synechocystis*, it is clear how the difference between standard and transitional conditions is higher and statistically significant respect to the one between transitional and proterozoic conditions.

Specie	Macromolecular Ratio	Standard Condition	Transitional Condition	Proterozoic Condition
***Synechocystis* sp. PCC6803**	Carbohydrates/Protein	0.612^{a} (0.157)	4.530^{b} (0.366)	1.823^{c} (0.525)
	Lipid/Protein	0.054^{a} (0.018)	1.075^{b} (0.149)	0.597^{c} (0.235)
	Carbohydrate/Lipid	11.5^{a} (0.967)	4.24^{b} (0.276)	3.18^{b} (0.689)
***Synechococcus* sp. WH7803**	Carbohydrates/Protein	1.94^{a} (0.39)	1.76^{a} (0.23)	N.A.
	Lipid/Protein	0.06^{a} (0.014)	0.08^{a} (0.013)	N.A.
	Carbohydrate/Lipid	31.2^{a} (1.30)	22^{b} (0.97)	N.A.

Table 22 *Molecular pool ratios. Standard deviation is indicated in brackets, different letters indicate statistically different values. NA indicates the impossibility to perform the experiment for the proterozoic condition.*

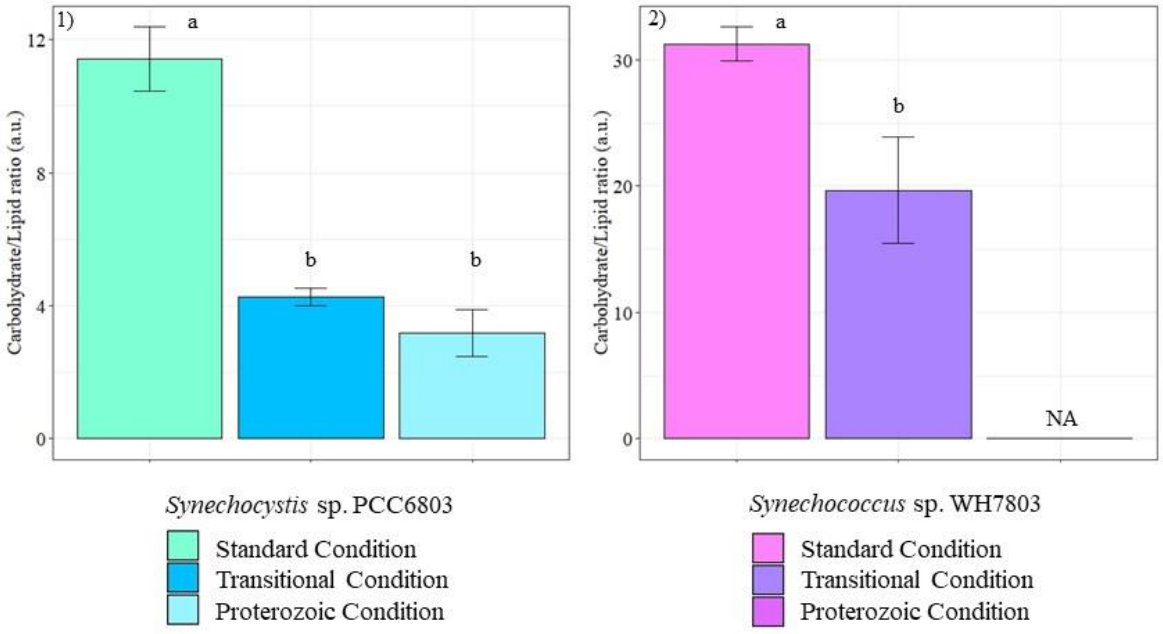

Figure 35 *Carbohydrate/Lipid ratio. 1) Synechocystis sp. PCC6803; the error bars represent the standard deviations and different letters indicate statistically different values. Each column is representative of 3 biological replicates (p <0.0001; ANOVA and Tukey test as post hoc). 2) Synechococcus sp. WH7803; the error bars represent the standard deviations and different letters indicate statistically different values. Each column is representative of 3 biological replicates (t-Test, p =0.0105). NA indicated the impossibility to perform the experiment for the proterozoic condition.*

Furthermore, comparing how both species react to the transitional condition it is important to point out how in *Synechocystis* the value in the transitional condition is almost a third of the one in standard condition while in *Synechococcus* the value decreases down to 2/3 respect the one in the standard condition.

The lipid/protein ratio changes greatly in *Synechocystis* (**Figure 36** and **Table 22**): the value increase from 0.06 in standard condition up to 1 in the transitional one. There is also a small decrease between transitional and proterozoic conditions. On the other hand, in *Synechococcus*, the value remains constant. The last ratio analyzed is the one between carbohydrates and proteins (**Figure 37**). Also, in this case, *Synechococcus* shows the consistency of values between the two analyzed conditions. In *Synechocystis* instead, the ratio value increases seven and a half times from standard to transitional conditions.

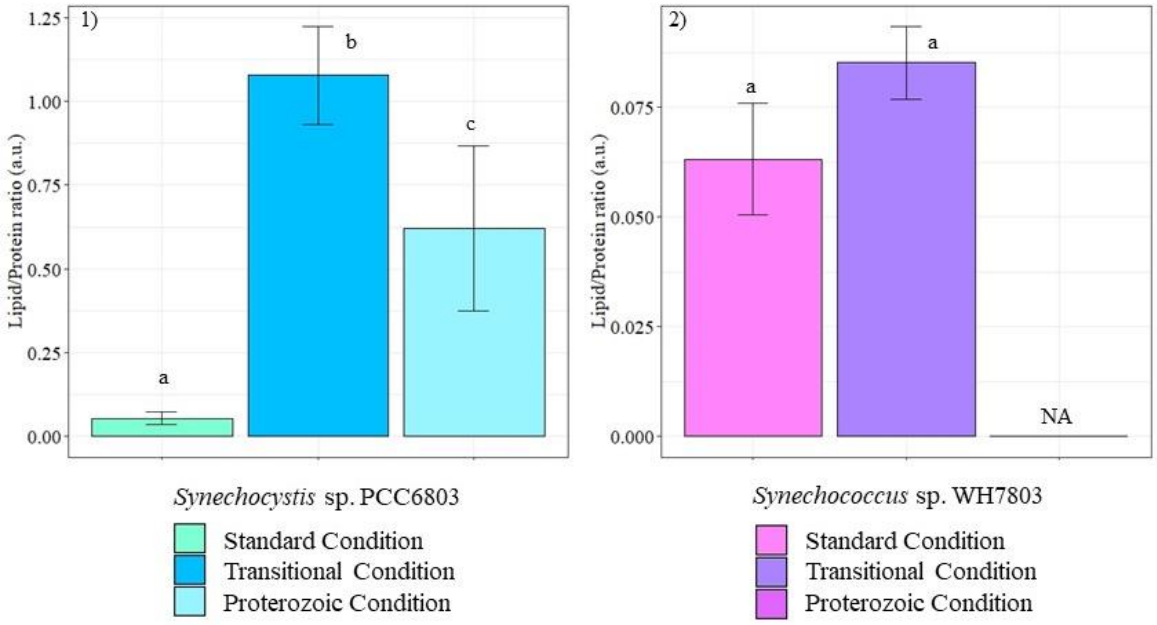

Figure 36 *Lipid/Protein ratio. 1) Synechocystis sp. PCC6803; the error bars represent the standard deviations and different letters indicate statistically different values. Each column is representative of 3 biological replicates (p =0.0008; ANOVA and Tukey test as post hoc). 2) Synechococcus sp. WH7803; the error bars represent the standard deviations and different letters indicate statistically different values. Each column is representative of 3 biological replicates (t-Test, p >0.05). NA indicated the impossibility to perform the experiment for the proterozoic condition.*

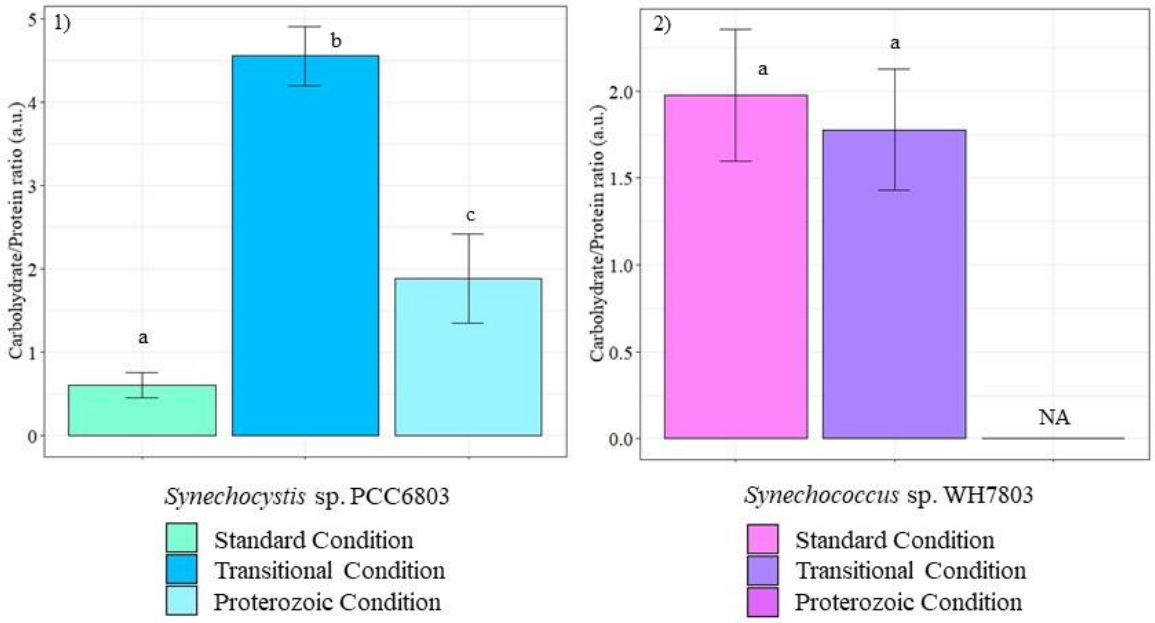

Figure 37 *Carbohydrate/Protein ratio. 1) Synechocystis sp. PCC6803; the error bars represent the standard deviations and different letters indicate statistically different values. Each column is representative of 3 biological replicates (p =0.0001; ANOVA and Tukey test as post hoc). 2) Synechococcus sp. WH7803; the error bars represent the standard deviations and different letters indicate statistically different values. Each column is representative of 3 biological replicates (t-Test, p >0.05). NA indicates the impossibility to perform the experiment for the proterozoic condition.*

3.3.3 Element composition

3.3.3.1 Carbon and Nitrogen amount

The elemental quotas as mg per g of dry weight were analyzed (**Table 23**). Analyzing first the most important abundant elements in cyanobacterial cells, it's clear how carbon content, for example, varied in both species (**Figure 38**). In this case, despite the ANOVA analyses returns a $p<0.05$ in Synechocystis, from the graph it is possible to detect a difference between the transitional condition and the other two. This difference is also underlined in **Figure 39** where is possible to compare the biological replicates within single conditions. Nitrogen, on the other hand, undergoes a statistically significant decrease in both specie from standard to transitional conditions (**Figure 38**, **Figure 39** and **Figure *40***).

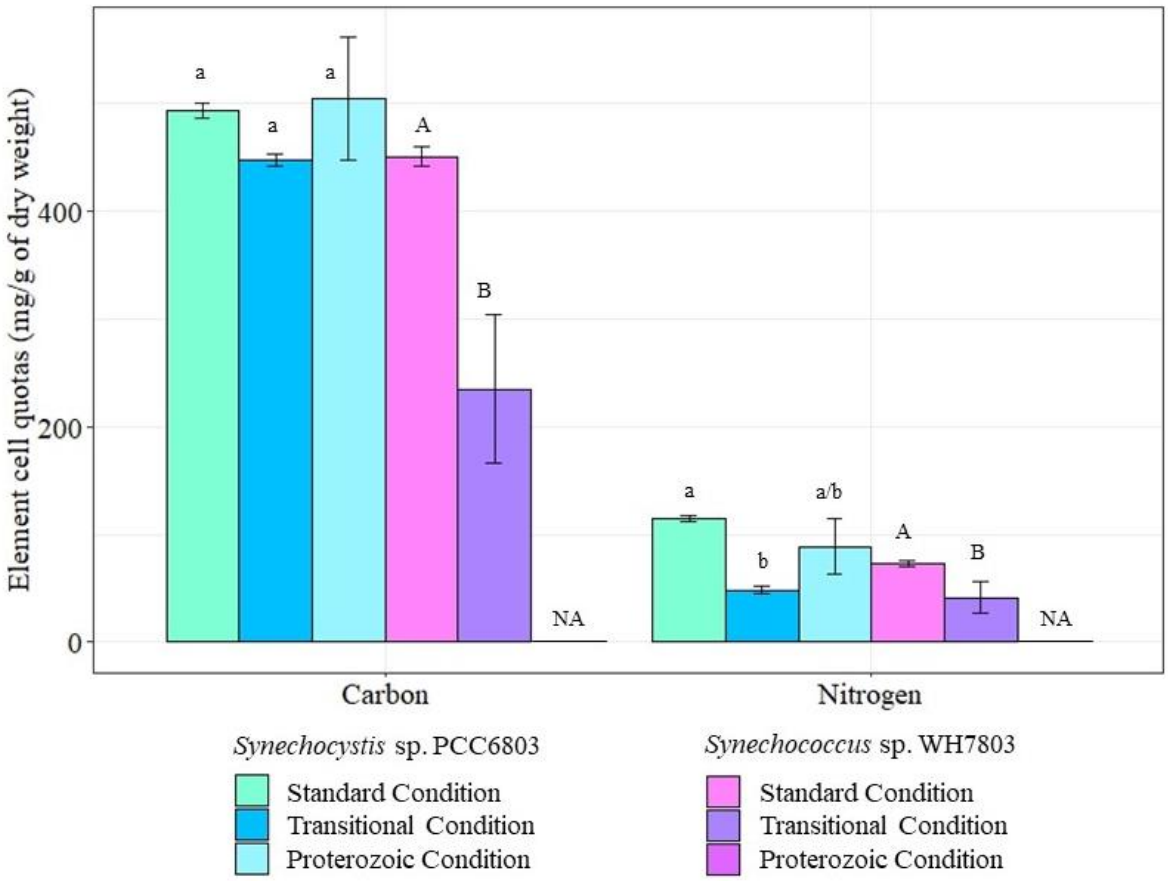

Figure 38 *Carbon and Nitrogen quotas calculated in mg in g of dry weight in Synechocystis sp. PCC6803 [Carbon: p >0.05; One-way ANOVA test and Tukey test as post hoc; Nitrogen: p = 0.02732; KRUSKAL – WALLIS test and PAIRWISE test as post hoc] and in Synechococcus sp. WH7803 cells. The error bars represent the standard deviations and different letters indicate statistically different values [Carbon: p <0.05; Nitrogen: p <0.05; t-Test]. The error bars represent the standard deviations while different letters indicate statistically different values. Each column is representative of 3 biological replicates. NA indicates the impossibility to perform the experiment for the proterozoic condition.*

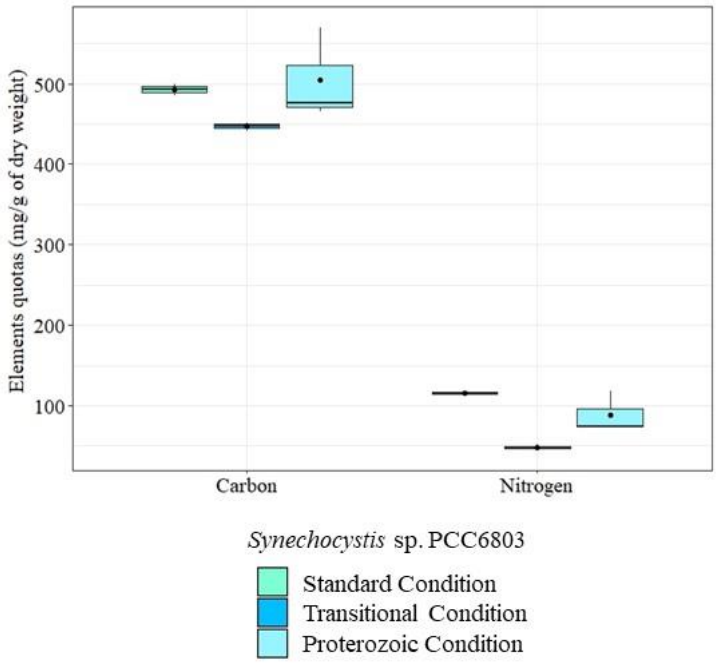

Figure 39 *Carbon and Nitrogen quotas calculated in mg in g of dry weight for Synechocystis sp. PCC6803. Each box is representative of 3 biological replicates and represents the interquartile range of a specific condition: the black spot represents the mean of the sample while the black line is the median and represents the second quartile Q_2. Above the line is the upper quartile Q_3 while below the line is the lower quartile Q_1. The lines that come out from each box represent the minimum (lower) and the maximum (higher) value in the data.*

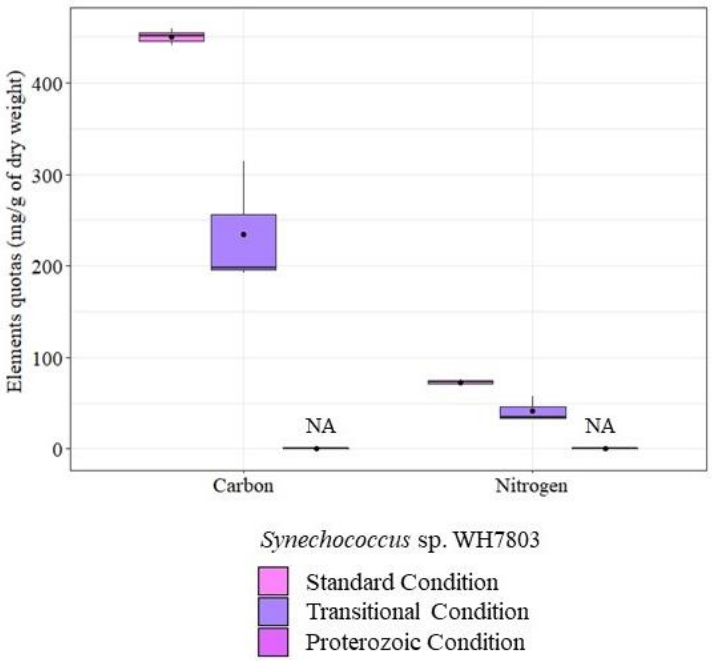

Figure 40 *Carbon and Nitrogen quotas calculated in mg in g of dry weight for Synechococcus sp. WH7803. Each box is representative of 3 biological replicates and represents the interquartile range of a specific condition: the black spot represents the mean of the sample while the black line is the median and represents the second quartile Q_2. Above the line is the upper quartile Q_3 while below the line is the lower quartile Q_1. The lines that come out from each box represent the minimum (lower) and the maximum (higher) value in the data. NA indicates the impossibility to perform the experiment.*

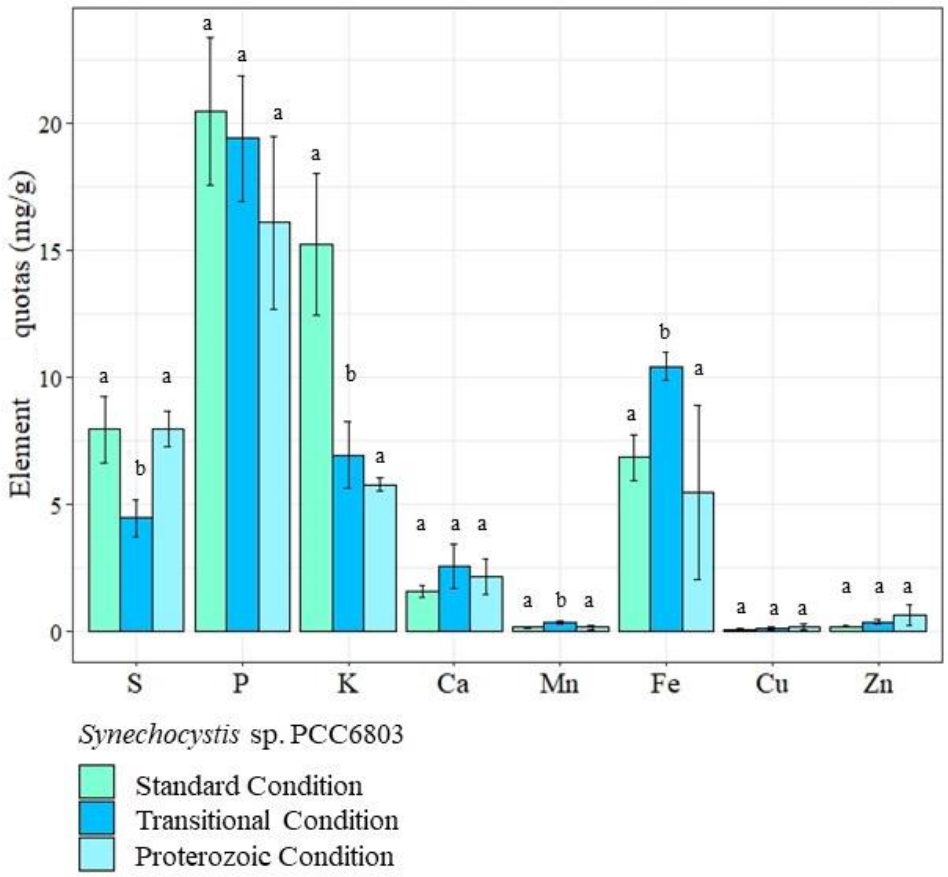

Figure 41 *Sulfur, Phosphorus, Potassium, Calcium, Magnesium, Iron, Copper and Zinc quotas for Synechocystis sp. PCC6803 calculated in mg in g of dry weight. The error bars represent the standard deviations and different letters indicate statistically different values. Each column is representative of 3 biological replicates. For each element, an ANOVA analysis was performed.*

Among other elements, *Synechocystis* presents an important difference in sulfur quotas of transitional condition, which results much lower than the standard and the proterozoic ones (**Figure 41**). Other variations, not considering those trace elements with a high error within the instrumental replicates, are detected in iron and potassium, once again, between standard and transitional conditions (**Figure 41**).

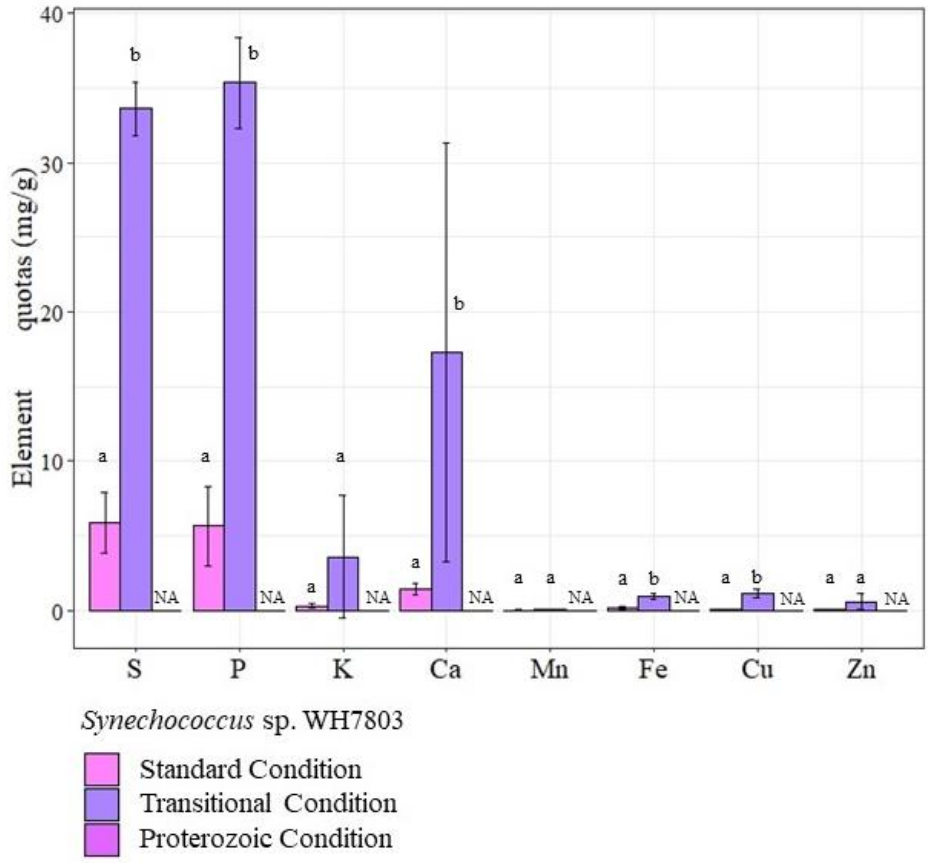

Figure 42 *Sulfur, Phosphorus, Potassium, Calcium, Magnesium, Iron, Copper and Zinc quotas for Synechococcus sp. WH7803 calculated in mg in g of dry weight. The error bars represent the standard deviations and different letters indicate statistically different values. Each column is representative of 3 biological replicates. For each element, a t-Test analysis was performed. NA indicates the impossibility to analyze/perform the experiment for the proterozoic condition.*

In *Synechococcus* (**Figure 42**), on the other hand, the differences are more detectable: the variation in sulfur quotas is higher between standard and transitional conditions and in this case, there is an increase unlike in *Synechocystis*. In seawater species also the phosphorus, calcium and iron quotas increase from standard to transitional conditions underling a higher response in cell composition under limiting environment (**Figure 42**).

Despite the variation in the total amount of single elements (**Table 23**), the cell ratios between the most important elements for cyanobacteria (**Table 24**), which means carbon, nitrogen, sulfur, and phosphorus, are maintained almost constant in *Synechocystis*. The only two appreciable exceptions are the carbon/nitrogen ratio in the transitional condition that increases respect to the other two, and the carbon/sulfur ration also in the transitional condition (**Table 24**).

Conditions	**Standard (mg/g of dry weight)**		**Transitional (mg/g of dry weight)**		**Proterozoic (mg/g of dry weight)**	
Elements	PCC6803	WH7803	PCC6803	WH7803	PCC6803	WH7803
C	492^{a} (7.09)	451^{A} (9.37)	447^{a} (5.28)	235^{B} (68.5)	504^{a} (57.2)	N.A.
N	115^{a} (2.70)	73.0^{A} (2.77)	48.2^{b} (3.53)	41.6^{B} (14.2)	$88.5^{a/b}$ (25.8)	N.A.
S	7.97^{a} (1.31)	5.87^{A} (2.03)	4.49^{b} (0.73)	33.7^{B} (1.78)	7.99^{a} (0.70)	N.A.
P	20.5^{a} (2.91)	5.64^{A} (2.63)	19.4^{a} (2.47)	35.4^{B} (3.05)	16.1^{a} (3.40)	N.A.
K	15.3^{a} (2.79)	0.29^{A} (0.17)	6.95^{a} (1.30)	3.59^{A} (4.16)	5.79^{a} (0.27)	N.A.
Ca	1.60^{a} (0.23)	1.41^{A} (0.40)	2.57^{a} (0.86)	17.3^{A} (14.1)	2.18^{a} (0.72)	N.A.
Mn	0.19^{a} (0.03)	0.01^{A} (0.002)	0.38^{b} (0.07)	0.05^{A} (0.05)	0.18^{a} (0.07)	N.A.
Fe	6.85^{a} (0.93)	0.16^{A} (0.05)	10.4^{a} (0.55)	0.93^{B} (0.18)	5.50^{a} (3.41)	N.A.
Cu	0.09^{a} (0.04)	0.02^{A} (0.01)	0.14^{a} (0.04)	1.08^{B} (0.29)	0.22^{a} (0.10)	N.A.
Zn	0.23^{a} (0.03)	0.05^{A} (0.02)	0.40^{a} (0.08)	0.59^{A} (0.54)	0.65^{a} (0.40)	N.A.

Table 23 *Principal element amount in the experimental organism under the tested environments, the standard deviation is indicated in brackets and different letters represent a statistical significance ($p<0.05$). Also, in this case, 3 biological replicates were used. Due to an important error between instrumental replicates, some of the standard deviations are so important that is not possible to discriminate differences between conditions. NA indicates the impossibility to analyze/perform the experiment for the proterozoic condition.*

Specie	Elements Ratio	Standard Condition	Transitional Condition	Proterozoic Condition
***Synechocystis* sp. PCC6803**	C:N	4.28[a] (0.079)	9.31[b] (0.581)	5.88[a] (0.918)
	C:P	24.4[a] (3.49)	23.3[a] (3.43)	32.6[a] (9.46)
	C:S	63[a] (10.5)	101.4[b] (16.6)	63.4[a] (8.63)
	N:P	5.70[a] (0.76)	2.53[a] (0.54)	5.82[a] (2.70)
	N:S	14.7[a] (2.45)	11[a] (2.33)	11.1[a] (3.37)
	P:S	2.58[a] (0.20)	4.36[b] (0.55)	2.01[a] (0.30)
***Synechococcus* sp. WH7803**	C:N	6.18[a] (0.17)	5.71[a] (0.29)	N.A.
	C:P	91.8[a] (39.5)	6.61[b] (1.57)	N.A.
	C:S	83.6[a] (29.9)	6.97[b] (1.88)	N.A.
	N:P	14.9[a] (6.38)	1.17[b] (0.33)	N.A.
	N:S	13.5[a] (4.80)	1.23[b] (0.39)	N.A.
	P:S	0.94[a] (0.11)	1.05[a] (0.04)	N.A.

Table 24 *Elements ration. Standard deviation is indicated in brackets and different letters represent a statistically significant difference.*

Specie	Conditions	Redfield Ratio
***Synechocystis* sp. PCC6803**	Standard Condition	C : N : P : S 24 : 5.6 : 1 : 0.39
	Transitional Condition	C : N : P : S 23 : 2.5 : 1 : 0.23
	Proterozoic Condition	C : N : P : S 31 : 5.5 : 1 : 0.49
***Synechococcus* sp. WH7803**	Standard Condition	C : N : P : S 80 : 13 : 1 : 1.04
	Transitional Condition	C : N : P : S 6.6 : 1.7 : 1 : 0.95
	Proterozoic Condition	----------

Table 25 *Redfield ratio based on* ***Table 23*** *and* ***Table 24*** *values.*

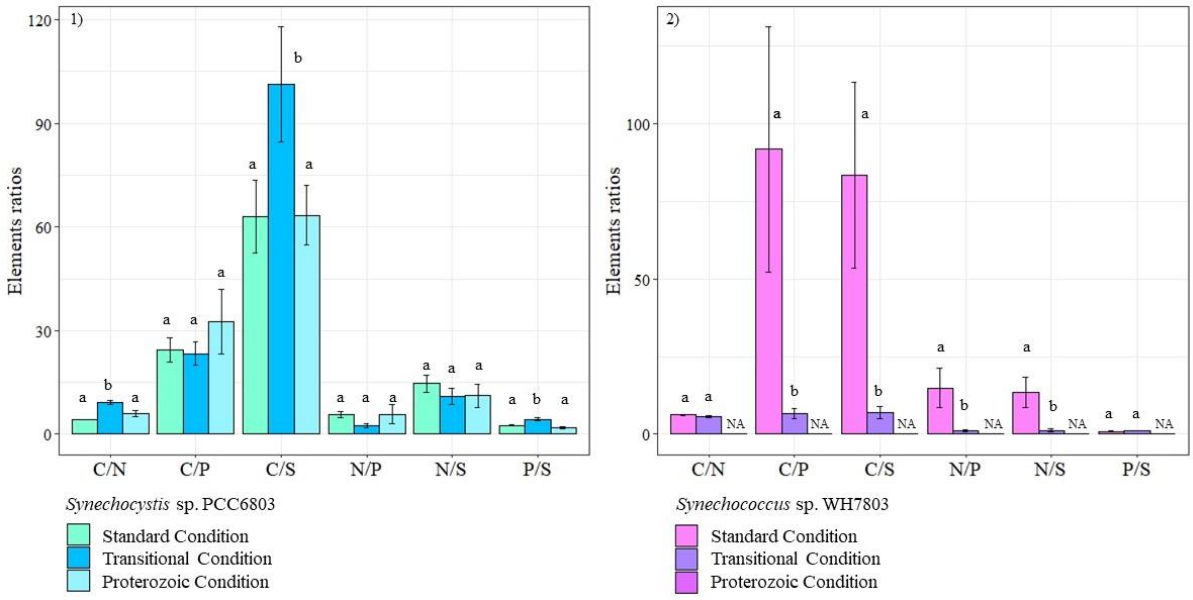

Figure 43 *Element ratios inside Synechocystis sp. PCC6803 (ANOVA) and Synechococcus sp. WH7803 (t-Test) culture, the error bars represent the standard deviations and different letters represent a statistically significant difference. Each column is representative of 3 biological replicates. NA indicated the impossibility to analyze/perform the experiment for the proterozoic condition.*

From elements quantification is also possible to obtain the Redfield ratio for each condition as shown in **Table 25**: normalizing everything to phosphorous, it is possible to underline some variations (Giordano and Prioretti, 2016; Redfield, 1934). In *Synechocystis* for example, the transitional condition ratio appears very different from the other two conditions ones. In *Synechococcus*, instead, results show how the ratio change completely in the transitional condition where sulfur becomes the limiting element rather than phosphorous.

On the other hand, *Synechococcus* shows important decreases in all ratio, except for the carbon/nitrogen ratio that is maintained constant between standard and transitional conditions (**Table 24**). As a general comment, *Synechocystis* seems to be more stable than *Synechococcus* if it undergoes stressful environmental conditions.

“E quindi uscimmo a riveder le stelle.”

La Divina Commedia
Inferno
Canto Trentaquattresimo – 139

“Thence we came out, and saw again the stars.”

La Divina Commedia
Hell
Chapter Thirty – 139

DISCUSSION

It is overall recognized that the evolution of oxygenic photosynthesis in ancient cyanobacteria had a great role in influencing the progression of the redox state of the planet (Hamilton et al., 2016). This concept links their development with the creation of the present atmosphere, making the understanding of their evolution even more complicated. Problems about the timing of their evolution are related especially with the detection of some gaseous oxygen before the GOE (whiff of oxygen - (Anbar et al., 2007; Crowe et al., 2013; Scott et al., 2008) that could imply the presence of some photosynthetic microorganisms. Theoretically, it can be either (1) that oxygenic photosynthesis evolved around 2.4Gyr ago and oxygenated the atmosphere and then the oceans; or (2) that oxygen consumption corresponded to photosynthetic production for the first millions of years of cyanobacterial history. In the second case, the GOE would take place a long time after the evolution of oxygenic photosynthesis due to several biological and geochemical phenomena, enclosed, but not only, the increase of oxygenic photosynthesis rate (Grula, 2012; Knoll and Nowak, 2017). Recent studies (Cardona, 2015; Cardona et al., 2015) demonstrate that the evolution of oxygenic photosynthesis took place prior the evolution of oxidative phototroph and, some theories proposed that cyanobacteria evolved before the great oxygenation event in freshwater environments (Sánchez-Baracaldo, 2015; Sánchez-Baracaldo et al., 2017).

However, it is generally accepted that before 2.5Gyr ago, the atmosphere was poor of free oxygen (at least less than 10 -5 PAL, Pavlov and Kasting, 2002) and overall much less oxidizing than the actual one (Papineau et al., 2007b). The first stable presence of oxygen in the atmosphere seems to happen between 2.4 and 2.1Gyr ago and is today identified as GOE (Lyons et al., 2014). Most of the data supporting the GOE development during the Paleoproterozoic period are based on sedimentary records, in particular on the presence/absence of (1) the iron deposits and (2) of the sulfur deposits. The presence of Banded Iron Formations (BIFs) and pyrite in oceanic sediments (Farquhar et al., 2010b; Fischer and Knoll, 2009; Hamilton et al., 2016) along with the lack of red beds in continental sediments confirmed the lower level of oxygen in the Archean atmosphere (Canfield, 2014; Fischer et al., 2016b; Pavlov and Kasting, 2002). The oxygenation of the atmosphere has continued for the most part of the Proterozoic Eon, during which there was the alternation of huge oxidation events (at least two - Lyons et al., 2014) and several ice periods (Hoffman, 2016; Hoffman et al., 2017). Finally, at the beginning of Phanerozoic eon, the level of

atmospheric oxygen arrived at the present atmospheric level, after at least 2.0Gyr from the GOE (Canfield, 2005; Hamilton et al., 2016).

Eventually, the increase in the molecular oxygen availability had 2 main consequences, connected to each other. First of all, (A) molecular oxygen started to compete for the active site of Rubisco in micro autotrophs (Rickaby and Eason Hubbard, 2019), secondly, (B) the environment underwent a shift in the general oxidizing level (Papineau et al., 2007). An experimental approach that uses the setup of a reconstructed precambrian environment is useful to investigate evolutive constraints on specific metabolisms (Giordano et al., 2018; Ratti et al., 2011, 2013).

(A) Cyanobacteria evolved the oxygenic photosynthesis in an anoxic environment that, despite the evolution of oxygen, remained at least hypoxic and highly unstable until the GOE occurred at the end of the proterozoic eon (Anbar et al., 2007; Grula, 2012; Knoll and Nowak, 2017; Lyons et al., 2014). In this situation, the specificity of the RubisCO enzyme for CO_2 was not fundamental since there was not enough O_2 to strongly compete for its active site. Moreover, it can be hypnotized that during the paleoproterozoic, geochemical oxygen consumption was important (Knoll and Nowak, 2017). When the oxygenic photosynthesis rate increased, due to adaptation of their physiology to a changing environment, gaseous oxygen increased and became highly competitive in several biochemical reactions, first of all for the active site of RubisCO. This idea seems to find confirmation in the variation of oxygen net production curve which was analyzed within the reconstructed precambrian environment set up for this work (**Figure 24**). Indeed, if the O_2 produced during the photosynthesis reactions is recycled in the photorespiration pathway of the cell with high efficiency, a higher light intensity is needed to arrive at a net O_2 production. This explains the higher compensation point which moves from 23 to 190µmol photons/$m^2 \cdot s^{-1}$(**Figure 24** and **Table 16**). This idea is reinforced by the timing of carboxysome evolution, which is 0.3Gya ago (Rae et al., 2013). Indeed, carboxysome and the whole carbon concentration mechanisms pathway evolved after the amount of oxygen in the atmosphere and in the ocean became so high that the RubisCO enzyme was probably not able anymore to guarantee a suitable carbon fixation. Indeed, in that changing situation, its specificity for CO_2 relative to O_2 was not enough anymore to assure the cell an efficient inorganic carbon fixation rate.

(B) The shift in the oxidizing level of the environmental (Papineau et al., 2007), force an increase in power demand to perform basal metabolism. Indeed, main assimilation pathways (for the incorporation of C, N, S in organic pools) need reducing power in the form of available electrons to be performed. Since oxygen outside and inside the cell acts as an electron sink (Knoll and Nowak, 2017), tighter control on the redox power usage in the cell can be present. The whole-cell physiology was also deeply affected by the new level of oxidative stress induced by reactive oxygen species (Fischer et al., 2016a). Within this context, the different reactions of experimental organisms to the paleo-reconstruct environment can be interpreted and explained both at the physiological level and considering their evolutionary history.

The first important data set regards those variations detected in the growth, which underline the effect of oxygen and nutrients availability variations.

The results of this study show that the availability of dissolved oxygen influenced cell growth in both species. In particular, the specie evolved more recently, *Synechococcus* sp. WH7803 (Sánchez-Baracaldo, 2015) was not able to grow in a reconstructed proterozoic environment (**Figure 20**), while *Synechocystis* sp. PCC6803 (which is identified as an ancient species - Sánchez-Baracaldo, 2015) was able to survive both in transitional and proterozoic environments despite the stressful conditions present in those conditions (**Figure 20**). Furthermore, data showed that *Synechococcus* specie had a better growth rate in the transitional conditions rather than in the standard conditions. These results suggest that this species evolved in an environment where (1) sulfur was limiting compared to the modern ocean, and (2) the oxic conditions were similar to the present ones rather than those in the proterozoic eon. This interpretation supports the *Synechococcus* sp. WH7803 evolution during the phanerozoic eon (Sánchez-Baracaldo, 2015). On the other hand, results underline also that *Synechocystis* sp. PCC6803 can survive in both (1) an environment with low nutrients and (2) in a hypoxic environment as demonstrated by other works (Thomas et al., 2005). These results are supported by Hermann and collaborators' work (Herrmann and Gehringer, 2019) who recently performed a set of experiments based on archean environmental conditions and freshwater cyanobacterial physiology. In this work (Herrmann and Gehringer, 2019), *Gloeobacter violaceus*, which is the most ancient species of oxygenic photosynthesis cyanobacteria present on the planet today; and *Chroococcidiopsis thermalis*, a salt-tolerant freshwater cyanobacteria, were cultured under different oxic conditions coupled with salinity variation. The purpose was to investigate the

faculty of modern descendants of ancient freshwater cyanobacteria to survive and grow under brackish and marine conditions. This capacity may have allowed them to give rise to ocean species which have caused the GOE (Herrmann and Gehringer, 2019). Herrman's work supported the hypothesis of cyanobacterial evolution in the freshwater environment and subsequent transition in the marine one. These findings endorse the idea of a more ancient evolution for *Synechocystis* sp. PCC6803, probably in a limiting and changing environment. This hypothesis of freshwater cyanobacteria evolution reinforces the Sanchez-Baracaldo phylogenetic approach, which claims the origin of cyanobacteria in freshwater ancient environment (Sánchez-Baracaldo, 2015; Sánchez-Baracaldo et al., 2017; Schirrmeister et al., 2016). Secondly, ancient freshwater cyanobacteria evolved specific physiological mechanisms that allowed them to conquer the precambrian ocean (Sánchez-Baracaldo, 2015; Sánchez-Baracaldo et al., 2017; Schirrmeister et al., 2016). On the other hand, Tria and collaborators suggested instead that cyanobacteria evolved in the ocean and only later they spread in all the aquatic environments on the planet (Tria et al., 2017). These theories are still under discussion but results from this work endorse the "freshwater origin theory".

Detected differences in growth rate can also be influenced by different nitrogen sources available in the growth media: (1) NO_3^{2-} in the standard conditions and (2) NH_4^+ in transitional and proterozoic ones. In *Synechocystis*, growth rate decreases changing from NO_3^{2-} to NH_4^+, while in *Synechococcus* an increase was observed. These results can be interpreted considering the oxidation level of the nitrogen compound or the toxicity of the molecules itself. NH_4^+ requires less energy than nitrate to be acquired and assimilated by the cell, thus cells should prefer ammonium over nitrate following the so called "metabolic cost hypothesis". However, this theory is still debated since is not real for all picocyanobacteria specie (Collier et al., 2012). Nevertheless, it was observed that iron concentration in the growth medium can influence the nitrogen assimilation pathway. For example, Kudo and collaborators reported that under low iron concentration, *Synechococcus* cell growth faster with NH_4^+ than with nitrate (Kudo and Harrison, 1997). Moreover, Raven calculated that nitrate assimilation requires a high amount of iron (60%) since nitrate and nitrite reductase possess Fe cluster (Raven, 1988). As a consequence, extra iron is required for nitrate assimilation compared to ammonium one (Schoffman et al., 2016). One recent work, however, underlines the role of specific enzymatic limitation in the nitrate assimilation pathway (Collier et al., 2012). This may be more important than the "metabolic cost hypothesis" for nitrate vs ammonium discrimination (Collier et al., 2012). Furthermore,

ammonium can become toxic for photosynthetic organisms since it increases the speed of photodamage in the PSII, but some works reported that *Synechocystis* sp. PCC6803 is able to constrain this kind of effect (Drath et al., 2008).

Synechocystis was able to survive in low nutrient transitional and proterozoic conditions even though oxygen concentration was very different: cell density decreased in both transitional and proterozoic conditions (**Figure 20**) in response to low iron, sulfur and nitrogen concentrations. *Synechococcus* showed a similar trend: in transitional condition, with low iron, sulfur and nitrogen concentrations, a decrease in cell density was observed (**Figure 20**). These results confirmed previous work on *Synechococcus* sp. WH7803 growth under starving iron conditions (Kudo and Harrison, 1997). Despite variation in growth rate and in cell density, the carbon/nitrogen cell ratio (**Figure 43** and **Table 24**) results to be homeostatic in response to different experimental conditions in both *Synechocystis* and *Synechococcus* (**Table 24**). The only exception is represented by a higher C/N ratio in Synechocystis cells grown under transitional conditions as compared to other treatments (**Table 24**). It might be due to the protein content which decreased only in the transitional condition (**Table 24**).

In *Synechocystis*, considering differences between standard and transitional conditions, we observed (1) a decrease in proteins, (2) an increase in carbohydrates and (3) in lipids (4) and an increase in the C/N ratio. Considering instead the differences between standard and proterozoic condition, in *Synechocystis* resulted (1) a maintained value of proteins, (2) an increase in carbohydrates and (3) in lipids (4) while the C/N ratio is maintained stable. In *Synechococcus*, again considering differences between standard and transitional conditions, we observed an increase (1) in proteins, (2) in carbohydrates and (3) in lipids. Nevertheless, Redfield ratios vary between different experimental conditions (**Table 25**).

Interestingly, iron quotas per cell varied between the experimental conditions. In *Synechocystis*, the iron amount in mg per g of dry weight increases from standard to transitional conditions, while there was a decrease from standard to proterozoic conditions despite the dissolved iron was maintained constant in the three media (**Figure 41**). This reaction underlines probably an improvement of iron uptake. The same variation was found in *Synechococcus*: iron amount increases from standard to transitional condition despite iron concentration in the growth medium decreases (**Figure 42**). As reported in other studies (Kudo and Harrison, 1997), iron starvation in *Synechococcus* implies lower carbon and nitrogen content as observed in this work (**Table 23** and **Table 25**).

In both *Synechocystis* and *Synechococcus*, an increase in the redox index was also observed from standard to transitional conditions. (**Figure 30**). In both species when this increase is observed, also an increase in the lipid pool is detected (**Figure 32** and **Figure 34**). Since the reduction index increase implies a decrease in the unsaturated carbon chain, and a consequent decrease in the amount of energy stored in this compound (Alkorta and Elguero, 2006), the increase in lipid content is justified since lipids are important energetic store molecules. The increase in lipid content implies thought a different strategy in-store energy inside the cell. Furthermore, the variation of macromolecular pools, C/N ratio and reduction index between standard and proterozoic conditions can be considered for *Synechocystis*. In this case, protein content is maintained constant with carbon and nitrogen ones (consequently also the C/N ratio is constant). Also, in this case, an increase in the lipid compound corresponds to an increase in the reduction index (**Figure 30**). The increase in the macromolecular pools inside the cell is possible under starvation since the cell density decrease, as was observed in this work. An increase in stored molecular pools corresponds, on the other hand, to a lower number of cells that can be maintained in this situation. In this contest, the overall richness of cell culture is higher, but the cell density has decreased.

Variations in growth rates can be linked with those detected in the biomass productivity and in the variation of iron and sulfur cell quotas since those elements are used as cofactors for several metabolic enzymes. Indeed, carbon, nitrogen and sulfur metabolic pathways enclose proteins that have reaction centers with Fe-S cluster. The photosystems and the electron chain require, for example, at least 22 iron atoms (Raven, 1990; Raven et al., 1999) to perform the light reaction during photosynthesis, while nitrite and nitrate reductase have one Fe_4-S_4 cluster each (Flores et al., 2005). Furthermore, several enzymes involved in sulfur assimilation contain cysteine residues, above all ATPS enzyme (Giordano and Prioretti, 2016).

Since variations in the dissolved oxygen availability lead to a variation in the element concentration, cofactors' availability has changed too (Fike et al., 2015) and might have influenced physiology through time. Iron and sulfur variations in particular influenced greatly the evolution and the spread of photosynthetic phytoplankton. Oxygen accumulation led to an increase of oxygenic photosynthesis over anoxygenic photosynthetic bacteria for example (Knoll and Nowak, 2017). In this contest, it is important to mention the iron hypothesis (Martínez-García et al., 2014; Tagliabue et al., 2017) and the sulfur facilitation hypothesis (Giordano and Prioretti, 2016; Prioretti and Giordano, 2016; Ratti et al., 2011).

According to the iron hypothesis, an increase of dust-borne iron in the ocean has driven phytoplankton blooms through ages (Martínez-García et al., 2014). Cyanobacteria, as well as other photosynthetic organisms, have high iron quotas *per cell* as said (Raven, 1990; Raven et al., 1999). Therefore, under low iron conditions (as transitional and proterozoic conditions in this work can be considered) growth is expected to be limited, as actually was shown in the results. In the modern oxic condition where iron is a limiting element, the high amount of iron should be positive in some regions, however, the excess of iron is demonstrated to be dangerous for organisms with oxygenic photosynthesis complex as cyanobacteria due to the production of reactive oxygen species (ROS) between Fe(II) and oxygen (Swanner et al., 2015a, 2015b). This information suggests the huge importance of redox environmental conditions on marine cell physiology rather than the simple availability of nutrients. This idea is confirmed by the inability of *Synechococcus* to grow in proterozoic eon where the redox conditions are completely different than today. Some works (Swanner et al., 2015a, 2015b) confirmed these findings underling the role of environmental oxic conditions on cyanobacteria physiology. Swanner and collaborators grew different *Synechococcus* species under different iron and oxic conditions to test the physiological effect. It was demonstrated that elevated Fe(II) levels in hypoxic/anoxic conditions resulted in a decrease in growth rates in marine *Synechococcus* genus. The reason was found in ROS production associated with Fe(II) rich medium (Swanner et al., 2015a).

On the other hand, the increase in sulfur availability during eons, up to the levels present in the modern ocean, allowed the increase in the abundance of those microalgae containing a and c chlorophyll, since they have a higher sulfur cell quotas (Ratti et al., 2011). From this information, the sulfur facilitation hypothesis (Giordano and Prioretti, 2016; Prioretti and Giordano, 2016; Ratti et al., 2011) was proposed to explain the picophytoplankton evolution during times. This theory underlines the importance of sulfur metabolic pathway in cyanobacteria and unicellular algae, especially considering the redox power high cost of sulfate assimilation pathway (Giordano and Prioretti, 2016). This hypothesis also links sulfur metabolism with the oxidizing level of the environment. In proterozoic eon, the CO_2/O_2 ratio was higher than today, with the advantage of CO_2, and the oxygenic photosynthesis theoretically increases. Thus, the cell will have more available ATP produced by the photosynthetic reactions. Besides, considering the decrease in redox power availability in the cell due to the oxygenation of the planet, a tighter regulation on

cell metabolism was required to discriminate in which metabolic pathway invest the power available (Hamilton et al., 2016).

Everything considered, and recalling the regulation of ATPS enzyme, the activity of the redox-regulated ATP sulfurylase isoform should be higher than today in the proterozoic environment since there were high levels of redox power (and probably also of ATP, obtain from the new oxygenic photosynthesis in a CO_2 rich environment) rather than today where the redox power is limiting in the cell. On the other hand, the not redox-regulated ATPS isoform shouldn't show any appreciable variation. Yet, the ATPS activity showed a great decrease from standard to proterozoic conditions in *Synechocystis*, and, moreover, a small increase of the enzyme activity from transitional to proterozoic conditions. On the other hand, the ATPS activity in *Synechococcus* presented an enormous decrease from standard to transitional conditions. Nevertheless, S quotas in *Synechococcus* increases greatly (**Figure 42**), underling an improvement of S acquisition from the environment. In *Synechocystis* instead, there is a decrease in transitional condition compared to standard and proterozoic ones (**Figure 41**). Interpreting this data, a higher effect due to sulfate availability rather than oxygen concentration can be underlined. From results, it can be said that the O_2 accumulation in the environment might not have been the only, or neither the strongest, evolutive constraint for redox regulation in ATPS enzymes since the variation between standard and transitional conditions are stronger than those between transitional and proterozoic conditions regarding enzyme activity itself.

"Vuolsi così colà dove si puote
ciò che si vuole, e più non dimandare."

La Divina Commedia
Inferno
Canto Terzo – 95,96

"Thus is it yonder willed, where there is power
to do whate'er is willed; so ask no more!"

La Divina Commedia
Hell
Chapter Third – 95,96

CONCLUSION

The results from this work allowed to point out some information:

→ A changing in redox power deeply affects growth in selected cyanobacteria species, indeed, important differences were detected in both cyanobacteria growth rate under different culture conditions.

→ Both nutrient limitation and redox power variation have effect on the ATPS activity, but nutrient concentration proves to be more important. The differences between ATPS activity between standard and transitional conditions were indeed bigger than those between standard and proterozoic conditions (where was possible to detect them) underling a stronger effect of nutrients on the protein activity.

→ Nutrient availability affects elements and macromolecular profiles in cyanobacteria suggesting a modification of the physiology in order to survive to a challenging environment.

From these observations, it is possible to conclude that the oxygenation of the planet might not have been the only evolutive constraint for redox regulation in ATPS enzymes. Moreover, these information support the theory which states cyanobacteria evolved in the freshwater environment and only secondly conquered the seawater environment.

LIST OF FIGURES

LIST OF TABLES

BIBLIOGRAPHY

Alkorta, I., and Elguero, J. (2006). The carbon–carbon bond dissociation energy as a function of the chain length. Chem. Phys. Lett. *425*, 221–224.

Altermann, W., and Kazmierczak, J. (2003). Archean microfossils: a reappraisal of early life on Earth. Res. Microbiol. *154*, 611–617.

Anbar, A.D. (2008). Elements and Evolution. Science *322*, 1481–1483.

Anbar, A.D., and Knoll, A.H. (2002). Proterozoic Ocean Chemistry and Evolution: A Bioinorganic Bridge? Science *297*, 1137–1142.

Anbar, A.D., Duan, Y., Lyons, T.W., Arnold, G.L., Kendall, B., Creaser, R.A., Kaufman, A.J., Gordon, G.W., Scott, C., Garvin, J., et al. (2007). A Whiff of Oxygen Before the Great Oxidation Event? Science *317*, 1903–1906.

Badger, M.R., and Price, G.D. (2003). CO2 concentrating mechanisms in cyanobacteria: molecular components, their diversity and evolution. J. Exp. Bot. *54*, 609–622.

Badger, M.R., Hanson, D., and Price, G.D. (2002). Evolution and diversity of CO2 concentrating mechanisms in cyanobacteria. Funct. Plant Biol. *29*, 161–173.

Badger, M.R., Price, G.D., Long, B.M., and Woodger, F.J. (2006). The environmental plasticity and ecological genomics of the cyanobacterial CO2 concentrating mechanism. J. Exp. Bot. *57*, 249–265.

Behrenfeld, M.J., Bale, A.J., Kolber, Z.S., Aiken, J., and Falkowski, P.G. (1996). Confirmation of iron limitation of phytoplankton photosynthesis in the equatorial Pacific Ocean. Nature *383*, 508–511.

Bekker, A., Holland, H.D., Wang, P.-L., Iii, D.R., Stein, H.J., Hannah, J.L., Coetzee, L.L., and Beukes, N.J. (2004). Dating the rise of atmospheric oxygen. Nature *427*, 117–120.

Bergman, B., Sandh, G., Lin, S., Larsson, J., and Carpenter, E.J. (2013). Trichodesmium – a widespread marine cyanobacterium with unusual nitrogen fixation properties. Fems Microbiol. Rev. *37*, 286–302.

von Bohlen, A. (2009). Total reflection X-ray fluorescence and grazing incidence X-ray spectrometry — Tools for micro- and surface analysis. A review. Spectrochim. Acta Part B At. Spectrosc. *64*, 821–832.

Bothe, H., Schmitz, O., Yates, M.G., and Newton, W.E. (2010). Nitrogen Fixation and Hydrogen Metabolism in Cyanobacteria. Microbiol. Mol. Biol. Rev. *74*, 529–551.

Boyle, R.A., Clark, J.R., Poulton, S.W., Shields-Zhou, G., Canfield, D.E., and Lenton, T.M. (2013). Nitrogen cycle feedbacks as a control on euxinia in the mid-Proterozoic ocean. Nat. Commun. *4*, 1533.

Brocks, J.J., Logan, G.A., Buick, R., and Summons, R.E. (1999). Archean Molecular Fossils and the Early Rise of Eukaryotes. Science *285*, 1033–1036.

Brocks, J.J., Buick, R., Summons, R.E., and Logan, G.A. (2003). A reconstruction of Archean biological diversity based on molecular fossils from the 2.78 to 2.45 billion-year-old Mount Bruce Supergroup, Hamersley Basin, Western Australia. Geochim. Cosmochim. Acta *67*, 4321–4335.

Bryant, D.A. (2006). The Molecular Biology of Cyanobacteria (Springer Science & Business Media).

Burnap, R.L., Hagemann, M., and Kaplan, A. (2015). Regulation of CO2 Concentrating Mechanism in Cyanobacteria. Life *5*, 348–371.

Burnell, J.N. (1984). Sulfate Assimilation in C4 Plants: Intercellular and Intracellular Location of ATP Sulfurylase, Cysteine Synthase, and Cystathionine β-Lyase in Maize Leaves. Plant Physiol. *75*, 873–875.

Butterfield, N.J. (2015). Proterozoic photosynthesis – a critical review. Palaeontology *58*, 953–972.

Cameron, J.C., Wilson, S.C., Bernstein, S.L., and Kerfeld, C.A. (2013). Biogenesis of a Bacterial Organelle: The Carboxysome Assembly Pathway. Cell *155*, 1131–1140.

Canfield, D.E. (1998). A new model for Proterozoic ocean chemistry. Nature *396*, 450–453.

Canfield, D.E. (2004). The evolution of the Earth surface sulfur reservoir. Am. J. Sci. *304*, 839–861.

Canfield, D.E. (2005). THE EARLY HISTORY OF ATMOSPHERIC OXYGEN: Homage to Robert M. Garrels. Annu. Rev. Earth Planet. Sci. *33*, 1–36.

Canfield, D.E. (2014). Oxygen: A Four Billion Year History (Princeton University Press).

Canfield, D.E., Habicht, K.S., and Thamdrup, B. (2000). The Archean Sulfur Cycle and the Early History of Atmospheric Oxygen. Science *288*, 658–661.

Cardona, T. (2015). A fresh look at the evolution and diversification of photochemical reaction centers. Photosynth. Res. *126*, 111–134.

Cardona, T., Murray, J.W., and Rutherford, A.W. (2015). Origin and Evolution of Water Oxidation before the Last Common Ancestor of the Cyanobacteria. Mol. Biol. Evol. *32*, 1310–1328.

Chen, J., Hanke, A., Tegetmeyer, H.E., Kattelmann, I., Sharma, R., Hamann, E., Hargesheimer, T., Kraft, B., Lenk, S., Geelhoed, J.S., et al. (2017). Impacts of chemical gradients on microbial community structure. ISME J. *11*, 920–931.

Cohen, Y., and Gurevitz, M. (2006). The Cyanobacteria—Ecology, Physiology and Molecular Genetics. In The Prokaryotes, (Springer, New York, NY), pp. 1074–1098.

Cord-Ruwisch, R., Seitz, H.-J., and Conrad, R. (1988). The capacity of hydrogenotrophic anaerobic bacteria to compete for traces of hydrogen depends on the redox potential of the terminal electron acceptor. Arch. Microbiol. *149*, 350–357.

Crowe, S.A., Døssing, L.N., Beukes, N.J., Bau, M., Kruger, S.J., Frei, R., and Canfield, D.E. (2013). Atmospheric oxygenation three billion years ago. Nature *501*, 535–538.

Domenighini, A., and Giordano, M. (2009). Fourier Transform Infrared Spectroscopy of Microalgae as a Novel Tool for Biodiversity Studies, Species Identification, and the Assessment of Water Quality1. J. Phycol. *45*, 522–531.

Drake, H.L., and Akagi, J.M. (1978). Dissimilatory reduction of bisulfite by Desulfovibrio vulgaris. J. Bacteriol. *136*, 916–923.

Dufresne, A., Ostrowski, M., Scanlan, D.J., Garczarek, L., Mazard, S., Palenik, B.P., Paulsen, I.T., de Marsac, N.T., Wincker, P., Dossat, C., et al. (2008). Unraveling the genomic mosaic of a ubiquitous genus of marine cyanobacteria. Genome Biol. *9*, R90.

Erb, T.J., and Zarzycki, J. (2018). A short history of RubisCO: the rise and fall (?) of Nature's predominant CO2 fixing enzyme. Curr. Opin. Biotechnol. *49*, 100–107.

Falkowski, P.G. (2004). The Evolution of Modern Eukaryotic Phytoplankton. Science *305*, 354–360.

Falkowski, P.G., and Godfrey, L.V. (2008). Electrons, life and the evolution of Earth's oxygen cycle. Philos. Trans. R. Soc. Lond. B Biol. Sci. *363*, 2705–2716.

Falkowski, P.G., and Raven, J.A. (2013). Aquatic Photosynthesis: (Second Edition) (Princeton University Press).

Fanesi, A., Raven, J.A., and Giordano, M. (2014). Growth rate affects the responses of the green alga Tetraselmis suecica to external perturbations. Plant Cell Environ. *37*, 512–519.

Farley, J.R., Cryns, D.F., Yang, Y.H., and Segel, I.H. (1976). Adenosine triphosphate sulfurylase from penicillium chrysogenum. Steady state kinetics of the forward and reverse reactions. J. Biol. Chem. *251*, 4389–4397.

Farquhar, J., and Wing, B.A. (2003). Multiple sulfur isotopes and the evolution of the atmosphere. Earth Planet. Sci. Lett. *213*, 1–13.

Farquhar, J., Bao, H., and Thiemens, M. (2000). Atmospheric Influence of Earth9s Earliest Sulfur Cycle. Science *289*, 756–758.

Farquhar, J., Wu, N., Canfield, D.E., and Oduro, H. (2010a). Connections between Sulfur Cycle Evolution, Sulfur Isotopes, Sediments, and Base Metal Sulfide Deposits. Econ. Geol. *105*, 509–533.

Farquhar, J., Wu, N., Canfield, D.E., and Oduro, H. (2010b). Connections between Sulfur Cycle Evolution, Sulfur Isotopes, Sediments, and Base Metal Sulfide Deposits. Econ. Geol. *105*, 509–533.

Fike, D.A., Bradley, A.S., and Rose, C.V. (2015). Rethinking the Ancient Sulfur Cycle. Annu. Rev. Earth Planet. Sci. *43*, 593–622.

Fischer, W.W. (2008). Biogeochemistry: Life before the rise of oxygen. Nature *455*, 1051–1052.

Fischer, W.W., and Knoll, A.H. (2009). An iron shuttle for deepwater silica in Late Archean and early Paleoproterozoic iron formationOrigin of Late Archean and Early Paleoproterozoic iron formation. GSA Bull. *121*, 222–235.

Fischer, W.W., Hemp, J., and Johnson, J.E. (2016a). Evolution of Oxygenic Photosynthesis. Annu. Rev. Earth Planet. Sci. *44*, 647–683.

Fischer, W.W., Hemp, J., and Valentine, J.S. (2016b). How did life survive Earth's great oxygenation? Curr. Opin. Chem. Biol. *31*, 166–178.

Flores, E., Frías, J.E., Rubio, L.M., and Herrero, A. (2005). Photosynthetic nitrate assimilation in cyanobacteria. Photosynth. Res. *83*, 117–133.

Flynn, T.M., O'Loughlin, E.J., Mishra, B., DiChristina, T.J., and Kemner, K.M. (2014). Sulfur-mediated electron shuttling during bacterial iron reduction. Science *344*, 1039–1042.

Fukuzawa, H., Ogawa, T., and Kaplan, A. (2012). The Uptake of CO<Subscript>2</Subscript> by Cyanobacteria and Microalgae. In Photosynthesis, (Springer, Dordrecht), pp. 625–650.

Gill, B.C., Lyons, T.W., and Frank, T.D. (2008). Behavior of carbonate-associated sulfate during meteoric diagenesis and implications for the sulfur isotope paleoproxy. Geochim. Cosmochim. Acta *72*, 4699–4711.

Giordano, M., and Prioretti, L. (2016). Sulphur and Algae: Metabolism, Ecology and Evolution. In The Physiology of Microalgae, (Springer, Cham), pp. 185–209.

Giordano, M., Pezzoni, V., and Hell, R. (2000). Strategies for the Allocation of Resources under Sulfur Limitation in the Green Alga Dunaliella salina. Plant Physiol. *124*, 857–864.

Giordano, M., Kansiz, M., Heraud, P., Beardall, J., Wood, B., and McNaughton, D. (2001). Fourier Transform Infrared Spectroscopy as a Novel Tool to Investigate Changes in Intracellular Macromolecular Pools in the Marine Microalga Chaetoceros Muellerii (bacillariophyceae). J. Phycol. *37*, 271–279.

Giordano, M., Beardall, J., and Raven, J.A. (2005). CO2 CONCENTRATING MECHANISMS IN ALGAE: Mechanisms, Environmental Modulation, and Evolution. Annu. Rev. Plant Biol. *56*, 99–131.

Giordano, M., Olivieri, C., Ratti, S., Norici, A., Raven, J.A., and Knoll, A.H. (2018). A tale of two eras: Phytoplankton composition influenced by oceanic paleochemistry. Geobiology *16*, 498–506.

Greene, R.M., Geider, R.J., and Falkowski, P.G. (1991). Effect of iron limitation on photosynthesis in a marine diatom. Limnol. Oceanogr. *36*, 1772–1782.

Griffin, B.M., Schott, J., and Schink, B. (2007). Nitrite, an Electron Donor for Anoxygenic Photosynthesis. Science *316*, 1870–1870.

Grula, J.W. (2012). Rethinking the Paleoproterozoic Great Oxidation Event: A Biological Perspective. ArXiv12036701 Astro-Ph.

Habicht, K.S., Canfield, D.E., and Rethmeier, J. (1998). Sulfur isotope fractionation during bacterial reduction and disproportionation of thiosulfate and sulfite. Geochim. Cosmochim. Acta *62*, 2585–2595.

Habicht, K.S., Gade, M., Thamdrup, B., Berg, P., and Canfield, D.E. (2002). Calibration of Sulfate Levels in the Archean Ocean. Science *298*, 2372–2374.

Hamilton, T.L., Bryant, D.A., and Macalady, J.L. (2016). The role of biology in planetary evolution: cyanobacterial primary production in low-oxygen Proterozoic oceans. Environ. Microbiol. *18*, 325–340.

Hayes, J.M., and Waldbauer, J.R. (2006). The carbon cycle and associated redox processes through time. Philos. Trans. R. Soc. Lond. B Biol. Sci. *361*, 931–950.

Herrmann, A.J., and Gehringer, M.M. (2019). An investigation into the effects of increasing salinity on photosynthesis in freshwater unicellular cyanobacteria during the late Archaean. Geobiology *17*, 343–359.

Ho, S.Y.W., and Phillips, M.J. (2009). Accounting for Calibration Uncertainty in Phylogenetic Estimation of Evolutionary Divergence Times. Syst. Biol. *58*, 367–380.

Hoffman, P.F. (2013). The Great Oxidation and a Siderian snowball Earth: MIF-S based correlation of Paleoproterozoic glacial epochs. Chem. Geol. *362*, 143–156.

Hoffman, P.F. (2016). Cryoconite pans on Snowball Earth: supraglacial oases for Cryogenian eukaryotes? Geobiology *14*, 531–542.

Hoffman, P.F., Abbot, D.S., Ashkenazy, Y., Benn, D.I., Brocks, J.J., Cohen, P.A., Cox, G.M., Creveling, J.R., Donnadieu, Y., Erwin, D.H., et al. (2017). Snowball Earth climate dynamics and Cryogenian geology-geobiology. Sci. Adv. *3*, e1600983.

House, C.H., Schopf, J.W., McKeegan, K.D., Coath, C.D., Harrison, T.M., and Stetter, K.O. (2000). Carbon isotopic composition of individual Precambrian microfossils. Geology *28*, 707–710.

Javaux, E.J., and Lepot, K. (2018). The Paleoproterozoic fossil record: Implications for the evolution of the biosphere during Earth's middle-age. Earth-Sci. Rev. *176*, 68–86.

Johnson, J.E. (2019). From minerals to metabolisms: Evidence for life before oxygen from the geological record. Free Radic. Biol. Med. *140*, 126–137.

Johnston, D.T., Wolfe-Simon, F., Pearson, A., and Knoll, A.H. (2009). Anoxygenic photosynthesis modulated Proterozoic oxygen and sustained Earth's middle age. Proc. Natl. Acad. Sci. *106*, 16925–16929.

Kansiz, M., Heraud, P., Wood, B., Burden, F., Beardall, J., and McNaughton, D. (1999). Fourier Transform Infrared microspectroscopy and chemometrics as a tool for the discrimination of cyanobacterial strains. Phytochemistry *52*, 407–417.

Karlson, A.M.L., Duberg, J., Motwani, N.H., Hogfors, H., Klawonn, I., Ploug, H., Barthel Svedén, J., Garbaras, A., Sundelin, B., Hajdu, S., et al. (2015). Nitrogen fixation by cyanobacteria stimulates production in Baltic food webs. AMBIO *44*, 413–426.

Kendall, C., and Caldwell, E.A. (1998). Chapter 2 - Fundamentals of Isotope Geochemistry. In Isotope Tracers in Catchment Hydrology, C. Kendall, and J.J. McDONNELL, eds. (Amsterdam: Elsevier), pp. 51–86.

Klatt, J.M., Al-Najjar, M.A.A., Yilmaz, P., Lavik, G., de Beer, D., and Polerecky, L. (2015). Anoxygenic Photosynthesis Controls Oxygenic Photosynthesis in a Cyanobacterium from a Sulfidic Spring. Appl. Environ. Microbiol. *81*, 2025–2031.

Knoll, A.H., and Nowak, M.A. (2017). The timetable of evolution. Sci. Adv. *3*.

Knoll, A.H., Bergmann, K.D., and Strauss, J.V. (2016). Life: the first two billion years. Philos. Trans. R. Soc. B Biol. Sci. *371*, 20150493.

Kolber, Z.S., Barber, R.T., Coale, K.H., Fitzwateri, S.E., Greene, R.M., Johnson, K.S., Lindley, S., and Falkowski, P.G. (1994). Iron limitation of phytoplankton photosynthesis in the equatorial Pacific Ocean. Nature *371*, 145–149.

Kudo, I., and Harrison, P.J. (1997). Effect of Iron Nutrition on the Marine Cyanobacterium Synechococcus Grown on Different N Sources and Irradiances1. J. Phycol. *33*, 232–240.

Kump, L.R. (2008). The rise of atmospheric oxygen. Nature *451*, 277–278.

Kump, L.R., and Barley, M.E. (2007). Increased subaerial volcanism and the rise of atmospheric oxygen 2.5 billion years ago. Nature *448*, 1033–1036.

Leavitt, W.D., Bradley, A.S., Santos, A.A., Pereira, I.A.C., and Johnston, D.T. (2015). Sulfur Isotope Effects of Dissimilatory Sulfite Reductase. Front. Microbiol. *6*.

Lindh, M.V., Maillot, B.M., Shulse, C.N., Gooday, A.J., Amon, D.J., Smith, C.R., and Church, M.J. (2017). From the Surface to the Deep-Sea: Bacterial Distributions across Polymetallic Nodule Fields in the Clarion-Clipperton Zone of the Pacific Ocean. Front. Microbiol. *8*.

Liu, L.-N. (2016). Distribution and dynamics of electron transport complexes in cyanobacterial thylakoid membranes. Biochim. Biophys. Acta BBA - Bioenerg. *1857*, 256–265.

Liu, C.L., and Peck, H.D. (1981). Comparative bioenergetics of sulfate reduction in Desulfovibrio and Desulfotomaculum spp. J. Bacteriol. *145*, 966–973.

Lowry, O.H., Rosebrough, N.J., Farr, A.L., and Randall, R.J. (1951). Protein measurement with the Folin phenol reagent. J. Biol. Chem. *193*, 265–275.

Lyons, T.W., Reinhard, C.T., and Planavsky, N.J. (2014). The rise of oxygen in Earth/'s early ocean and atmosphere. Nature *506*, 307–315.

Martínez-García, A., Sigman, D.M., Ren, H., Anderson, R.F., Straub, M., Hodell, D.A., Jaccard, S.L., Eglinton, T.I., and Haug, G.H. (2014). Iron Fertilization of the Subantarctic Ocean During the Last Ice Age. Science *343*, 1347–1350.

McFadden, G.I. (2001). Primary and Secondary Endosymbiosis and the Origin of Plastids. J. Phycol. *37*, 951–959.

Melis, A., and Chen, H.-C. (2005). Chloroplast sulfate transport in green algae – genes, proteins and effects. Photosynth. Res. *86*, 299–307.

Miyashita, H., Ikemoto, H., Kurano, N., Adachi, K., Chihara, M., and Miyachi, S. (1996). Chlorophyll d as a major pigment. Nature *383*, 402.

Moore, J.K., Doney, S.C., Glover, D.M., and Fung, I.Y. (2001). Iron cycling and nutrient-limitation patterns in surface waters of the World Ocean. Deep Sea Res. Part II Top. Stud. Oceanogr. *49*, 463–507.

Moore, L.R., Post, A.F., Rocap, G., and Chisholm, S.W. (2002). Utilization of different nitrogen sources by the marine cyanobacteria Prochlorococcus and Synechococcus. Limnol. Oceanogr. *47*, 989–996.

Mooy, B.A.S.V., Rocap, G., Fredricks, H.F., Evans, C.T., and Devol, A.H. (2006). Sulfolipids dramatically decrease phosphorus demand by picocyanobacteria in oligotrophic marine environments. Proc. Natl. Acad. Sci. *103*, 8607–8612.

Ozaki, K., Thompson, K.J., Simister, R.L., Crowe, S.A., and Reinhard, C.T. (2019). Anoxygenic photosynthesis and the delayed oxygenation of Earth's atmosphere. Nat. Commun. *10*, 1–10.

Painter, P.R., and Marr, A.G. (1967). Inequality of mean interdivision time and doubling time. Microbiology *48*, 155–159.

Palmucci, M., Ratti, S., and Giordano, M. (2011). Ecological and Evolutionary Implications of Carbon Allocation in Marine Phytoplankton as a Function of Nitrogen Availability: A Fourier Transform Infrared Spectroscopy Approach1. J. Phycol. *47*, 313–323.

Papineau, D., Mojzsis, S.J., and Schmitt, A.K. (2007a). Multiple sulfur isotopes from Paleoproterozoic Huronian interglacial sediments and the rise of atmospheric oxygen. Earth Planet. Sci. Lett. *255*, 188–212.

Papineau, D., Mojzsis, S.J., and Schmitt, A.K. (2007b). Multiple sulfur isotopes from Paleoproterozoic Huronian interglacial sediments and the rise of atmospheric oxygen. Earth Planet. Sci. Lett. *255*, 188–212.

Partensky, F., and Garczarek, L. (2010). Prochlorococcus: Advantages and Limits of Minimalism. Annu. Rev. Mar. Sci. *2*, 305–331.

Partensky, F., Blanchot, J., and Vaulot, D. (1999). Differential distribution and ecology of Prochlorococcus and Synechococcus in oceanic waters: a review. Bull.-Inst. Oceanogr. MONACO-NUMERO Spec. 457–476.

Pavlov, A. a., and Kasting, J. f. (2002). Mass-Independent Fractionation of Sulfur Isotopes in Archean Sediments: Strong Evidence for an Anoxic Archean Atmosphere. Astrobiology *2*, 27–41.

Peterson, G.L. (1977). A simplification of the protein assay method of Lowry et al. which is more generally applicable. Anal. Biochem. *83*, 346–356.

Pfennig, N., Widdel, F., Postgate, J.R., Postgate, J.R., and Kelly, D.P. (1982). The bacteria of the sulphur cycle. Philos. Trans. R. Soc. Lond. B Biol. Sci. *298*, 433–441.

Ph.D, A.H.C. (1923). CXVII. The total reflexion of X-rays. Lond. Edinb. Dublin Philos. Mag. J. Sci. *45*, 1121–1131.

Planavsky, N.J., Asael, D., Hofmann, A., Reinhard, C.T., Lalonde, S.V., Knudsen, A., Wang, X., Ossa, F.O., Pecoits, E., Smith, A.J.B., et al. (2014). Evidence for oxygenic photosynthesis half a billion years before the Great Oxidation Event. Nat. Geosci. *7*, 283–286.

Porra, R.J., Thompson, W.A., and Kriedemann, P.E. (1989). Determination of accurate extinction coefficients and simultaneous equations for assaying chlorophylls a and b extracted with four different solvents: verification of the concentration of chlorophyll standards by atomic absorption spectroscopy. Biochim. Biophys. Acta BBA-Bioenerg. *975*, 384–394.

Price, G.D. (2011). Inorganic carbon transporters of the cyanobacterial CO2 concentrating mechanism. Photosynth. Res. *109*, 47–57.

Price, G.D., Badger, M.R., Woodger, F.J., and Long, B.M. (2008). Advances in understanding the cyanobacterial CO2-concentrating-mechanism (CCM): functional components, Ci transporters, diversity, genetic regulation and prospects for engineering into plants. J. Exp. Bot. *59*, 1441–1461.

Prioretti, L., and Giordano, M. (2016). Direct and indirect influence of sulfur availability on phytoplankton evolutionary trajectories. J. Phycol. *52*, 1094–1102.

Prioretti, L., Gontero, B., Hell, R., and Giordano, M. (2014). Diversity and regulation of ATP sulfurylase in photosynthetic organisms. Front. Plant Sci. *5*.

Prioretti, L., Lebrun, R., Gontero, B., and Giordano, M. (2016). Redox regulation of ATP sulfurylase in microalgae. Biochem. Biophys. Res. Commun. *478*, 1555–1562.

Rae, B.D., Long, B.M., Badger, M.R., and Price, G.D. (2013). Functions, Compositions, and Evolution of the Two Types of Carboxysomes: Polyhedral Microcompartments That Facilitate CO2 Fixation in Cyanobacteria and Some Proteobacteria. Microbiol. Mol. Biol. Rev. *77*, 357–379.

Rasmussen, B., Fletcher, I.R., Brocks, J.J., and Kilburn, M.R. (2008). Reassessing the first appearance of eukaryotes and cyanobacteria. Nature *455*, 1101–1104.

Ratti, S., Knoll, A.H., and Giordano, M. (2011). Did sulfate availability facilitate the evolutionary expansion of chlorophyll a+c phytoplankton in the oceans? Geobiology *9*, 301–312.

Ratti, S., Knoll, A.H., and Giordano, M. (2013). Grazers and Phytoplankton Growth in the Oceans: an Experimental and Evolutionary Perspective. PLoS ONE *8*, e77349.

Raven, J.A. (1990). Predictions of Mn and Fe use efficiencies of phototrophic growth as a function of light availability for growth and of C assimilation pathway. New Phytol. *116*, 1–18.

Raven, J.A., Evans, M.C.W., and Korb, R.E. (1999). The role of trace metals in photosynthetic electron transport in O<Subscript>2</Subscript>-evolving organisms. Photosynth. Res. *60*, 111–150.

REDFIELD, A.C. (1934). On the proportions of organic derivatives in sea water and their relation to the composition of plankton. James Johnstone Meml. Vol. 176–192.

Rees, C.E. (1973). A steady-state model for sulphur isotope fractionation in bacterial reduction processes. Geochim. Cosmochim. Acta *37*, 1141–1162.

Rickaby, R.E.M., and Eason Hubbard, M.R. (2019). Upper ocean oxygenation, evolution of RuBisCO and the Phanerozoic succession of phytoplankton. Free Radic. Biol. Med. *140*, 295–304.

Robbins, L.J., Lalonde, S.V., Planavsky, N.J., Partin, C.A., Reinhard, C.T., Kendall, B., Scott, C., Hardisty, D.S., Gill, B.C., Alessi, D.S., et al. (2016). Trace elements at the intersection of marine biological and geochemical evolution. Earth-Sci. Rev. *163*, 323–348.

Robinson, P.K. (2015). Enzymes: principles and biotechnological applications. Essays Biochem. *59*, 1–41.

Ruan, Z., Prášil, O., and Giordano, M. (2018). The phycobilisomes of Synechococcus sp. are constructed to minimize nitrogen use in nitrogen-limited cells and to maximize energy capture in energy-limited cells. Environ. Exp. Bot. *150*, 152–160.

Saito, M.A., Sigman, D.M., and Morel, F.M.M. (2003). The bioinorganic chemistry of the ancient ocean: the co-evolution of cyanobacterial metal requirements and biogeochemical cycles at the Archean–Proterozoic boundary? Inorganica Chim. Acta *356*, 308–318.

Sánchez-Baracaldo, P. (2015). Origin of marine planktonic cyanobacteria. Sci. Rep. *5*.

Scanlan, D.J. (2003). Physiological diversity and niche adaptation in marine Synechococcus. In Advances in Microbial Physiology, (Academic Press), pp. 1–64.

Scanlan, D.J., Ostrowski, M., Mazard, S., Dufresne, A., Garczarek, L., Hess, W.R., Post, A.F., Hagemann, M., Paulsen, I., and Partensky, F. (2009). Ecological Genomics of Marine Picocyanobacteria. Microbiol. Mol. Biol. Rev. *73*, 249–299.

Schirrmeister, B.E., Vos, J.M. de, Antonelli, A., and Bagheri, H.C. (2013). Evolution of multicellularity coincided with increased diversification of cyanobacteria and the Great Oxidation Event. Proc. Natl. Acad. Sci. *110*, 1791–1796.

Schirrmeister, B.E., Gugger, M., and Donoghue, P.C.J. (2015). Cyanobacteria and the Great Oxidation Event: evidence from genes and fossils. Palaeontology *58*, 769–785.

Schirrmeister, B.E., Sanchez-Baracaldo, P., and Wacey, D. (2016). Cyanobacterial evolution during the Precambrian. Int. J. Astrobiol. *15*, 187–204.

Scott, C., Lyons, T.W., Bekker, A., Shen, Y., Poulton, S.W., Chu, X., and Anbar, A.D. (2008). Tracing the stepwise oxygenation of the Proterozoic ocean. Nature *452*, 456–459.

Scott, K.M., Henn-Sax, M., Harmer, T.L., Longo, D.L., Frame, C.H., and Cavanaugh, C.M. (2007). Kinetic isotope effect and biochemical characterization of form IA RubisCO from the marine cyanobacterium Prochlorococcus marinus MIT9313. Limnol. Oceanogr. *52*, 2199–2204.

Settle, F.A. (1997). Handbook of Instrumental Techniques for Analytical Chemistry (Prentice Hall PTR).

Shih, P.M., Occhialini, A., Cameron, J.C., Andralojc, P.J., Parry, M.A.J., and Kerfeld, C.A. (2016). Biochemical characterization of predicted Precambrian RuBisCO. Nat. Commun. *7*.

Shih, P.M., Hemp, J., Ward, L.M., Matzke, N.J., and Fischer, W.W. (2017). Crown group Oxyphotobacteria postdate the rise of oxygen. Geobiology *15*, 19–29.

Sim, M.S., Paris, G., Adkins, J.F., Orphan, V.J., and Sessions, A.L. (2017). Quantification and isotopic analysis of intracellular sulfur metabolites in the dissimilatory sulfate reduction pathway. Geochim. Cosmochim. Acta *206*, 57–72.

Sim, M.S., Ogata, H., Lubitz, W., Adkins, J.F., Sessions, A.L., Orphan, V.J., and McGlynn, S.E. (2019). Role of APS reductase in biogeochemical sulfur isotope fractionation. Nat. Commun. *10*, 44.

Six, C., Thomas, J.-C., Garczarek, L., Ostrowski, M., Dufresne, A., Blot, N., Scanlan, D.J., and Partensky, F. (2007). Diversity and evolution of phycobilisomes in marine Synechococcusspp.: a comparative genomics study. Genome Biol. *8*, R259.

Smith, B.C. (2011). Fundamentals of Fourier Transform Infrared Spectroscopy, Second Edition (CRC Press).

Smith, E., and Morowitz, H.J. (2016). The Origin and Nature of Life on Earth by Eric Smith.

Soo, R.M., Hemp, J., Parks, D.H., Fischer, W.W., and Hugenholtz, P. (2017). On the origins of oxygenic photosynthesis and aerobic respiration in Cyanobacteria. Science *355*, 1436–1440.

Stanier, R.Y., Kunisawa, R., Mandel, M., and Cohen-Bazire, G. (1971). Purification and properties of unicellular blue-green algae (order Chroococcales). Bacteriol. Rev. *35*, 171–205.

Stüeken, E.E., Kipp, M.A., Koehler, M.C., and Buick, R. (2016). The evolution of Earth's biogeochemical nitrogen cycle. Earth-Sci. Rev. *160*, 220–239.

Summons, R.E., Jahnke, L.L., Hope, J.M., and Logan, G.A. (1999). 2-Methylhopanoids as biomarkers for cyanobacterial oxygenic photosynthesis. Nature *400*, 554–557.

Swanner, E.D., Mloszewska, A.M., Cirpka, O.A., Schoenberg, R., Konhauser, K.O., and Kappler, A. (2015a). Modulation of oxygen production in Archaean oceans by episodes of Fe(II) toxicity. Nat. Geosci. *8*, 126–130.

Swanner, E.D., Wu, W., Hao, L., Wüstner, M.L., Obst, M., Moran, D.M., McIlvin, M.R., Saito, M.A., and Kappler, A. (2015b). Physiology, Fe(II) oxidation, and Fe mineral formation by a marine planktonic cyanobacterium grown under ferruginous conditions. Front. Earth Sci. *3*.

Tagliabue, A., Bowie, A.R., Boyd, P.W., Buck, K.N., Johnson, K.S., and Saito, M.A. (2017). The integral role of iron in ocean biogeochemistry. Nature *543*, 51–59.

Takahashi, H., Kopriva, S., Giordano, M., Saito, K., and Hell, R. (2011). Sulfur Assimilation in Photosynthetic Organisms: Molecular Functions and Regulations of Transporters and Assimilatory Enzymes. Annu. Rev. Plant Biol. *62*, 157–184.

Takahashi, H., Buchner, P., Yoshimoto, N., Hawkesford, M.J., and Shiu, S.-H. (2012). Evolutionary Relationships and Functional Diversity of Plant Sulfate Transporters. Front. Plant Sci. *2*.

Tamagnini, P., Axelsson, R., Lindberg, P., Oxelfelt, F., Wünschiers, R., and Lindblad, P. (2002). Hydrogenases and Hydrogen Metabolism of Cyanobacteria. Microbiol. Mol. Biol. Rev. *66*, 1–20.

Thauer, R.K., Jungermann, K., and Decker, K. (1977). Energy conservation in chemotrophic anaerobic bacteria. Bacteriol. Rev. *41*, 100–180.

Thode, H.G., Macnamara, J., and Fleming, W.H. (1953). Sulphur isotope fractionation in nature and geological and biological time scales. Geochim. Cosmochim. Acta *3*, 235–243.

Thomas, D.J., Sullivan, S.L., Price, A.L., and Zimmerman, S.M. (2005). Common freshwater cyanobacteria grow in 100% CO2. Astrobiology *5*, 66–74.

Uitz, J., Claustre, H., Gentili, B., and Stramski, D. (2010). Phytoplankton class-specific primary production in the world's oceans: Seasonal and interannual variability from satellite observations. Glob. Biogeochem. Cycles *24*, GB3016.

Ward, L.M., Kirschvink, J.L., and Fischer, W.W. (2016). Timescales of Oxygenation Following the Evolution of Oxygenic Photosynthesis. Orig. Life Evol. Biospheres *46*, 51–65.

Watanabe, M., and Ikeuchi, M. (2013). Phycobilisome: architecture of a light-harvesting supercomplex. Photosynth. Res. *116*, 265–276.

Whitton, B.A., and Potts, M. (2012). Introduction to the Cyanobacteria. In Ecology of Cyanobacteria II, (Springer, Dordrecht), pp. 1–13.

Williford, K.H., Ushikubo, T., Schopf, J.W., Lepot, K., Kitajima, K., and Valley, J.W. (2013). Preservation and detection of microstructural and taxonomic correlations in the carbon isotopic compositions of individual Precambrian microfossils. Geochim. Cosmochim. Acta *104*, 165–182.

Yamamoto, Y., and Shiah, F.-K. (2010). Relationship between cell growth and frequency of dividing cells of Microcystis aeruginosa. Plankton Benthos Res. *5*, 131–135.

Zwirglmaier, K., Jardillier, L., Ostrowski, M., Mazard, S., Garczarek, L., Vaulot, D., Not, F., Massana, R., Ulloa, O., and Scanlan, D.J. (2008). Global phylogeography of marine Synechococcus and Prochlorococcus reveals a distinct partitioning of lineages among oceanic biomes. Environ. Microbiol. *10*, 147–161.